Dissertation
submitted to the
Combined Faculty of Mathematics, Engineering
and Natural Sciences
of Heidelberg University, Germany
for the degree of
Doctor of Natural Sciences

Put forward by
Lars Helge Heyen
born in: Georgsmarienhütte
Oral examination: 07.06.2023

On the lower particle number limit of fluid dynamics and the derivation of transport coefficients from microscopic theory

Abstract

Motivated by results from heavy-ion collisions we investigate the lower particle number limit of the applicability of fluid dynamics. We model the expansion of ultracold atoms in two dimensions suited to study this question experimentally and successfully predict the qualitative scaling of the elliptic flow with the particle number. For a fluid released from a harmonic trap with fluid static initial conditions, the dynamics can be reduced to ordinary differential equations by using Lagrange coordinates and solved for specific cases. Finding discrepancies between these results and experiments, we simulate the ideal fluid evolution of initial conditions fitted to experimental data, which shows that a system of ten strongly interacting ^{6}Li atoms behaves like a fluid at early times of the expansion.

The second problem addressed in this thesis is the non-perturbative prediction of shear viscosity for a real scalar quantum field theory with quartic interaction. We formulate the shear viscosity as a derivative of the quantum effective action and employ functional renormalization group methods to go beyond the perturbative regime. We construct a minimal ansatz and formulate flow equations for all free parameters. In the current form this leads to a trivial prediction for the shear viscosity which can be remedied by small changes to the interaction.

Zusammenfassung

Erkenntnissen aus Schwerionenkollisionen folgend untersuchen wir, bis zu welchen Teilchenzahlen Fluiddynamik noch anwendbar ist. Wir modellieren die Expansion von ultrakalten Atomen in zwei Dimensionen, die geeignet sind, diese Frage zu untersuchen, und schätzen erfolgreich die qualitative Abhängigkeit des elliptischen Flusses von der Teilchenzahl ab. Für ein Fluid, das aus einer harmonischen Falle mit fluidstatischen Anfangsbedingungen freigelassen wird, kann die Dynamik auf gewöhnliche Differentialgleichungen reduziert und in speziellen Fällen gelöst werden. Wir finden Diskrepanzen zwischen diesen Resultaten und Experimenten und simulieren die Entwicklung eines idealen Fluids mit an experimentelle Daten angepassten Anfangsbedingungen. Diese zeigt, dass ein System von zehn stark wechselwirkenden ^{6}Li-Atomen sich in der Frühphase der Expansion wie ein Fluid verhält.

Das zweite Problem mit dem sich diese Arbeit auseinandersetzt, ist die nicht-perturbative Vorhersage der Scherviskosität für die Quantenfeldtheorie eines reellen Skalarfelds mit quartischer Wechselwirkung. Wir formulieren die Scherviskosität in Form von Ableitungen der effektiven Wirkung und benutzen Methoden der funktionalen Renormierungsgruppe, um Vorhersagen jenseits von Störungstheorie treffen zu können. Dazu konstruieren wir einen minimalen Ansatz und formulieren Flussgleichungen für alle darin enthaltenen freien Parameter. In der jetzigen Form resultiert dies in einer trivialen Scherviskosität. Dieses Problem kann durch kleine Änderungen der effektiven Wechselwirkungsstärke behoben werden.

Contents

Acronyms

BBGKY	Bogoliubov, Born, Green, Kirkwood, Yvon
BCS	Bardeen, Cooper, Schrieffer
BEC	Bose-Einstein condensate
FLRW	Friedmann, Lemaître, Robertson, Walker
KMS	Kubo, Martin, Schwinger
QFT	quantum field theory
QGP	quark-gluon plasma

Units

Unless explicitly stated otherwise, units are assumed to be chosen such that $c = 1$, $\hbar = 1$, $k_B = 1$. In some cases, these constants will still be written out for purposes of clarity.

Metric signature

This thesis uses a mostly-plus signature, $(-, +, +, +)$, for all occurrences of the space-time metric $g_{\mu\nu}$.

Introduction

In classical physics, the one particle problem without any external forces is trivial. The problem of two particles interacting via newtonian gravitational force is also easy to solve. But already at three gravitationally interacting particles a closed form solution in terms of elementary functions is not possible [1], although for systems without net angular momentum there is a solution by Sundman that is a slowly converging infinite series in powers of $t^{1/3}$ [2]. In general the problem gets more difficult for higher numbers of particles and when taking into account quantum and relativistic effects. Yet physics is able to consistently describe certain classes of large systems with plenty of substructure on the microscopic level. Instead of predicting individual particle trajectories these effective descriptions focus on the dynamics of macroscopic properties that capture statistical properties of the system. The resulting concepts like temperature remain meaningful across a wide range of systems which might require vastly different descriptions in the microscopic regime. Equilibrium thermodynamics formulates relations between these macroscopic quantities and requires only knowledge of a single thermodynamic potential [3], and thereby the equation of state, as input from the underlying system. The dynamics in reaction to slight deviations from equilibrium can be encoded in transport coefficients. Overall, the macroscopic description only depends on the microscopic details in an indirect fashion as it usually determined more by the present symmetries and breakings thereof than the precise couplings [4].

One very successful macroscopic theory of out-of-equilibrium matter is fluid dynamics which can be derived as a consequence of conservation laws for the long time and large scale behavior of many-particle systems [5]. Its applications span many orders of magnitude in temperature and size, reaching from the classical flow of everyday liquids and gases to astrophysical phenomena and processes on much smaller scales like superfluidity in cold atomic gases [6] and the expansion of a quark gluon plasma in a collision of heavy ions at high energies [7]. In the collisional systems the litmus test of fluidlike behavior are the elliptic flow v_2 and higher order momentum anisotropies of the final state particles [8–10]. The fraction of the initial spatial anisotropy ε_n that translates into the momentum profile can be compared to predictions from fluid dynamic simulations. In recent years, specifically small systems like proton-proton collisions have gained a lot of attention due to the surprising stability of the fluid dynamic description down to very low particle numbers [11, 12]. These results call into question whether the separation of scales and local thermal equilibrium assumed to be necessary for fluidlike behavior can even be achieved [13].

In this thesis I will focus on two central questions. First, **what is the lower**

particle number limit of the applicability of fluid dynamics? We define fluidlike behavior as mass density, local velocity and energy density following their fluid dynamic equations of motion for some equation of state and transport coefficients resulting from the interactions between particles. The two edge cases are very clear. A single isolated particle cannot interact and thus fails to qualify while a macroscopic liquid with $N \sim 10^{23}$ particles fulfills the criteria. The data from small collisional systems suggests that the transition already happens at a small number ($N \leq 100$) of particles [14] that are still very strongly interacting. This multiplicity region is difficult to precisely probe in heavy-ion collisions, but can be investigated in expanding clouds of ultracold atoms. These systems allow for precise tuning of the interaction strength by using Feshbach resonances [15]. Elliptic flow in ultracold atoms has already been studied for different atoms and interaction strengths [16–25]. However, the particle numbers in these experiments are still comparatively large ($N \sim 10^5$ in [16]). Recent developments in experimental techniques allow for the preparation of very few ($N \leq 14$) fermionic particles in a harmonic oscillator ground state with high fidelity [26–28]. This opens up the possibility for a comparison between fluid dynamic predictions and experimental results in the mesoscopic regime which is already too large to be solved exactly, but also small enough that the applicability of a statistical description is highly questionable.

The second question of this thesis is: **How can we understand, and possibly predict, transport properties of a fluid in terms of an underlying quantum field theory?** In this thesis I will discuss specifically the prediction of shear viscosity for a real scalar field theory with a quartic interaction term. This problem has been investigated before [29, 30], but only in a perturbative fashion which cannot capture the strongly interacting systems one would intuitively expect fluid dynamic behavior from on a macroscopic scale. Considering shear viscosity as a static susceptibility, it is possible to relate it to a two-point function of the energy momentum tensor [31, 32] which in turn can be expressed as a functional derivative of the quantum effective action. This enables an approach using functional renormalization group methods that are valid beyond the perturbative regime [33].

Outline

Chapter 1 gives a brief overview over fluid dynamics and its application in the systems we will work with. The equations of motion of fluid dynamics are derived both as a special case of kinetic theory and from conservations laws with a focus on the difference in the assumptions between the two approaches. Lagrange coordinates are introduced as a comoving coordinate system that has a direct interpretation as a description of test particle trajectories. I shortly outline the role of fluid dynamics in heavy-ion collisions and its primary indicator, the elliptic flow v_2. Due to systematic uncertainties in the limit of small multiplicities, I move to a system of ultracold atoms, summarizing the phenomena of superfluidity and Feshbach resonances. I explore the special case of diverging scattering length and make predictions about isotropic expansion and oscillation behavior. The chapter concludes with the experimental techniques used to

achieve the well-controlled few particle systems needed for probing the lower particle number limit of fluid dynamics. In chapter 2, I present both analytical and numerical predictions for fluid behavior in few particle systems. I discuss the appropriate equation of state to be used in the description of the cold atom system and settle with a fit to data obtained from quantum Monte Carlo simulations in the many particle limit. This equation of state, together with a fluid static initial condition, makes it possible to reduce the continuity and Euler equation to a set of ordinary differential equation in Lagrange coordinates. Observing a mismatch between experimental data and fluid static initial conditions, I compare numerical simulations starting from fitted initial conditions to results from experiments. From the agreement between the data and a simulation with rescaled pressure I conclude that fluidlike behavior is present at early times in a system of $N = 10$ strongly interacting ^{6}Li atoms. Chapter 3 formulates functional renormalization group flow equations for the shear viscosity of a real scalar field theory with quartic interaction. I give an introduction to quantum field theory in thermal equilibrium as well as linear response theory. The Green-Kubo relations make it possible to formulate the shear viscosity in terms of a two-point correlation function of the energy momentum tensor or, equivalently, a second metric derivative of the quantum effective action. I explore a non-relativistic limit of the real scalar theory that could simplify calculations, but choose not to use it due to its complex metric dependency. Functional renormalization group methods allow for a non-perturbative approach to obtaining the quantum effective action using the Wetterich equation starting from a minimalist ansatz I present. From the results of the previous sections I derive flow equations for the free parameters of the ansatz as well as the shear viscosity. While the given approximation of the effective action is found to be at a fixed point in parameter space and thus produces trivial results, small changes to the ansatz can remedy this issue. The last chapter is a summary of the obtained results and a short outlook over some future avenues of research.

Chapter 1

Fluid dynamics

Fluid dynamics is a robust framework that gives a macroscopic description of systems that one would intuitively call a fluid or gas and also some that one might not identify as such. In the following discussion of the basics, I will focus on the assumptions that are made in order to arrive at the well-known equations that govern fluid motion. I will approach this in two different ways, the first being a derivation of continuity and Euler equations from kinetic theory. The second ansatz is centered around conservation laws and identifications independent of the assumptions already contained in kinetic theory.

1.1 Derivation from kinetic theory

With the first discussions of what is known today as kinetic theory going back more than two centuries, kinetic theory has a long history as a successful description linking microscopic and macroscopic understanding of collisional systems. I will introduce the basic concepts of kinetic theory starting from analytical mechanics following the discussions in [3] and [34]. Fluid dynamics is derived as a special case, describing the dynamics of certain moments of the phase space distribution. Lastly, I will discuss the involved assumptions and scales associated with this ansatz.

1.1.1 Basics of kinetic theory

In order to derive fluid dynamics from kinetic theory, we need to first consider the basic rules of that theory. Kinetic theory starts from a system of N classical particles whose motion is described by a Hamiltonian H. For the sake of simplicity, from this point on I will assume that there is only one species of particles, all particles are affected in the same way by external forces and interactions only involve two particles, even though that is not necessary for the derivation to work. Such a system is uniquely identified by its position in $6N$-dimensional phase space at any point in time. The Hamiltonian gives a clear prescription of what trajectory through phase space the system will take. In a statistical setting, in which we only work with a distribution function f_N in phase space, this can be formulated as the Liouville equation,

$$\partial_t f_N + \{f_N, H\} = 0 \,, \tag{1.1}$$

where $\{\cdot, \cdot\}$ denote the Poisson brackets with respect to all $6N$ generalized coordinates and momenta. In terms of potentials this is

$$\partial_t f_N + \sum_{i=0}^{N} \frac{\vec{p_i}}{m} \cdot \vec{\nabla}_{q_i} f_N - \sum_{i=0}^{N} \vec{\nabla}_{q_i} \left(V^{(\text{ext})} + \sum_{j=1, j \neq i}^{N} V_{ij}^{(\text{int})} \right) \cdot \vec{\nabla}_{p_i} f_N = 0 \,. \qquad (1.2)$$

The potential $V^{(\text{ext})}$ sums up all external forces and $V_{ij}^{(\text{int})}$ denotes the interaction potential between particles i and j and depends on both of their positions. By considering a statistical setting we also made another assumption about the system, which is that the number of particles is sufficiently large that a statistical treatment is justified. However, in a macroscopic setting complete knowledge of the full N-particle phase space distribution is unrealistic to assume.

One can marginalise the distribution by integrating out all particles but a certain number n, reducing it to

$$f_n = \int f_N \, \mathrm{d}^3 q_{n+1} \, \mathrm{d}^3 p_{n+1} \cdots \mathrm{d}^3 q_N \, \mathrm{d}^3 p_N \,. \qquad (1.3)$$

This object no longer follows a homogeneous differential equation since the effects of the marginalised particles on the still present ones has to be considered,

$$\begin{aligned}
\partial_t f_n + \sum_{i=0}^{n} \frac{\vec{p_i}}{m} \cdot \vec{\nabla}_{q_i} f_n - \sum_{i=0}^{n} \vec{\nabla}_{q_i} \left(V^{(\text{ext})} + \sum_{j=1, j \neq i}^{n} V_{ij}^{(\text{int})} \right) \cdot \vec{\nabla}_{p_i} f_n \\
= (N - n) \sum_{i=1}^{n} \int \vec{\nabla}_{q_i} V_{i,n+1}^{(\text{int})} \cdot \vec{\nabla}_{p_i} f_{n+1} \, \mathrm{d}^3 q_{n+1} \, \mathrm{d}^3 p_{n+1} \,.
\end{aligned} \qquad (1.4)$$

This is not a closed equation. In order to determine the dynamics of f_n, knowledge of f_{n+1} is necessary which in turn relies on the next higher order, recursively back to the closed full N-body case described by the Liouville equation. This is the Bogoliubov–Born–Green–Kirkwood–Yvon (BBGKY) hierarchy.

In order to get to a predictive theory, kinetic theory makes two decisions. First, it works with the one particle phase space density $f_1 = f(t, \vec{q}, \vec{p})$. Second, it makes the assumption of molecular chaos. On the mathematical side, molecular chaos means that the two particle phase space density f_2 can be expressed as a function of the one-particle distribution f. With this, the lowest order equation of the BBGKY hierarchy becomes closed and can be expressed as the Boltzmann equation,

$$\partial_t f + \frac{\vec{p}}{m} \cdot \vec{\nabla}_q f - \vec{\nabla}_q V^{(\text{ext})} \cdot \vec{\nabla}_p f = \mathcal{C}[f] \,. \qquad (1.5)$$

The collision kernel $\mathcal{C}[f]$ is a functional of the distribution encoding the interactions between particles. The physical interpretation of the molecular chaos hypothesis is that the correlations between the phase space positions of particles participating in a collision can be neglected, both before and after the collision. Since the scattering necessarily introduces some correlation between the particles which is discarded, this

introduces a time direction into an otherwise reversible process. This makes it possible to derive Boltzmann's H-theorem [34], the kinetic theory version of the second law of thermodynamics, from the unitary dynamics of the Liouville equation.

A commonly chosen form of the collision kernel is

$$\mathcal{C}[f](t, \vec{q}, \vec{p}) = \int W(\vec{p}_1, \vec{p}_2, \vec{p}_3, \vec{p})[f(t, \vec{q}, \vec{p}_1)f(t, \vec{q}, \vec{p}_2) - f(t, \vec{q}, \vec{p}_3)f(t, \vec{q}, \vec{p})] \, \mathrm{d}^3 p_1 \, \mathrm{d}^3 p_2 \, \mathrm{d}^3 p_3 \tag{1.6}$$

with a probability measure W of two particles colliding to go from momenta $(\vec{p}_1, \vec{p}_2)$ to $(\vec{p}_3, \vec{p})$ [3]. We can add different assumptions about the collisions in the system into this weight function. Momentum conservation can be enforced by making the probability of any process violating it vanish,

$$W(\vec{p}_1, \vec{p}_2, \vec{p}_3, \vec{p}) \sim \delta\left((\vec{p}_1 + \vec{p}_2) - (\vec{p}_3 + \vec{p})\right), \tag{1.7}$$

which represents three constraints and reduces the weight to a function of only three momenta. In general, conserved quantities within the collision are identified or conversely enforced via

$$\int g(\vec{p}) \, \mathcal{C}[f](t, \vec{q}, \vec{p}) \, \mathrm{d}^3 p = 0 \tag{1.8}$$

for some function of the momentum $g(\vec{p})$. The corresponding functions for conservation of particle number, momentum and non-relativistic kinetic energy are $g(\vec{p}) = 1$, $\vec{p}$ and $\vec{p}^2/2m$ respectively. Together with the assumption of rotational invariance of the interaction potential and the invariance of the scattering process under Galilean boosts, the probability distribution can be made to only depend on the center of mass energy and scattering angle. A linearized version of the Boltzmann equation can be obtained by using the relaxation time approach,

$$\mathcal{C}[f](t, \vec{q}, \vec{p}) = \frac{f(t, \vec{q}, \vec{p}) - f_{\mathrm{leq}}(t, \vec{q}, \vec{p})}{\tau}, \tag{1.9}$$

where f_{leq} is a local equilibrium distribution, which solves the collisionless Boltzmann equation, that the system approaches on the time scale τ.

1.1.2 Free streaming

An important special case is the one in which the collision terms vanish. This is most commonly the case when the system in question becomes so dilute that interactions between the particles can reasonably be neglected. In that case the Boltzmann equation in the absence of external forces becomes

$$\partial_t f + \frac{p}{m} \cdot \nabla f = 0. \tag{1.10}$$

This is in general solved by

$$f(t, x, p) = f_0\left(x - \frac{p}{m}t, p\right), \tag{1.11}$$

for some initial phase space distribution $f_0 = f(t = 0)$. This behavior is called free streaming. If we were to translate this back into a description of individual particles, it would mean that every particle moves with a constant velocity since there are no collisions which could redistribute momenta. In particular, this contains the conservation of momentum expectation values, since the time dependence can be integrated out.

1.1.3 Fluid dynamics as a special case of kinetic theory

The step towards fluid dynamics from this point is not very large. The quantities that we are interested in are formulated much in the language of equilibrium thermodynamics. When in equilibrium we have a constant particle number N and energy E in a fixed volume V. In fluid dynamics we promote these global variables to local ones. We consider volume densities of extensive variables, like number, entropy and energy density, while intensive properties, like pressure and temperature, remain. This contains the assumption that the concepts that we know from equilibrium still carry meaning. Usually, this is considered acceptable as long as deviations from the equilibrium within a neighborhood of any point are sufficiently small. A system that fulfills this criterion is said to be in local thermodynamic equilibrium.

Fluid dynamic variables can be expressed as momentum space expectation values of the phase space distribution. The two main ones we are going to discuss are the local fluid density $\rho(t, \vec{x})$ and the local fluid velocity $\vec{u}(t, \vec{x})$. The fluid velocity is not directly related to an equilibrium variable, but instead quantifies the local motion, and thus departure from global equilibrium, of an infinitesimal volume of matter. The local density and velocity are defined as

$$
\begin{aligned}
\rho(t, \vec{x}) &= \int m f(t, \vec{x}, \vec{p}) \, \mathrm{d}^3 p \;, \\
\vec{u}(t, \vec{x}) &= \frac{1}{\rho(t, \vec{x})} \int \vec{p} f(t, \vec{x}, \vec{p}) \, \mathrm{d}^3 p \;.
\end{aligned}
\tag{1.12}
$$

If the scattering processes between particles are reversible, the momentum integral of the collision kernel vanishes and we can formulate the continuity equation directly as a consequence of the Boltzmann equation,

$$
\partial_t \rho + \vec{\nabla} \cdot (\rho \vec{u}) = 0 \,.
\tag{1.13}
$$

We can do a similar thing for the fluid velocity by first multiplying with the momentum vector and subsequent integration,

$$
\begin{aligned}
\partial_t (\rho \vec{u}) + \vec{\nabla} \cdot \underline{T} - \rho \nabla V^{(ext)} &= \int \vec{p} \, \mathcal{C}[f] \, \mathrm{d}^3 p \;, \\
T_{ij} &:= \int \frac{p_i p_j}{m} f \, \mathrm{d}^3 p \;.
\end{aligned}
\tag{1.14}
$$

The right-hand-side of equation (1.14) vanishes if we demand momentum conservation. The object T_{ij} is the momentum flux density tensor, or stress tensor, and at this point

still a dynamical quantity. Its equation of motion would depend on the third order moment of the phase space distribution. Such a hierarchy again arises since only the set of all moments fully encodes the information of the full phase space distribution. The fluid velocity equation is commonly simplified by replacing the momentum flux density by

$$T_{ij} = \rho u_i u_j + \mathcal{T}_{ij} \,, \tag{1.15}$$

with the tensor $\mathcal{T}$ which transforms as a scalar under Galilean boosts. With this, we come to the better known form (neglecting external forces)

$$\rho(\partial_t + \vec{u} \cdot \vec{\nabla})\vec{u} + \vec{\nabla} \cdot \underline{\mathcal{T}} = 0 \,. \tag{1.16}$$

In order to arrive at a closed set of equations, a truncation is chosen. A very common choice is to assume that the stress tensor consists only of a pressure contribution, which leads to the Euler equation,

$$
\begin{aligned}
T_{ij} &= \rho u_i u_j + P\delta_{ij} \,, \\
\rho(\partial_t + \vec{u} \cdot \vec{\nabla})\vec{u} + \vec{\nabla}P &= 0 \,.
\end{aligned}
\tag{1.17}
$$

This and the continuity equation do not form a closed set of equations yet since the pressure P is not fixed. For that, one usually uses a thermodynamic equation of state appropriate to the system in question and expresses the pressure as some function of the density. The choice of stress tensor (1.17) is also motivated by the fact that it is the lowest order expansion in derivatives of velocity with the correct symmetries and index structure. Notably, such an approximation of the full dynamic momentum flux density tensor does not necessarily converge, although it can be very robust in some specific cases [35]. In general, it can only serve as an asymptotic series in the case of small gradients in velocity. The next higher order in derivatives introduces dissipative terms that are associated with bulk (ζ) and shear viscosity (η). Including these effects leads to the Navier-Stokes equation for fluid velocity (neglecting external forces for simplicity),

$$
\begin{aligned}
T_{ij} &= \rho u_i u_j + P\delta_{ij} - \zeta(\vec{\nabla} \cdot \vec{u})\delta_{ij} - \eta\sigma_{ij} \,, \\
\sigma_{ij} &= \partial_i u_j + \partial_j u_i - \frac{2}{3}(\vec{\nabla} \cdot \vec{u})\delta_{ij} \,, \\
\rho(\partial_t + \vec{u} \cdot \vec{\nabla})\vec{u} + \vec{\nabla}P - \eta\Delta\vec{u} - \left(\zeta + \frac{\eta}{3}\right)\vec{\nabla}(\vec{\nabla} \cdot \vec{u}) &= 0 \,.
\end{aligned}
\tag{1.18}
$$

Like the pressure, the viscosities cannot be obtained from within the framework of fluid dynamics, but instead have to be supplied externally.

The last central fluid dynamic quantity is the local energy density e. It encodes the kinetic energy of the particles,

$$e(t, \vec{x}) := \int \frac{\vec{p}^2}{2m} f(t, \vec{x}, \vec{p}) \, \mathrm{d}^3 p = \sum_i T_{ii}(t, \vec{x}) \,. \tag{1.19}$$

As before, we can use the Boltzmann equation and the conservation of kinetic energy in collisions to find the evolution of this quantity,

$$\partial_t e + \vec{\nabla} \cdot (e\vec{u}) + \vec{\nabla} \cdot (\mathcal{T}\vec{u}) + \vec{\nabla} \cdot \vec{q} = 0$$

$$q_i = \frac{1}{2m^2} \int (p_i - mu_i)(\vec{p} - m\vec{u})^2 f \, \mathrm{d}^3 p \ . \tag{1.20}$$

This introduces the heat flux $\vec{q}$ as a third order momentum moment of the phase space distribution. Its dynamics depends again on a combination of higher order moments. We can expand the heat flux as

$$\vec{q} = -\kappa \vec{\nabla} T \ , \tag{1.21}$$

introducing the heat conductivity κ as a new transport coefficient and expressing the temperature in terms of the fluid dynamic variables e and ρ by using the thermodynamic equation of state. As this ansatz contains a gradient, it is part of the same derivative expansion as the stress tensor. At zeroth order, neglecting dissipative processes altogether, it makes sense to also neglect any dissipation of heat, hence the heat flux vanishes. In relativistic hydrodynamics the connection between viscosities and heat flux becomes even more apparent since the latter can be added to the relativistic energy momentum tensor in a manner consistent with the equations [5].

We end up with five equations, the continuity equation, the three components of the velocity equation and the energy equation, for $2 + 2d + (d^2 + d)/2 = 14$ unknowns $(\rho, \vec{u}, e, \underline{T}, \vec{q})$. In a relativistic setting this series of equations for the momentum moments of the phase space distribution can be closed at any finite order for specific collision kernels [36]. In our non-relativistic context we eliminate the 9 degrees of freedom associated with the momentum flux density and the heat flux by making a derivative expansion. This, however, adds four more unknown quantities in the pressure P and the transport coefficients η, ζ and κ. The pressure is fixed by the thermodynamic equation of state while the expressions for the transport coefficients have to be obtained from a deeper understanding of the microscopic theory, through e.g. linear response theory in section 3.2). This leaves us with the five fluid dynamic variables and their associated equations.

1.1.4 Assumptions of this ansatz

In summary, the kinetic theory approach to fluid dynamics makes several assumptions. These can be grouped as the ones needed for the basic applicability of kinetic theory and the ones made within the fluid dynamic context. Among the latter the assumption of the symmetries of the scattering process are fairly restrictive in terms of the symmetries they imply, but also fairly generic in that they are applicable to a wide range of underlying microscopic theories. The assumptions about the form of the energy momentum tensor are based on the derivative expansion. This necessitates some properties of the macroscopic situation that fluid dynamics might be applied to. Specifically, it asks that the spatial gradients in fluid velocity as well as the expansion coefficients are small. Since the viscosities are dimensionful expansion parameters,

their smallness can only be formulated in relation to other quantities. The ratio of shear viscosity to entropy density η/s is conjectured and in some cases proven to be bounded from below [37]. This allows it to function as an indicator of the "ideal-ness" of fluids. The closer a fluid is to saturating the boundary, the better the ideal fluid approximation should work. The smallness of gradients is also important for the presence of local thermal equilibrium.

On the side of the assumptions necessary for the standard formulation of kinetic theory, the more relevant one is the molecular chaos hypothesis. Neglecting the corre-lation of two particles after a collision can be justified if there is no observer particle which would interact with both and thus probe their correlation. In other words, a dilute system, in which particles spend most of their time flying freely and only very little scattering with others, is favored when it comes to molecular chaos. It also favors systems which have a large total number of particles where correlations are spread out far and hence less relevant. This is also in line with the assumption that statistical methods are applicable.

1.1.5 Scales in fluid dynamics

For the validity of the kinetic theory ansatz multiple quantities are demanded to be "small" or "large". For dimensionless quantities like the total particle number that is not necessarily consistently defined, but is mostly a matter of convention independent of the choice of units. For dimensionful quantities, however, there needs to be some point of reference in order for these statements to have any meaning. This effectively transforms the statements into ones about dimensionless quantities again. In this section, I will introduce the common scales used in fluid dynamics and express the conditions from the previous section as statements about dimensionless combinations.

In order to identify scales in our system, we first need to look at the system itself. While in theory a fluid system can be arbitrarily large, in practice any realization will have a finite size which we associate with a length scale L. The first internal scale we introduce is the typical interparticle distance

$$d_n = \left(\frac{\rho}{m}\right)^{-1/3} . \tag{1.22}$$

In a system with only short range forces between the particles, the interparticle dis-tance is the lower limit for any length scales that involve effects between particles. The most well-known of those is the mean free path,

$$\lambda_{\mathrm{mfp}} = \frac{m}{\sigma\rho} , \tag{1.23}$$

which is defined as the average length that a test particle can move in a given density between two scatterings in a system with scattering cross section σ. With this we can construct the Knudsen number,

$$\mathrm{Kn} = \frac{\lambda_{\mathrm{mfp}}}{L} , \tag{1.24}$$

which is a dimensionless quantity that scales inversely with the average number of collisions that a particle undergoes when moving across the entire system. If the Knudsen number is large the particles will barely scatter at all and the system is effectively free streaming. On the other hand, a small value implies many scatterings which bring the system closer to the local equilibrium that favors a fluid description. In that sense, the Knudsen number quantifies how much a system deviates from strongly interacting fluid dynamics towards free streaming.

If we are in the fluid regime, we can find a typical fluid velocity v of the system. It can be compared to the speed of sound c_s that is determined by the thermodynamic equation of state as $c_s^2 = \partial p / \partial \rho |_{s/n}$. This leads to the Mach number,

$$\mathrm{Ma} = v/c_s \,, \tag{1.25}$$

which quantifies the compressibility of the fluid in question. Lastly, in order to quantify the importance of viscous corrections, we put their contribution to the momentum flux density ($\sim \eta v/L$) in relation to that of the kinetic energy term ($\sim \rho v^2$) in form of the Reynolds number,

$$\mathrm{Re} = \frac{\rho v L}{\eta} \,. \tag{1.26}$$

Taking into account that bulk viscous corrections depend on the compressibility of the system, the derivative expansion can be considered to be controlled by $\mathrm{Ma}^2 \mathrm{Re}^{-1}$ [38, 39]. The smaller this parameter is, the smaller the influence of the derivative corrections to the stress tensor. It can be argued that in some cases this expansion is equivalent to one for small Knudsen number [40]. However, all these dimensionless scales rely on a microscopic picture of colliding particles and might thus not be applicable to non-collisional fluid dynamics.

1.2 Derivation from conservation principles

For situations involving fluids in which kinetic theory also naturally applies, the ansatz described above is a great choice as it allows treating objects like the stress tensor or the heat flux as dynamical if one wants to make the truncation at a later point. However, experiments observe fluid dynamic behavior in systems like ultracold helium [41, 42] which do not have a clear underlying picture of colliding particles. This implies that fluid dynamics can be applied outside the range of applicability of kinetic theory and not just to a subset of it. In this section, I will look into a different ansatz to derive the same equations of motions for the hydrodynamic variables based on a different set of assumptions, following along the lines of [5].

Since we want to arrive at equations for the same fluid dynamic variables, we again assume that the system we want to describe is in local thermal equilibrium. In order to find equations of motion, this time we make use of the global version of the conservation laws we applied to the individual collisions in the previous section. The conserved quantities we are considering are the total mass, momentum and energy of the system.

In terms of the microscopic Hamiltonian, the latter two correspond to global symmetries with respect to translations in both space and time. The conservation of mass and, without particles decaying or combining, equivalently particle number is less easy to pin to a specific symmetry. In quantum mechanics it corresponds to the hermiticity of the Hamilton operator while in a quantum field theory of a complex scalar field it is the result of a global $U(1)$ symmetry. For each of the conserved quantities we can define a corresponding density $(\rho_m, \vec{\rho}_p, \rho_e)$ and claim that the time derivative of the spatial integral over each of these quantities vanishes, e.g.

$$\partial_t \int_{\mathbb{R}^3} \mathrm{d}^3x \, \rho_m = \partial_t m_{\mathrm{tot}} = 0 \,. \tag{1.27}$$

With no possibility of creating new mass, and motion of mass being continuous, one can argue that any change of total mass within a finite volume can only come from matter flowing across the boundary of said volume,

$$\int_V \mathrm{d}^3x \, \partial_t \rho_m + \int_{\partial V} \mathrm{d}\vec{A} \cdot \vec{J}_m = 0 \,. \tag{1.28}$$

We can make similar arguments for energy and momentum to find a vector and a (0,2)-tensor field $\underline{J}_p, \vec{J}_e$, which we will call flux densities, that fulfill an equation of the same type. As opposed to mass, however, it is possible to violate conservation of total momentum in a finite volume by means of forces exerted by sources outside the volume. We summarize these as an external force density $\vec{f}_{\mathrm{ext}}$ that, when integrated over a finite volume, gives the sum of all external forces acting on a that volume. These statements hold for an arbitrarily chosen connected volume. Taking all this into consideration and making use of Gauss' law, we can reformulate the conservation laws in a differential form,

$$\begin{aligned}
\partial_t \rho_m + \vec{\nabla} \cdot \vec{J}_m &= 0 \,, \\
\partial_t \vec{\rho}_p + \vec{\nabla} \cdot \underline{J}_p &= \vec{f}_{\mathrm{ext}} \,, \\
\partial_t \rho_e + \vec{\nabla} \cdot \vec{J}_e &= 0 \,.
\end{aligned} \tag{1.29}$$

For simplicity, we will neglect external forces in the following. What remains is to identify the densities and flux densities with the local thermodynamic variables. For the mass density that is easily done as the product of the thermodynamic particle number density n and the single particle mass m. For the momentum density and the mass flux density one can argue by the momentum flux's behavior under Galilean boosts that they must be identical. Momentum determines the change of position of any masses and thus their flow. We can introduce the local fluid velocity to formulate this as a hydrodynamic variable,

$$\vec{\rho}_p = \vec{J}_m =: \rho \vec{u} \,. \tag{1.30}$$

This allows us to express the first equation of (1.29) in the well-known form of the continuity equation,

$$\partial_t \rho + \vec{\nabla} \cdot (\rho \vec{u}) = 0 \,. \tag{1.31}$$

The next object to identify is the momentum flux density. While from our intuition from kinetic theory this should be the momentum flux density tensor as defined in (1.14), this is not immediately clear just from conservation laws. The specific form of the stress tensor in the previous section was, however, only an expansion of some a priori independent dynamic variable in a series of derivatives of the fluid velocity. Under the same assumptions about the smallness of gradients we can identify terms in the same way as before. The difference is that we have no link to a momentum space expectation value. Therefore, we will also call the momentum flux density a stress tensor and use the same symbol T_{ij} because as long as it is not considered an independent dynamic variable it is defined via the same terms. This also carries the implication that the momentum flux density is symmetric in its two indices. In kinetic theory that directly follows from the definition. In this framework that property is guaranteed if the system in question is rotationally invariant, i.e. there are no internal torques. For convenience of notation we again split $T_{ij} = \rho u_i u_j + \mathcal{T}_{ij}$. This, in combination with the continuity equation (1.31), allows us to write

$$\rho(\partial_t + \vec{u} \cdot \vec{\nabla})\vec{u} + \vec{\nabla} \cdot \mathcal{T} = 0 \, . \tag{1.32}$$

We can again obtain the Euler and Navier-Stokes equations for the corresponding choices of the stress tensor. As for the energy equation, the energy density is just a quantity that we will continue to use within the fluid dynamic framework as $e = \rho_e$. Energy flowing into a volume can come from multiple sources. The first is particles physically moving across the boundary, carrying both energy itself and interacting with the particles already in the volume. From a thermodynamic perspective this can be viewed as a particle moving against pre-existing pressure, performing work to enter the volume. In addition, work can also be done by particles moving along the surface of the volume exerting shear forces on it. Another contribution is random scattering processes at the boundary which transport energy into the volume without net particle motion. This part is what we associate with the thermodynamic concept of heat which we will add as a heat flux $\vec{q}$. Including these aspects, the total energy flux density takes the form

$$(J_e)_i = (e\delta_{ij} + \mathcal{T}_{ij})u_j + q_i \, . \tag{1.33}$$

This lets us write down the energy equation of fluid dynamics,

$$\partial_t e + \vec{\nabla} \cdot (e\vec{u}) + \vec{\nabla} \cdot (\mathcal{T}\vec{u}) + \vec{\nabla} \cdot \vec{q} = 0 \, . \tag{1.34}$$

However, the heat flux remains undefined in this approach. It needs to be determined by additional assumptions in the same way that the truncation of the stress tensor is decided in a way appropriate to the problem at hand. We can use the same approximation as before in equation (1.21) reintroducing the heat conductivity. In this way, we end up with the same 5 equations and 14 unknowns as we should. This is reduced to the 5 fluid dynamic variables and equations by the derivative expansion complemented by three transport coefficients and one thermodynamic equation of state.

1.2.1 Assumptions of the ansatz

The difference in getting to the equations of fluid dynamics compared to the previous ansatz is mostly an exchange of microscopic and macroscopic assumptions. We no longer require the molecular chaos hypothesis or make statements about conserved quantities in individual particle collisions. Instead we demand macroscopic conservation laws for mass, momentum, energy and angular momentum to be in place. In their differential form these formulate relations between densities and fluxes. The former are identified with the thermodynamic variables. The identification between mass flux and momentum density is fixed by symmetry. However, both momentum and energy flux density are introduced as new quantities that are not understood on the microscopic level to the degree that stress tensor and heat flux are by equations (1.14) and (1.20). We associate them with the same derivative expansion in the same transport coefficients, but these are to be understood purely as a macroscopic material properties of the fluid.

With this ansatz we trade assumptions about the underlying microscopic theory against understanding the microscopic implications of the fluid description. But this also allows to be a bit more free in the interpretation of the fluid dynamic variables. Since it follows a similar conservation law, it is possible to formulate a continuity equation for the probability distribution of a quantum-mechanical wave function (see also section 1.5.1). We also still make use of thermodynamic quantities and the derivative expansion and are thus reliant on the assumption of local thermal equilibrium. There is, however, evidence that suggests close to fluidlike behavior of systems for which local equilibrium is very unlikely to be reached [13].

1.3 Lagrange coordinates

Finding a simple solution to a physical problem often requires using a suitable set of coordinates for its description. In fluid dynamics one such choice that is commonly used in numerical calculations in e.g. biophysics [43] are the Lagrange coordinates, discussed here roughly following [44, 45]. Their basic idea is to describe a trajectory for every infinitesimally small fluid parcel in order to encode the motion of the entire fluid. In that sense it can be called a comoving coordinate system. This corresponds to a non-linear change in coordinates. The central object of that description is the quantity $\vec{r}(t, \vec{R})$ that determines the position of the fluid parcel at some time t that was at position $\vec{R}$ at a fixed initial time t_0. By this definition, we can connect the parcel position to the local fluid velocity via its time derivative,

$$\vec{u}(t, \vec{r}(t, \vec{R})) = \partial_t \vec{r}(t, \vec{R}) \,. \tag{1.35}$$

For the density we simply replace its spatial dependence by one on the parcel position. This allows us to write

$$(\partial_t + \vec{u} \cdot \vec{\nabla})\rho(t, \vec{r}) = \frac{\mathrm{d}}{\mathrm{d}t}\rho(t, \vec{r}(t, \vec{R})) \,. \tag{1.36}$$

14

The last ingredient that we need in order to rewrite the continuity and Euler equations is the divergence of the fluid velocity,

$$\vec{\nabla} \cdot \vec{u}(t, \vec{r}) = \frac{\partial}{\partial r_k} \frac{\partial}{\partial t} r_k(t, \vec{R}) = \left[\frac{\partial}{\partial r_k} R_j(t, \vec{r}) \right] \frac{\partial}{\partial t} \frac{\partial}{\partial R_j} r_k(t, \vec{R}) \,. \tag{1.37}$$

For shortness of notation we introduce symbols for the Jacobi matrix, its inverse and its determinant,

$$\begin{aligned} J_{jk}(t, \vec{R}) &= \frac{\partial}{\partial R_j} r_k(t, \vec{R}) \\ I_{kj}(t, \vec{r}) &= \frac{\partial}{\partial r_k} R_j(t, \vec{r}) \\ J(t, \vec{R}) &= \det(J_{jk}(t, \vec{R})) \,. \end{aligned} \tag{1.38}$$

With this and the Jacobi identity, we can write

$$\vec{\nabla} \cdot \vec{u}(t, \vec{r}) = I_{kj}(t, \vec{r}) \frac{\partial}{\partial t} J_{jk}(t, \vec{R}) = \frac{1}{J(t, \vec{R})} \partial_t J(t, \vec{R}) \,. \tag{1.39}$$

The continuity equation (1.31) takes the form

$$\frac{\mathrm{d}}{\mathrm{d}t} \rho(t, \vec{r}(t, \vec{R})) + \frac{\rho(t, \vec{r}(t, \vec{R}))}{J(t, \vec{R})} \frac{\mathrm{d}}{\mathrm{d}t} J(t, \vec{R}) = 0 \,, \tag{1.40}$$

which can be reformulated as

$$\frac{\mathrm{d}}{\mathrm{d}t} \ln[\rho(t, \vec{r}(t, \vec{R})) J(t, \vec{R})] = 0 \,. \tag{1.41}$$

Considering that at initial time the fluid parcel has not had any opportunity to move, i.e. $\vec{r}(t, \vec{R}) = \vec{R}$ and hence $J(t_0, \vec{R}) = 1$, we can express the density at any point in time as a rescaling of the initial density,

$$\rho(t, \vec{r}(t, \vec{R})) = \frac{\rho(t_0, \vec{R})}{J(t, \vec{R})} \,. \tag{1.42}$$

Thus the density is completely determined by its initial configuration and the Jacobian of the change of coordinates. That Jacobian and the fluid velocity are themselves fully determined by the exact form of the parcel position. The dynamics of the fluid parcels are governed by the equivalent to the velocity equation. In this discussion, we choose to neglect the energy equation and dissipative effects. The Euler equation can then be formulated as a differential equation of the parcel position,

$$\rho(t, \vec{r}) \frac{\mathrm{d}^2}{\mathrm{d}t^2} r_k(t, \vec{R}) + \frac{\partial}{\partial r_k} P(t, \vec{r}) = 0 \,. \tag{1.43}$$

The derivative with respect to r_k can again be rewritten as a combination of inverse Jacobi matrix and initial parcel position derivative. On top of that, we replace the pressure by the chemical potential μ by using $n = \partial P / \partial \mu$. This leaves us with

$$J_{jk}(t, \vec{R}) \frac{\mathrm{d}^2}{\mathrm{d}t^2} r_k(t, \vec{R}) + \frac{1}{m} \frac{\partial}{\partial R_j} \mu(t, \vec{r}(t, \vec{R})) = 0 \,. \qquad (1.44)$$

The initial conditions are given by

$$\begin{aligned}
\vec{r}(t_0, \vec{R}) &= \vec{R} \,, \\
\frac{\mathrm{d}}{\mathrm{d}t} \vec{r}(t_0, \vec{R}) &= \vec{u}(t_0, \vec{R}) \,.
\end{aligned} \qquad (1.45)$$

The equation of state relates μ to the density which closes the equations in a way whose time dependence is given by the transformation Jacobian.

Formulating expectation values in Lagrange coordinates shows another advantage of the comoving picture. The time evolution of the density scales with the inverse transformation Jacobian. This lets us change the integration variable from the current parcel position to the initial one in order to absorb that time dependence. As long as we can express the current parcel position in terms its initial value, we can therefore formulate every spatial expectation value with respect to the initial density,

$$\begin{aligned}
\langle f(\vec{x}) \rangle_{\rho(t,\vec{x})} &= \frac{1}{m_{\mathrm{tot}}} \int \mathrm{d}^d r \, f(\vec{r}) \rho(t, \vec{r}) = \frac{1}{m_{\mathrm{tot}}} \int \mathrm{d}^d r \, f(\vec{r}) \frac{\rho(t_0, \vec{R}(t, \vec{r}))}{J(t, \vec{R}(t, \vec{r}))} \\
&= \frac{1}{m_{\mathrm{tot}}} \int \mathrm{d}^d R \, f(\vec{r}(t, \vec{R})) \rho(t_0, \vec{R}) = \left\langle f(\vec{r}(t, \vec{R})) \right\rangle_{\rho(t_0, \vec{R})} \,.
\end{aligned} \qquad (1.46)$$

The time dependence of the expectation value is entirely contained in the transformation.

The main differences to the standard formulation of hydrodynamics are that the dynamics are entirely contained in the Euler equation (1.44) and that the initial density configuration explicitly enters the equations. In some special cases (see section 2.2.2) one can argue that the partial differential equation reduces to an ordinary one due to properties of the equation of state and the initial conditions. This makes the dynamics much easier to solve in the Lagrangian formulation than the standard Eulerian one that can only indirectly make use of symmetries in its initial density.

1.4 Fluid dynamics in heavy ion collisions

An important point in the history of collider experiments is the discovery of fluidlike behavior in high-energy collisions between heavy nuclei [7]. In this section I will shortly summarize the role and indicators of fluid dynamics in these collisions and lead to the central question of the lower particle number limit of these descriptions. More detailed discussions of fluid dynamics in collisional systems can be found in [38, 46] which this section is in part based on.

In the course of a collision of heavy ions, shortly after the atoms hit each other, their constituents form a quark gluon plasma (QGP). While this state of matter is a strongly interacting phenomenon, it is not immediately clear whether it also behaves fluidlike at least during a part of its expansion. In order to determine whether the fluid description is viable, one can make use of a qualitative feature of fluid dynamics. In the absence of external forces, the local velocities of the fluid system are mostly driven by pressure gradient forces. Assuming that the equation of state of the system is such that the pressure increases with increasing density, this means that matter is pushed away from dense clumps with an acceleration proportional to the gradient in density. Specifically, for a fluid with an elliptic density profile and no or isotropic initial fluid velocity that means that acceleration will be larger in the more strongly squeezed direction. At later times at which we assume interactions between the constituents of the fluid to be sparse, the shape of the fluid density will be fully determined by its widths in momentum space. Therefore, for any fluid with a strictly monotonously increasing equation of state, any initial elliptic shape will invert in the course of a free expansion. This anisotropy in the final state can be used as an indicator of collective flow as pointed out in the context of heavy-ion collisions by Ollitrault [10]. It can be put into a quantitative variable by identifying it as the second order term of a Fourier decomposition of the distribution in momentum space angles [8, 9]. It is usually labeled V_2 and in two dimensions, e.g. a reaction plane, defined as

$$V_2 = \int \mathrm{d}^2 p \, f(\vec{p}) e^{2i\phi_p} , \qquad (1.47)$$

where ϕ_p is the polar angle in momentum space and $f(\vec{p})$ is the observed distribution of particles in momentum space normalized to one. In the case of a heavy ion collision the latter reduces to an angular distribution of detected particles,

$$V_2 = \frac{1}{2\pi N} \int_0^{2\pi} \mathrm{d}\phi_p \frac{\mathrm{d}N}{\mathrm{d}\phi_p} e^{2i\phi_p} . \qquad (1.48)$$

The resulting complex Fourier factor can be decomposed into a magnitude $v_2 = |V_2|$ and an angle $\Phi_2 = \arg(V_2)$. The variable v_2 determines the ellipticity of the shape in momentum space and will be called elliptic flow from here on. The angular degree of freedom Φ_2 contains information about the orientation of the ellipse. For a system of non-interacting expanding particles the cloud shape becomes circular in the long time limit and the elliptic flow vanishes. As such the magnitude of the elliptic flow indicates how much the system differs from a non-interacting one. This has to be put into perspective with respect to the initial cloud shape. The more spatially anisotropic the fluid is initially, the larger will v_2 be in general. In order to account for this, one can introduce a measure for the spatial anisotropy via the normalized quadrupole moment of the spatial density [47],

$$\mathcal{E}_2 = -\frac{\int \mathrm{d}^2 x \, n(\vec{x}) |\vec{x}|^2 e^{2i\phi_x}}{\int \mathrm{d}^2 x \, n(\vec{x}) |\vec{x}|^2} , \qquad (1.49)$$

17

where n is the energy density which in a non-relativistic setting becomes the particle number density. This quantity can again be decomposed into what we will simply call the spatial ellipticity $\varepsilon_2 = |\mathcal{E}_2|$ and the angular information about the orientation of the cloud shape $\Psi_2 = \arg(\mathcal{E}_2)$.

Neglecting the orientation of the shapes, the natural choice for a quantity that might be comparable across different geometries is therefore v_2/ε_2. Using this ratio as an identifying feature of fluidlike behavior has many advantages. It is observable in convergent asymptotic behavior which makes it resilient to uncertainties in the time of the measurement, it is comparable between different initial geometries and it has few requirements to the equation of state. It does, however, also require knowledge of the initial state to some degree. In order to determine whether a shape inversion has occurred, one needs to have some information about the initial shape of the potential fluid. In general, this is not possible for high energy collisions. There are successful models to generate initial conditions for the fluid part of the expansion dynamics like T_{R}ENTo [48], but the impact parameter of any single collision is still random. This means that it is not possible to gain information by calculating v_2 as an average over all shots since it would vanish due to symmetry. This problem can be avoided by using correlations between the momenta of different final state particles within a single event [8] and calculating a quantity similar to the elliptic flow from e.g. a two-particle distribution function in momentum space,

$$v_2\{2\} = \left\langle \langle \cos(2(\phi_{p,1} - \phi_{p,2})) \rangle_{f_2(\phi_{p,1},\phi_{p,2})} \right\rangle_{\mathrm{events}} . \tag{1.50}$$

This concept can be generalized to N-particle correlations giving access to $v_2\{N\}$. Measurements of these observables can be performed for different types of collisions. In recent years, investigations of proton-proton (p-p) and proton-lead (p-Pb) collisions have gained interest since the elliptic flow generated in these small systems is comparable to that found in the collision of much heavier nuclei, like lead-lead (Pb-Pb) collisions, at the same multiplicity [11, 12, 14]. Notably, this stays true in the low multiplicity regime ($N_{\mathrm{ch}} < 100$). It is well-established that QGPs from Pb-Pb collisions can be reasonably treated as fluids. This tells us two things. First, the good agreement between the different collisions confirms that the observable $v_2\{2\}$ as an indicator is robust to changes in the underlying system. Second, the agreement with the p-p collisions in the low multiplicity regime implies that the small system shows very similar behavior to the heavier ones and is therefore at least in contention for fluidlike behavior. This is especially curious since the proton-proton system seemingly violates two of the basic requirements postulated earlier. Even down to a multiplicity of $\sim 20 - 30$ the hydrodynamic features seem to remain. Assuming that the effective number of particles in the fluid phase of the QGP is on the same order of magnitude as the final state leaves us with about fifty particles at the most. The smallness of this number calls into question whether a description in terms of local thermodynamic variables is viable. There are also good arguments that it is not possible to attain local equilibrium in these small systems since the time scales required for that are too long [13].

While using multiparticle correlations solves the problem of the unknown orientation of the impact parameter, it also introduces new issues. Final state particles that originate from the same decay process have inherently correlated momenta. This does not require any fluidlike behavior to be present in the system and introduces therefore systematic uncertainties to the elliptic flow. There are also other potential ways to build up these correlations without fluid dynamics [49]. The entirety of these contributions is commonly referred to as non-flow effects and introduces uncertainty to the measurements. The signal-to-noise ratio can be improved by using combinations of Fourier coefficients obtained from different orders of correlations [50], but still decreases with decreasing number of final state particles detected in a collision. This makes it very hard to obtain precise information about low-multiplicity events and by that a more robust understanding of smaller systems like proton-proton collisions. Therefore, in order to learn more about the applicability of fluid dynamics in very small systems, we cannot make use of the multiparticle correlations alone. This means we have to move the problem to a different experimental setup which allows us to control the initial state of the system so we can use one-particle expectation values.

1.5 Fluid dynamics in cold atomic systems

On the other end of the accessible temperature spectrum, 17 orders of magnitude lower [32, 51], one finds systems comprised of trapped cold atoms. In this section I will introduce the basic concepts of these systems that make them a good candidate for studying the limits of fluid dynamics.

1.5.1 Superfluidity

A system of bosonic atoms at sufficiently low temperatures and high densities will undergo Bose-Einstein condensation [52–54]. The ground state is macroscopically occupied and the dynamics of the system are mostly determined by an effective macroscopic wave function Ψ, called order parameter, and small perturbations on top of it. We neglect the perturbations for now and focus on the dynamics of the bulk of the Bose-Einstein condensate (BEC). In a BEC with interaction strength g in an external potential V_{ext} the dynamics of the order parameter can be described by the Gross-Pitaevskii equation [6],

$$i\partial_t \Psi = -\frac{\nabla^2}{2m}\Psi + V_{\text{ext}}\Psi + g|\Psi|^2\Psi\,. \tag{1.51}$$

This non-linear Schrödinger type equation is the result of treating the bulk of the field operator as a classical field and only considering the perturbations as an operator, $\hat{\Psi} = \Psi + \delta\hat{\Psi}$. This treatment can be justified by the aforementioned macroscopic ground state occupation [6]. We can split the order parameter into its absolute value and its complex phase and identify the former with the square root of the particle number density,

$$\Psi(t,x) = \sqrt{n(t,x)}e^{iS(t,x)}\,. \tag{1.52}$$

We can further identify the gradient of the phase with a velocity

$$\vec{u}(t, x) = \frac{1}{m}\vec{\nabla}S(t, x)\,.$$

(1.53)

In terms of the new variables the Gross-Pitaevskii equation takes the form

$$\partial_t n + \vec{\nabla}\cdot(n\vec{u}) = 0\,,$$

$$(\partial_t + \vec{u}\cdot\vec{\nabla})\vec{u} + \vec{\nabla}\left(V_{\text{ext}} + gn^2 - \frac{1}{m^2}\frac{\vec{\nabla}^2\sqrt{n}}{\sqrt{n}}\right) = 0\,,$$

(1.54)

which resemble the continuity and Euler equation. The acceleration in this system consists of three contributions: the external forces, the pressure term from interactions and a pressure term dependent on density gradients which we will call quantum pressure. The quantum pressure is often neglected under the assumption that it is of higher order in gradients which are assumed to be small. Notably, this is a case of inviscous and, up to quantised vortices, irrotational fluid dynamics. These are both defining features of superfluidity at zero temperature. Such behavior, however, is not limited to BECs and was originally discovered in helium [41, 42]. The theory of superfluidity was formulated by Landau in 1941 [55]. This description encompasses two additional key features. At finite temperatures the system can be described as a mixture of a superfluid and a normal one. The fraction of superfluid density decreases with increasing temperature down to zero at the critical temperature. The second feature is that superfluidity also breaks down if relative velocities become too large. If the relative velocity between the fluid and the boundary it flows along, e.g. a capillary, crosses a critical velocity v_c, this can create excitations which destabilize the superfluid behavior. This is usually formulated in terms of the Landau criterion,

$$v < v_c = \min\frac{\varepsilon(\vec{p})}{|\vec{p}|}\,,$$

(1.55)

where $\varepsilon(\vec{p})$ is the dispersion relation of the excitations [6]. Reintroducing the perturbations up to linear order into the Gross-Pitaevskii equation one finds the Bogoliubov dispersion law [6],

$$\varepsilon(\vec{p}) = \sqrt{\frac{\vec{p}^2}{2m}\left(\frac{\vec{p}^2}{2m} + 2gn\right)}\,.$$

(1.56)

From this directly follows that the critical velocity $v_c = \sqrt{gn/m}$ depends on the presence of interactions. A non-interacting Bose gas has a vanishing critical velocity and thus cannot form a superfluid in the presence of any motion. This result also tells us that superfluidity can break down if the fluid becomes too dilute, similar to how a classical fluid would tend towards free streaming in the dilute limit.

Notably, condensation and thereby superfluid behavior can also be found in some fermionic systems [56, 57]. The principle is similar to that of the related phenomenon of superconductivity in Bardeen-Cooper-Schriefer (BCS) theory [58]. Interacting fermions can form pairs that behave like effective bosons, allowing them to condense.

1.5.2 Feshbach resonances

The mechanism that allows these fermionic pairs to form at experimentally accessible temperatures is the so-called Feshbach resonance. In order to formulate how the interaction strength can be modified, I will first introduce basic concepts of scattering theory following [59]. In a system of two particles interacting via a potential that only depends on the distance between them, $\vec{r} = \vec{x}_1 - \vec{x}_2$, the quantum-mechanical wave function can be split into two factors. One is a trivial center of mass part, the other encapsulates the relative motion and is a solution of the Schrödinger equation

$$i\partial_t \Psi(t, \vec{r}) = \left(-\frac{\vec{\nabla}_r^2}{2\mu} + V(\vec{r}) \right) \Psi(t, \vec{r}), \tag{1.57}$$

with the reduced mass μ. Far away from the "collision" at $\vec{r} = 0$, we can approximate the incoming particles as a linear combination of the plane wave solutions of the free equation labeled by their momentum $\vec{k}$. The outgoing particles are modeled as a spherical wave modified by an angle dependent scattering amplitude $f(|\vec{k}|, \theta)$. The complete ansatz for the individual momentum modes away from the center of the collision is thus

$$\psi_{\vec{k}}(\vec{r}) \propto e^{i\vec{k}\cdot\vec{r}} + f(|\vec{k}|, \theta)\frac{e^{i|\vec{k}||\vec{r}|}}{|\vec{r}|}. \tag{1.58}$$

If the potential additionally only depends on the magnitude of the relative position and not its orientation, $V = V(|\vec{r}|)$, the angular dependence of the momentum modes can be expressed in terms of Legendre polynomials. In this way, the mode can be decomposed into in- and outgoing spherical waves for the different angular momentum modes where the scattering amplitude just introduces phase shifts δ_l,

$$f(|\vec{k}|, \theta) = \frac{1}{k} \sum_{l=0}^{\infty} (2l+1) e^{i\delta_l(|\vec{k}|)} \sin\left(\delta_l(|\vec{k}|)\right) P_l(\cos(\theta)). \tag{1.59}$$

It can be shown that for short range potentials, as are typical for interactions between neutral atoms, the isotropic part ($l = 0$) of the scattering amplitude dominates for small momenta [60]. The s-wave scattering length a is defined via the low momentum behavior of the isotropic phase shift as

$$a = -\lim_{|\vec{k}|\to 0} \frac{\tan\left(\delta_0(|\vec{k}|)\right)}{|\vec{k}|}, \tag{1.60}$$

and is sufficient to describe all the atomic scattering processes at near zero temperature we are interested in.

Following the discussion in [15], we will consider two scattering lithium atoms (^{6}Li) in their atomic ground states, meaning no angular momentum from the unpaired electron orbit ($L = 0$). The interaction potential between them can be estimated using the Born-Oppenheimer approximation. This potential depends strongly on whether the atoms' unpaired electrons are considered in a singlet ($S_{\text{tot}} = 0$) or triplet state

($S_\text{tot} = 1$) in the joint description of the two atoms. Of these two, the singlet state typically has the lower energy at large distances which we will call $E = 0$. The ingoing particles of a collision at low temperatures will have energies only slightly above zero. If the triplet potential has a bound state with energy close to zero, mixing occurs and can cause a phase shift depending on the difference in energy. In the case of ^{6}Li, the difference between triplet bound state and ingoing particle energy can be controlled by an external magnetic field B. The resulting modification of the s-wave scattering length can be expressed as [61]

$$a(B) = a_\text{bg} \left(1 - \frac{\Delta}{B - B_0} \right) , \qquad (1.61)$$

where Δ is the width of the resonance, B_0 the magnetic field at which resonance occurs and a_bg the scattering length off-resonance. This is a magnetic Feshbach resonance. The parameters in (1.61) differ depending on the hyperfine quantum numbers of the atoms participating in the collision. For a given mixture of states, the use of a Feshbach resonance thus makes it possible to tune the scattering length to the value desired in the experiment. This includes both positive and negative scattering lengths, corresponding to attractive and repulsive effective interactions respectively. The atoms can form both tightly bound molecule states for $1/a \gg 0$, which in larger systems can behave like a BEC, and much more loosely bound pairs of BCS type for $1/a \ll 0$. The transition between these two regimes is a smooth crossover (also called the BEC-BCS crossover) through a region of strong interactions [15].

1.5.3 Unitarity and non-relativistic conformal field theory

A special type of behavior of the cold atomic gas is found at exactly the point of resonance, at which the scattering length diverges ($1/|a| \to 0$), also called the unitary limit. This removes an external scale from the system which thereby recovers additional symmetry. In this section I will follow the discussion of Maki and Zhou [62] about properties of the emerging non-relativistic conformal field theory and present results obtained for isotropic expansion and oscillation behavior on that basis. The work discussed in this section was done in cooperation with Nils Becker and Stefan Floerchinger.

We start from a description similar to the Gross-Pitaevskii equation, but adapted for fermion fields,

$$
\begin{aligned}
H(g) = \sum_\sigma \int \mathrm{d}^3x \, \psi_\sigma^\dagger(x) \left(-\frac{\nabla^2}{2m} + V_\text{ext}(x) \right) \psi_\sigma(x) \\
+ g(\Lambda) \sum_{\sigma,\sigma'} \int \mathrm{d}^3x \, \psi_\sigma^\dagger(x)\psi_{\sigma'}^\dagger(x)\psi_{\sigma'}(x)\psi_\sigma(x) ,
\end{aligned}
\qquad (1.62)
$$

where the summations are over all possible spin states and the field ψ_σ obeys a canonical equal time anticommutation relation. For our given problem we choose $V_\text{ext}(x) = 0$ at first. However, the scale invariance of the system can still be broken by a possible

scale dependence in the effective coupling $g(\Lambda)$ (discussed for the two-dimensional case in [63, 64]). The unitary case is only achieved when the interaction strength has a specific value g^* from which it no longer flows away during renormalisation. In a general dimension d this is fulfilled either by the trivial value $g^* = 0$ or by $g^* = 2 - d$ [65]. One can also define operators associated with non-relativistic scale (D) and conformal (C) transformations

$$D = \sum_\sigma \int \mathrm{d}^3x \, \psi_\sigma^\dagger(x) \left(-i\frac{3}{2} + \vec{x} \cdot \vec{p} \right) \psi_\sigma(x) \tag{1.63}$$

$$C = \sum_\sigma \int \mathrm{d}^3x \, \psi_\sigma^\dagger(x) \frac{\vec{x}^2}{2} \psi_\sigma(x) \,. \tag{1.64}$$

These operators form a closed algebra with the scale invariant Hamiltonian $H_s = H(g^*)$

$$\begin{aligned}
[H_s, C] &= -iD \\
[D, H_s] &= 2iH_s \\
[D, C] &= -2iC \,.
\end{aligned} \tag{1.65}$$

On field operators that have been evolving according to H_s,

$$\psi_s(r, t) = e^{iH_s t} \psi_s(r) e^{-iH_s t} \,, \tag{1.66}$$

these operators act as

$$\begin{aligned}
e^{-iD\lambda} \psi_s(r, t) e^{iD\lambda} &= e^{-\lambda\frac{3}{2}} \psi_s \left(r' = re^{-\lambda}, t' = te^{-2\lambda} \right) \\
e^{-iC\lambda} \psi_s(r, t) e^{iC\lambda} &= \frac{1}{(1 - \lambda t)^{\frac{3}{2}}} \exp\left(-i\frac{r^2}{2} \frac{\lambda}{1 - \lambda t} \right) \\
&\qquad \psi_s \left(r' = \frac{r}{1 - \lambda t}, t' = \frac{t}{1 - \lambda t} \right) \,.
\end{aligned} \tag{1.67}$$

These transformations can be embedded into a larger group containing also spatial and time translations, spatial rotations and Galileian boosts, called the Schrödinger group [66]. The Hamiltonian of the fermions at unitarity forms a closed algebra with all of the associated generators (being invariant under the space-time transformations). For a system of harmonically trapped fermions, the external potential term $V_{\mathrm{ext}}(x) = m\omega^2 \vec{x}^2/2$ can also be expressed as the generator of conformal transformations. For simplicity of notation, we choose units such that the trapped Hamiltonian can be written simply as

$$H = H_s + C \,. \tag{1.68}$$

This makes it possible to express the eigenstates of the system as a tower of states labeled with an integer energy quantum number l and a superindex n for all other quantum numbers that determines which tower the state is part of [62],

$$\begin{aligned}
H \left| O_l^n \right\rangle &= E_l^n \left| O_l^n \right\rangle \\
E_l^n &= 2l + E_0^n \,.
\end{aligned} \tag{1.69}$$

We will refer to these as conformal tower states in the following. All states of a tower can be constructed from any one state within the tower using ladder operators $L_\pm$

$$L_\pm = H_s - C \pm iD$$

$$|O_l^n\rangle = \frac{1}{c_l}(L_+)^l |O_0^n\rangle \tag{1.70}$$

$$|c_l|^2 = \prod_{k=1}^{l} \left[k^2 + (E_0^n - 1)k \right] .$$

By formulating the set of operators (H_s, D, C) in terms of (H, L_+, L_-) it is also possible to use this structure for expansion dynamics.

In order to make predictions about the behavior of observables, we formulate the state of the system, following Maki and Zhou [62], via the one-particle density matrix expressed in terms of the tower states. For simplicity, we assume that the system initially is in a pure state, $\rho = |\Psi_0\rangle\langle\Psi_0|$, and do not explicitly write out the spin sums. The one-particle density matrix then decomposes as

$$\begin{aligned} P_1(x_1, x_2, t) &= \langle\Psi_0|\psi^\dagger(x_2, t)\psi(x_1, t)|\Psi_0\rangle \\ &= \langle O_l^n|\Psi_0\rangle \left\langle\Psi_0\middle|O_{l'}^{n'}\right\rangle \left\langle O_{l'}^{n'}\middle|\psi^\dagger(x_2, t)\psi(x_1, t)\middle|O_l^n\right\rangle \\ &=: \Gamma_{l,l'}^{n,n'} \, \rho_{l,l'}^{n,n'}(x_1, x_2, t) \end{aligned} \tag{1.71}$$

where the initial conditions are entirely absorbed into $\Gamma_{l,l'}^{n,n'}$ while the dynamics are entirely contained in $\rho_{l,l'}^{n,n'}$. For the dynamical part, they found

$$\left[(1+t^2)\partial_t + t(\vec{x}_1 \cdot \vec{\nabla}_1 + \vec{x}_2 \cdot \vec{\nabla}_2 + 3) + i\frac{\vec{x}_1^2 - \vec{x}_2^2}{2} - i(E_l^n - E_{l'}^{n'})\right] \rho_{l,l'}^{n,n'}(\vec{x}_1, \vec{x}_2, t) = 0 . \tag{1.72}$$

The observable we are going to focus on is the moment of inertia,

$$I_{ij}(t) = \langle x_i x_j \rangle = \int \mathrm{d}^3x \, x_i x_j P_1(\vec{x}, \vec{x}, t) , \tag{1.73}$$

for which the differential equation (1.72) takes the form

$$\left[(1+t^2) - 2t\right] I_{ij}(t) = i \sum_{l,l',n,n'} (E_l^n - E_{l'}^{n'}) \int \mathrm{d}^3x \, x_i x_j \rho_{l,l'}^{n,n'}(\vec{x}, \vec{x}, t)\Gamma_{l,l'}^{n,n'} . \tag{1.74}$$

While Maki and Zhou continued to work out the late time behavior of this quantity and made perturbative out-of-unitarity, Nils Becker, Stefan Floerchinger, and I solved a special case of this equation exactly.

The assumption we make is that $\Gamma_{l,l'}^{n,n'} \sim \delta^{n,n'}$, which implies no interference between different towers. Accordingly, we will drop the n indices in further calculations. In

order to solve the equations, we split the moment of inertia, similarly to the density matrix, into a static initial and generic dynamical part,

$$I_{ij}(t) = \sum_n \sum_{l,l'} R_{ij}^{n,l,l'}(t) \Gamma_{l,l'}^{n,n}$$

$$R_{ij}^{n,l,l'}(t) := \int \mathrm{d}^3x \, x_i x_j \rho_{l,l'}^{n,n}(\vec{x}, \vec{x}, t)$$

(1.75)

Inserting this into equation (1.74) and comparing coefficients gives us an ordinary differential equation,

$$\left[(1+t^2)\partial_t - 2t - 2i(l-l')\right] R_{ij}^{n,l,l'} = 0 \,,$$

(1.76)

which is solved by

$$R_{ij}^{n,l,l'}(t) = C_{ij}^{n,l,l'}(t^2+1) \exp\left(2i(l-l')\tan^{-1}(t)\right) \,.$$

(1.77)

While the $C_{ij}^{n,l,l'}$ are infinitely many unknown constants, they are independent of the initial conditions in $\Gamma_{l,l'}^{n,n}$ and thus the same for all systems. In general, $R_{ij}^{n,l,l'}$ can be interpreted as a matrix element of a symmetric operator with two spatial indices with respect to the tower states. For our chosen action these states can be interpreted as eigenstates to the angular momentum operators L_z and L^2 of the Schrödinger algebra. This implies that for a given choice of (n, l, l'), as a consequence of the Wigner-Eckardt theorem, $R_{ij}^{n,l,l'}$ has not six degrees of freedom, but two.

There are special cases that we can solve completely. One such case is the isotropic free expansion of a cloud of fermions. By identifying

$$\sum_i I_{ii}(t) = \left\langle \vec{x}^2 \right\rangle(t) = \sum_n \Gamma_{l,l'}^{n,n} \left\langle O_{l'}^n | C(t) | O_l^n \right\rangle \,,$$

(1.78)

with $C(t) = e^{iH_st}Ce^{-iH_st} = C + tD + t^2 H_s$ we can express the trace of the moment of inertia in terms of the algebra operators. Rewriting this in terms of the ladder operators and trapped Hamiltonian yields

$$\sum_i R_{ii}^{n,l,l'} = \left\langle O_l^n | C(t) | O_{l'}^n \right\rangle = \frac{1}{2}\left[\delta_{l,l'} E_l^n - \frac{c_L^n}{2c_{L-1}^n}(\delta_{l,l'+1} + \delta_{l+1,l'})\right]$$
$$+ \frac{t}{2i}\frac{c_L^n}{c_{L-1}^n}(\delta_{l,l'+1} - \delta_{l+1,l'})$$
$$+ \frac{t^2}{2}\left[\delta_{l,l'}E_l^n + \frac{c_L^n}{2c_{L-1}^n}(\delta_{l,l'+1} + \delta_{l+1,l'})\right] \,,$$

(1.79)

where $L = \max(l, l')$. The expansion (without interference between towers) is thus only affected by mixing between neighboring tower states,

$$\left\langle \vec{x}^2 \right\rangle(t) = \sum_n (1+t^2) \sum_{l=0} \Gamma_{l,l}^{n,n} E_l^n + \frac{c_L^n}{c_{L-1}^n} \sum_{L=1} \left[(t^2-1)\mathrm{Re}(\Gamma_{L,L-1}^{n,n}) + 2t\,\mathrm{Im}(\Gamma_{L,L-1}^{n,n})\right] \,.$$

(1.80)

This result also nicely agrees with Zhou and Maki's prediction for initial conditions diagonal in (l, l') [62] which is $\langle \vec{x}^2 \rangle (t) = \langle \vec{x}^2 \rangle (t=0)(1 + \omega^2 t^2)$. In a similar fashion we can calculate the isotropic part of the oscillation of an atomic cloud while still trapped by evolving the tower states trivially with the trapped Hamiltonian instead,

$$\begin{aligned}
\langle O_l^n | e^{iHt} C e^{-iHt} | O_{l'}^n \rangle &= e^{i(E_l^n - E_{l'}^n)t} \langle O_l^n | C | O_{l'}^n \rangle \\
&= \frac{e^{i(E_l^n - E_{l'}^n)t}}{2} \left[\delta_{l,l'} E_l^n - \frac{c_L^n}{2c_{L-1}^n}(\delta_{l,l'+1} + \delta_{l+1,l'}) \right].
\end{aligned}$$
(1.81)

which translates into oscillatory behavior of the cloud as well

$$\begin{aligned}
\langle \vec{x}^2 \rangle_{\text{osc}} &= \sum_n \sum_{l=0} \Gamma_{l,l}^{n,n} E_l^n - \sum_{L=1} \frac{c_L^n}{c_{L-1}^n} \text{Re}(e^{2it}\Gamma_{L,L-1}^{n,n}) \\
&= \sum_n \sum_{l=0} \Gamma_{l,l}^{n,n} E_l^n + \sin(2t) \sum_{L=1} \frac{c_L^n}{c_{L-1}^n} \text{Im}(\Gamma_{L,L-1}^{n,n}) - \cos(2t) \sum_{L=1} \frac{c_L^n}{c_{L-1}^n} \text{Re}(\Gamma_{L,L-1}^{n,n}).
\end{aligned}$$
(1.82)

Again, we find that this quantity only depends on neighboring energy states in the initial condition. Non-relativistic conformal field theory is a powerful tool for analytical predictions in isotropically trapped ultracold gases. It is however limited by requiring knowledge about the ground states of each tower as well as how the initial condition projects onto the tower state basis. It also fails to capture behavior of two-dimensional systems due to the aforementioned existence of a quantum anomaly breaking the symmetry in that case [63, 64].

1.5.4 Experimental realization

In order to investigate fluidlike behavior in systems with few particles, I worked as part of a collaboration with the group led by Selim Jochim at the Physikalisches Institut of Heidelberg University. In this section I will roughly lay out the experimental techniques they use in the realization of ultracold atomic gases with $N \leq 14$ particles and their consequences for the theoretical considerations.

The cold atoms used in the experiments are specifically ^{6}Li atoms in the hyperfine states $|F = 1/2, m_F = -1/2\rangle$ and $|F = 3/2, m_F = -3/2\rangle$ which have a broad ($\Delta \approx 170$G) Feshbach resonance at $B_0 \approx 690$G [67]. The particles are trapped in the superposition of a single layer of an optical lattice, which effectively renders the problem two-dimensional, and an optical tweezer imposes an approximately harmonic potential on the particles within the plane [27, 28]. The desired small atom numbers are achieved by, following the method of [26], applying a magnetic field gradient and weakening the radial confinement until all but the lowest harmonic oscillator states are expelled from the trap. That means that the resulting few particle state is a ground state of the optical tweezer trap that has an equal number of atoms in either hyperfine state (usually written as e.g. $5 + 5$ particles for ten total atoms). Interactions between the particles can be controlled with the Feshbach resonance and quenched off

rapidly by exciting the atoms in the $|F = 3/2, m_F = -3/2\rangle$ state to the off-resonance $|F = 3/2, m_F = -1/2\rangle$ by means of a two-photon Raman transition [28]. Measurements in this system are performed by switching off the optical tweezer and imaging the positions of the atoms (discussed in [68]) after a fixed time of flight.

The most important implication of this for the theoretical calculations is the fact that we should not consider the system three dimensional but instead work with a two-dimensional description. Due to the fact that the system is only quasi two-dimensional, we need to consider appropriate corrections to the scattering length [69]. Instead of $1/a$ the correct parameter to indicate the transition between the BEC and BCS sides of the resonance becomes $\ln(k_F a_{2d})$ [70] ($\ll 0$ for BEC, $\gg 0$ for BCS side) where k_F is the Fermi momentum. Notably, in the quasi-2d system the effective scattering length is always positive such that stable two-particle bound states can exist on both sides of the crossover [70]. Beyond that, the change in dimensionality also affects thermodynamics which means that we need to consider different equations of state for our eventual fluid dynamic comparison to this system. These effects need to be considered, but do not change the nature of our calculations fundamentally. All in all this means that we have an effectively two-dimensional system of few fermionic atoms with controllable interaction via the Feshbach resonance and known initial geometry through the shape of the potential induced by the optical tweezer.

Chapter 2

Testing the low particle number limit

At this point we have established that there is evidence supporting the claim of fluid dynamic behavior in very small systems and that cold atomic systems are suited to study this due to their good control over the initial state geometry and particle interaction. This chapter lays out the concept of an experimental procedure, a theoretical approach to the prediction of the system's behavior in both real and momentum space and a comparison between numerical results and the experimental data measured and processed by the Ultracold Quantum Gases group at the Physikalisches Institut of Heidelberg University.

2.1 Qualitative expectations

In this section, I will introduce the general concept of a cold atom experiment that investigates the elliptic flow for a small number of particles as well as give a qualitative prediction of the scaling of v_2 with the particle number. I explore the non-interacting case and its non-flow contributions to the results and reason that effects due to particle interaction will come to dominate as the particle number increases. The work presented here was done in cooperation with Stefan Floerchinger, Giuliano Giacalone and Leena Tharwat and published in [71]. This section follows along the line of thought of that publication.

2.1.1 Experimental observable and schematic setup

As discussed before, the preferred indicator for potential fluid dynamic behavior is the ratio of initial spatial and late-time momentum anisotropy v_2/ε_2. The initial geometry and thereby ε_2 of the cold atom cloud is determined by the interaction strength and the trapping potential both of which are part of the experimental setup. Assuming we can always prepare the exact same N particle ground state, this means the initial anisotropy of the system will always be the same, at least statistically over all sufficiently large subsets of the measurements. In the following, we will assume a harmonic

two-dimensional trapping potential. It is fully determined by the trapping frequencies in each spatial direction, ω_x and ω_y and gives us an angular frame of reference for the expansion process. A fluid at rest in this trap would align the orientation of its shape with the axes of the ellipse defined by the equipotential lines. This lets us drop the angular information that would inherently be contained in $\mathcal{E}_2$ and V_2. At this point, the initial ellipticity could depend on up to four scalar degrees of freedom. While it would be possible to determine $\varepsilon_2(N, a, \omega_x, \omega_y)$ experimentally for each set of these, we consider only the spatial ellipticity of a one-particle, and thus non-interacting, ground state in the trap. In that case we find that the result only depends on the ratio of the trapping frequencies,

$$\varepsilon_2 = \frac{1 - \omega_y/\omega_x}{1 + \omega_y/\omega_x} \, . \tag{2.1}$$

In general, this will not be the exact initial ellipticity of any given N particle ground state. It does, however, give us a reference point close enough to an exact result which we can use to normalize any measurement of v_2. Also, this definition is independent of the internal physics of the cold atom system. The fact that ε_2 can be negative is a remainder of the original angular information that indicates along which of the coordinate axes the long axis of ellipse is oriented, reduced from a $U(1)$ to a $\mathbb{Z}_2$ degree of freedom.

The elliptic flow, on the other hand, will be determined from the time-of-flight measurement. That data provides us with a histogram of the particle positions that will approximate the complete one-particle distribution in space $n(x, y)$. Using the common assumption that, after a sufficiently long time of flight, the real space distribution will mirror the momentum distribution scaled with time, we can calculate the elliptic flow as

$$
\begin{aligned}
v_2 &= \langle \cos(2\phi_p) \rangle_{f(\vec{p}), \, t \to \infty} \approx \langle \cos(2\phi) \rangle_{n(x,y), \, t \to \infty} \\
&= \int \mathrm{d}x \, \mathrm{d}y \, n(x, y) \frac{x^2 - y^2}{x^2 + y^2} \, .
\end{aligned}
\tag{2.2}
$$

Here, again, the sign encodes the orientation of the anisotropy in relation to the axes of the trapping potential. We make use of the remaining angular information to distinguish between the inversion of shape ($v_2/\varepsilon_2 > 0$) and the for ideal fluids unexpected conservation of shape ($v_2/\varepsilon_2 < 0$). While in a large sample of particles the transition from the measured position histogram to the continuous distribution is reasonable, that becomes less certain if we only have a small number of particles in each image. This is not a problem as long as the same microscopic wave function $\psi(x)$ can be prepared within the trap initially. In that case, each shot samples the probability distribution given by $|\psi(x)|^2 = n(x)$ and we can combine the results of many measurements into one histogram in order to reproduce it.

This leaves us with a straightforward measurement procedure for the qualitative study of potential fluid dynamic behavior. A ground state of N particles is prepared for a fixed known scattering length a in a trap with known frequencies ω_x and ω_y. The trapping potential is turned off instantaneously and the particle cloud expands. After a sufficiently long fixed time of flight, the positions of the atoms are imaged, destroying

the state in the process. This measurement is repeated many times with the same initial conditions in order to reproduce the probability distribution as accurately as possible. From the initial trap configuration and the particle distribution at final time, we can construct v_2/ε_2 for this set of experimental parameters. This procedure can be performed for different numbers of particles in the initial state in order to get an understanding of the dependence of the normalized elliptic flow. Such a measurement, in fact, was already done for $N \sim 10^5$ atoms by O'Hara et al. [16] where they found an inversion of the atomic cloud's aspect ratio as it expanded. Following this, other experiments investigated elliptic flow under different aspects, for bosonic atoms [18, 19, 22] and mixes of different isotopes [23], for different interactions [20–22] and as a probe of viscosity [17, 24, 25]. However, all these previous studies were performed on systems with a macroscopic number of particles. In the following, we will explore the mesoscopic regime that is too complex for a full analytical treatment, but does not yet fall clearly into the range of collective descriptions.

2.1.2   Addressing non-flow contributions

The measurement we proposed is based purely on one-particle distributions with a known initial orientation and thereby avoids many of the difficulties and uncertainties that come with multiparticle correlations. In systems as small as the ones we are considering, however, we cannot neglect that on a microscopic level we are working with a marginalized N-particle wave function $\psi(t, x)$. Heisenberg's uncertainty tells us that even if the cloud of atoms is at zero temperature and at rest, there will be some variance of the momentum around zero. This is true even in a setting without interactions. Since we state fluid dynamics to be a result of interactions, any anisotropy in that initial momentum spread would give a contribution to the elliptic flow that is similar to the non-flow contributions in the high energy measurements. In a setting with many fermionic atoms like the system of O'Hara et al., this is not a significant problem because the fermions will fill up energy levels from the bottom up and form a Fermi sphere in momentum space that is isotropic regardless of the trap geometry and thus does not contribute to the elliptic flow. For the few-particle system we will first analyse the non-interacting case.

Without interactions, the system we are dealing with is that of a fixed number N of fermionic particles in an external potential. It is well-described by quantum mechanics as a state $|\Psi\rangle$ whose evolution is determined by the Schrödinger equation

$$i\partial_t |\Psi\rangle = H |\Psi\rangle \,, \tag{2.3}$$

with a Hamiltonian comprised of a kinetic and potential term for each particle,

$$H = \sum_{i=1}^{N} \frac{\vec{p}_i^2}{2m} + V(\vec{x}_i) \,. \tag{2.4}$$

Since this Hamiltonian separates additively into the same terms for each particle, we can construct an N particle solution from a product of one particle solutions $|\psi_{n,m}\rangle$.

Taking into account the necessary antisymmetrisation, we find

$$|\Psi\rangle = \frac{1}{\sqrt{N!}} \sum_{\sigma \in S_N} \text{sign}(\sigma) \bigotimes_{i=1}^{N} |\psi_{n_i,m_i}(\sigma(i))\rangle \,, \tag{2.5}$$

where S_N is the symmetric group containing all permutations of the numbers from one to N. This construction is also called the Slater determinant [72].

The first step is thus to solve the problem for only one particle. The potential we use is

$$V(\vec{x}) = \frac{m\omega_x^2}{2}x^2 + \frac{m\omega_y^2}{2}y^2 \,. \tag{2.6}$$

The solution to the resulting eigenstate problem of the one-particle Hamiltonian is well-known to be

$$\psi_{n_1,n_2}(\vec{x}) = \langle \vec{x}|\psi_{n_1,n_2}\rangle = \sqrt{\frac{m\sqrt{\omega_x\omega_y}}{2^{n+m}n_1!n_2!\pi}} H_{n_1}(\sqrt{m\omega_x}x) H_{n_2}(\sqrt{m\omega_y}y) e^{-\frac{m\omega_x^2}{2}x^2 - \frac{m\omega_y^2}{2}y^2} \,,$$

$$H|\psi_{n_1,n_2}\rangle = E_{n_1,n_2}|\psi_{n_1,n_2}\rangle \,,$$

$$E_{n_1,n_2} = (n_1 + 1/2)\omega_x + (n_2 + 1/2)\omega_y \,, \tag{2.7}$$

with the Hermite polynomials H_n. The representation in momentum space is very similar,

$$\psi_{n_1,n_2}(\vec{p}) = \langle \vec{p}|\psi_{n_1,n_2}\rangle$$

$$= \frac{1}{\sqrt{2^{n+m}n_1!\,n_2!\,\pi m\sqrt{\omega_x\omega_y}}} H_{n_1}\left(\frac{p_x}{\sqrt{m\omega_x}}\right) H_{n_2}\left(\frac{p_y}{\sqrt{m\omega_y}}\right) e^{-\frac{p_x^2}{2m\omega_x} - \frac{p_y^2}{2m\omega_y}} \,. \tag{2.8}$$

In the non-interacting scenario we are currently considering, expectation values of momentum quantities do not change over time, hence we can determine v_2 from the above representation via its standard definition (2.2). For the one-particle ground state that amounts to

$$v_2 = \langle \cos(2\phi_p)\rangle_{\psi_{0,0}} = \left\langle \frac{p_x^2 - p_y^2}{p_x^2 + p_y^2}\right\rangle_{\psi_{0,0}} = \frac{1 - \sqrt{\omega_y/\omega_x}}{1 + \sqrt{\omega_y/\omega_x}} \,, \tag{2.9}$$

which leads to the ratio v_2/ε_2 varying between 0.5 and 1 which is noticably larger than the results from high energy physics ($v_2/\varepsilon_2 \approx 0.3$, [73]) or the many particle limit ($v_2/\varepsilon_2 \approx 0.43$, from the data of [16]).

Returning to the case of N particles, there is another important thing to note. Since the particles are all indistiguishable from one another, we can formulate one-particle expectation values as observables in terms of position and momentum operators referring to just one particle. For any such operator $A = A(\vec{x}_i, \vec{p}_i)$ we can formulate its expectation value as

$$\langle A\rangle_\Psi = \frac{1}{N}\sum_{i=1}^{N}\langle A\rangle_{\psi_{n_i,m_i}} \,, \tag{2.10}$$

which is nothing but the average over all individual one particle expectation values for all sets of quantum numbers in the full state. We can also apply this to the elliptic flow and the total energy. The ground state for N particles at fixed trap aspect ratio will hence be the antisymmetric combination of the N lowest energy states of the one-particle system. In what order the quantum numbers increase will in general depend on the chosen trap ellipticity. With this, it is also possible to see the buildup of a Fermi sphere for large particle numbers. The ratio of the momentum variances in the two spatial dimensions,

$$\frac{\langle p_x^2 \rangle_\Psi}{\langle p_y^2 \rangle_\Psi} = \frac{\omega_x}{\omega_y} \frac{\left(\frac{1}{2} + \frac{1}{N} \sum_{i=1}^N n_i \right)}{\left(\frac{1}{2} + \frac{1}{N} \sum_{i=1}^N m_i \right)} , \tag{2.11}$$

depends on the aspect ratio of the trap and the ratio of average quantum numbers in the corresponding directions. We expect the latter to scale inversely proportional to the trap aspect ratio for ground states at larger particle numbers, which leads to an aspect ratio converging to unity, regardless of the trap geometry. This also manifests in the predictions of the elliptic flow shown in figure 2.1. The elliptic flow starts at very large values for a single particle but from there decreases roughly as the inverse of the particle number. The jumps around this trend are due to the discreteness of the particle number and quantum numbers.
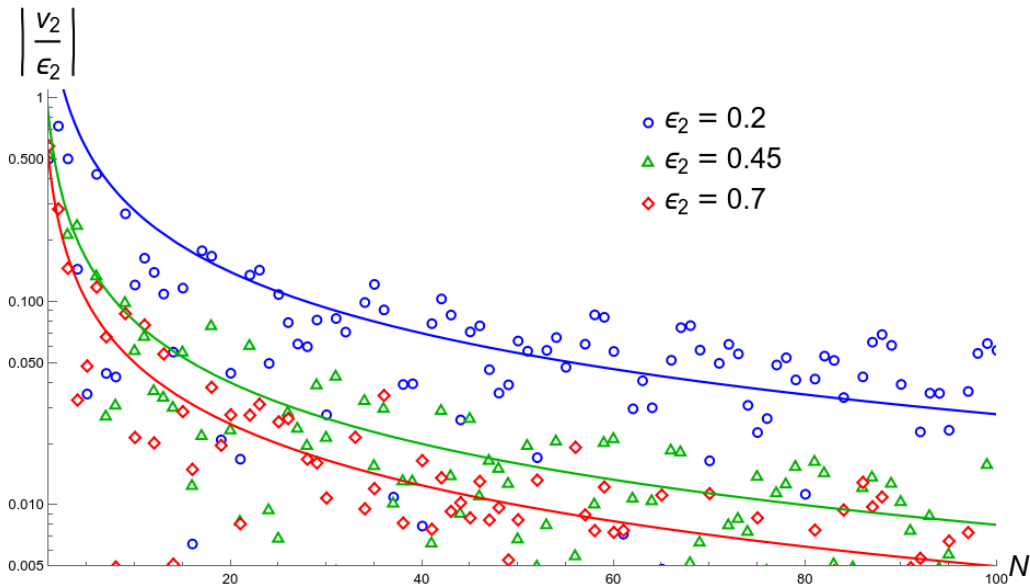

Figure 2.1: Predictions for the normalized elliptic flow v_2/ε_2 (disregarding the sign) of a non-interacting quantum harmonic oscillator ground state as a function of the particle number. The solid lines are all proportional to $1/N$ (blue: $2.8/N$, green: $0.8/N$, red: $0.5/N$) and are shown to illustrate the general trend of the data points. Adapted from [71].

One dimension of our system that we have consistently neglected so far is tempera-

ture. We can make use of the non-interacting scenario to test whether that is justified. At finite temperature, we can no longer work with a wave function, but instead formulate the state of the system as a density operator. In thermal equilibrium, the system is a mixture of all possible states weighted by their energy compared to the thermal energy scale $k_B T = \beta^{-1}$. For a system with just a single particle that can be expressed as

$$\rho = \frac{e^{-\beta H}}{\text{tr}(e^{-\beta H})} = \frac{1}{Z} \sum_{n=0}^{\infty} \sum_{m=0}^{\infty} |\psi_{n,m}\rangle \langle \psi_{n,m}| \, e^{-\beta(n\omega_x + m\omega_y)} \,,$$

$$Z = \sum_{n=0}^{\infty} e^{-\beta n\omega_x} \sum_{m=0}^{\infty} e^{-\beta m\omega_y} = \frac{1}{(1 - e^{-\beta\omega_x})(1 - e^{-\beta\omega_y})} \,.$$

(2.12)

Expectation values with respect to this density operator are calculated by

$$\langle A \rangle_\rho = \text{tr}(\rho A) \,. \tag{2.13}$$

For the single particle case we can calculate the variance of momentum explicity,

$$\langle p_x^2 \rangle = m\omega_x \left(\frac{1}{2} + \frac{1}{e^{\beta\omega_x} - 1} \right) \,. \tag{2.14}$$

From there, we can make a very similar argument as before since the ratio of momentum variances,

$$\frac{\langle p_y^2 \rangle}{\langle p_x^2 \rangle} = \frac{\omega_y}{\omega_x} \frac{\tanh(\beta\omega_x/2)}{\tanh(\beta\omega_y/2)} \,, \tag{2.15}$$

becomes unity in the limit of infinite temperature, $\beta \to 0$, which implies that the elliptic flow should also vanish. This is confirmed by the numerical results shown in figure 2.2 in which for numerical practicality we only considered the 100 lowest energy states for a given ellipticity. It is also consistent with the low temperature limit, $\beta \to \infty$, calculated before in (2.11) which simply becomes the trap frequency ratio for a single particle. For more than one particle this becomes much more complicated to express because even with a limited range of quantum numbers, the number of possible states grows rapidly with the particle number. We checked systems with up to $N = 4$ atoms numerically and found the same results of v_2 decreasing with increasing temperature. It is possible to make an analytical argument that the infinite temperature limit for any fixed number of particles is identical to the limit of infinite particle number at zero temperature. In both cases the elliptic flow is averaged over the entire spectrum of eigenstates with equal weights (see also appendix of [71]). Therefore, we can expect the asymptotic behavior

$$\lim_{\beta \to 0} v_2 = 0 \,, \tag{2.16}$$

for non-interacting particles, regardless of particle number.

In summary, this means that non-flow contributions due to the quantum nature of the system are very relevant in the limit of few particles, but decrease in importance
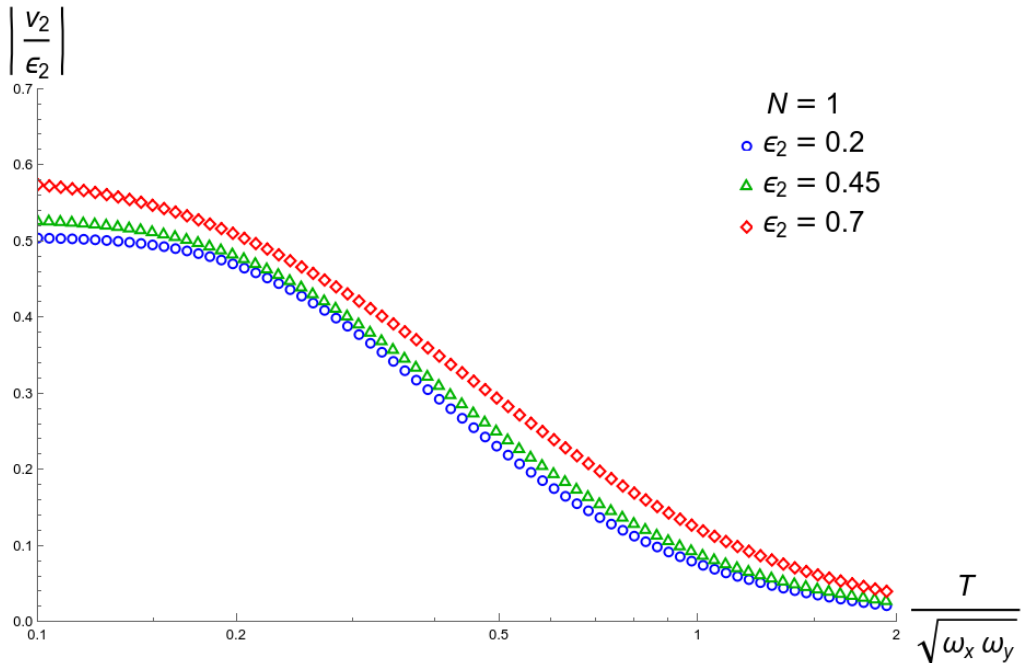
Figure 2.2: Predictions for the normalized elliptic flow v_2/ε_2 of a single particle harmonic oscillator ground state as a function of the dimensionless temperature scale $T/\sqrt{\omega_x \omega_y}$. Adapted from [71].

as the number of particles rises. Any deviation in temperature from the expected $T \approx 0$ would suppress these non-flow effects. Therefore, we will continue to neglect any effects from non-zero temperature as they would only decrease contributions of the initial state momentum variance that are present without interactions.

2.1.3 Qualitative prediction of elliptic flow

We have now studied the non-interacting case and its influence on the elliptic flow in much detail. In order to understand how this is modified by the presence of interactions, we start in the many particle limit in which fluid dynamics has already been proven to be applicable [16]. In that limit we also expect a kinetic theory description to be viable. That means we can make use of the the scales introduced in section 1.1.5 to determine how the applicability of fluid dynamics scales with the particle number from that point of view. The relevant dimensionless scale to answer that question is the Knudsen number Kn. Using a hard sphere model as the basis, we can see that the only quantity in the definition of the Knudsen number (1.24) that scales with the particle number in an equilibrium situation is the system size. In the two-dimensional case we are considering, the system length would scale like the square root of the particle number, $L \propto \sqrt{N}$. Under these simplifying assumptions, we obtain for the scaling of the Knudsen number with the particle number,

$$\text{Kn} \propto 1/\sqrt{N}\,. \tag{2.17}$$

34

While this specific result is a product of drastic simplifications, it shows the general trend that the Knudsen number decreases with increasing particle number in a fast manner, compared to e.g. a logarithmic scaling of the cross section with the interaction strength [70]. Fluid dynamics is expected to be applicable only if the Knudsen number is very small, Kn $\ll 1$. For larger values individual particle dynamics are expected to play too big a role to simplify them as just a density in space. A phase space description for e.g. free streaming can however still be viable. This also tells us that as the cloud of atoms expands, it will eventually lose any fluid dynamic properties it might have, since the product of particle density, contained in the mean free path, and system diameter in equation (1.24) will decrease as the cloud expands. A similar prediction can be made on the basis of a superfluid with a Bogoliubov dispersion relation (1.56). As the density decreases during expansion, so does the critical velocity. When the velocity of the expanding particles crosses this continuously decreasing limit, superfluidity breaks down.

In a fluid dynamic modeling of the system the elliptic flow is clearly non-vanishing. We expect that contribution to come only from interactions since the non-flow contributions are negligible in the many particle limit. This means that the elliptic flow will converge to its fluid dynamic value for large N. On the few particle side of the problem, we expect interactions to contribute less to the value of v_2 since there are fewer potential participants for any scattering event. In the extreme case of just one particle, we expect interactions not to contribute at all such that the elliptic flow is fully determined by non-flow effects. Combining this expectation of an interaction contribution converging to a macroscopic value from below with the non-flow contributions scaling roughly inversely with the particle number leads us to the qualitative prediction in figure 2.3. Depending on the balance between non-flow and collective parts we would expect either a monotonously decreasing curve converging to the fluid dynamic limit or a curve with a minimum after which the system goes back up to again the fluid dynamic prediction. This has been investigated experimentally by the Ultracold Quantum Gases group at Heidelberg University [74]. They found the second type of behavior with a minimum at $N = 2 + 2$ particles for their configuration of the interaction strength.

2.2 Quantitative theoretical predictions

After confirming qualitatively the presence of fluidlike behavior in these small atomic systems, we want to convince ourselves fully by making quantitative comparisons as well. In this section, I present methods to model the flow of the cold atom cloud. First, I establish a suitable approximation for the thermodynamic equation of state of the system based on experimental results from the many body case. Based on this, I make predictions for the evolution of the Thomas-Fermi type density profile predicted by fluid statics. By making further assumptions, the fluid dynamic predictions can be expanded to include global momentum space expectation values. These theoretical considerations lay the groundwork for the following numerical calculations. This was,
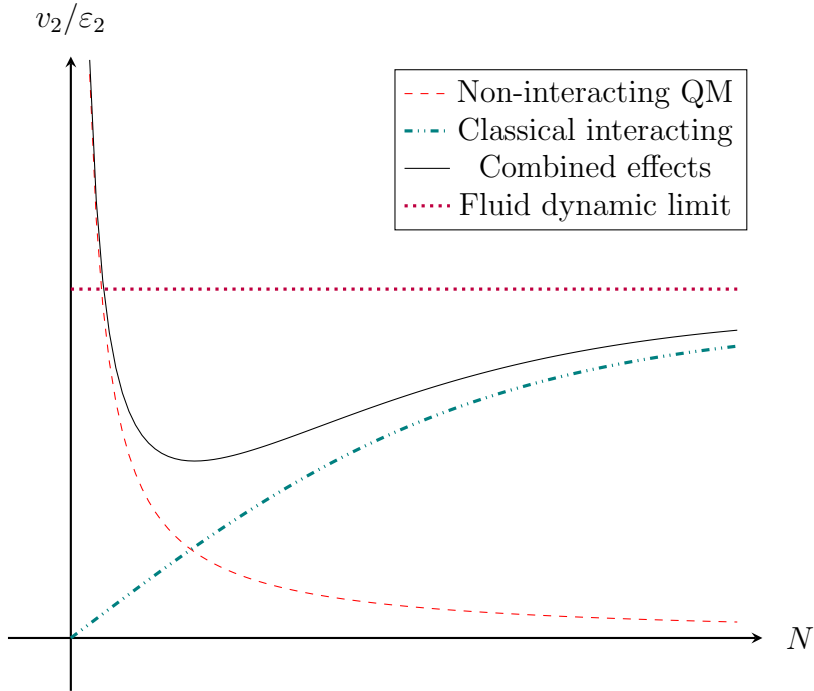
Figure 2.3: Qualitative sketch of the scaling of the elliptic flow with the particle number for an interacting system that expands after being released from an anisotropic harmonic trap. At low particle numbers we expect the influence of quantum effects (red dashed curve) to dominate while for larger numbers interactions (blue dot-dashed curve) play a more central role. The behavior of the combined system (solid black curve) could therefore have a minimum and will most likely converge to a macroscopic value (dotted purple line) in the many-particle limit. Adapted from [71].

again, done in cooperation with Stefan Floerchinger and Giuliano Giacalone.

2.2.1 Finding the right equation of state

The only external ingredient needed for a description of the cold atom system as an ideal fluid is its thermodynamic equation of state. Depending on which side of and how close to the Feshbach resonance the external magnetic field is set, the system can behave anywhere between weakly or strongly interacting Bose gas and strongly interacting or ideal Fermi gas. In general these types of behavior and the corresponding equations of state are descriptions of many-particle situations which clearly fall into the range of thermodynamics. Since we are trying to expand the boundaries of what we can reasonably describe with this kind of macroscopic language, we will make use of these concepts even in the few-particle case we are considering. We start with one of these edge cases. The thermodynamic properties of ideal Fermi gases have been studied extensively. From the constant density of states we know the equation of state

in the two-dimensional case with two possible hyperfine states to be [3]

$$n(\mu) = 2\lambda_T^{-2}\ln(1 + e^{\beta\mu}) \tag{2.18}$$

with the thermal wavelength

$$\lambda_T = \left(\frac{2\pi}{mk_BT}\right)^{1/2}. \tag{2.19}$$

In the low temperature limit $\beta \to 0$, this equation of state simplifies to

$$n(\mu) \approx 2\lambda_T^{-2}\beta\mu = \frac{m}{\pi}\mu \tag{2.20}$$

The pressure can be calculated from that particle density as

$$P(\mu, T \to 0) - P_0 = \frac{m}{2\pi}\mu^2 = \frac{\pi}{2m}n^2 = \frac{\pi}{2m^3}\rho^2 \tag{2.21}$$

Ignoring the constant shift, this is a polytropic equation of state, meaning it is mono-mial in density, $P = c\rho^\kappa$, with exponent $\kappa = 2$. From here on we will refer to this as the ideal Fermi pressure P_F.

Finding the equation of state for an interacting system is much more complicated from a theoretical point of view. There have however already been studies on this, both experimental and numerical [75–78], in the many-particle limit. These usually put the pressure in relation to the ideal Fermi one, so we will do the same. The relevant dimensionless scale as shortly discussed in section 1.5.4 is

$$\begin{aligned}\eta &= \ln(k_F a_{2d}), \\ k_F &= \sqrt{2\pi n},\end{aligned} \tag{2.22}$$

which puts the two-dimensional scattering length and the Fermi momentum, and thereby density, of the system into relation. The limit $\eta \to \infty$ captures the behavior of the cold atoms like an ideal Fermi gas, while the ideal Bose gas behavior is recovered for $\eta \to -\infty$. The strongly interacting case is expected when the scattering length and the interparticle spacing are comparable, at $\eta \approx 0$. Multiple approximations for different ranges of η have been compared to both experimental data and quantum Monte Carlo simulations covering the strongly interacting region [77]. Since we are considering a system that starts off dense enough to be near $\eta \approx 1$ at its peak density and only dilutes from there on, we matched an equation of state to the quantum Monte Carlo data from [76] of the region $\eta < 2$ as shown in figure 2.4. We approximated the multiplicative correction to the ideal Fermi pressure with an exponential function,

$$\frac{P}{P_F} \approx \alpha_1 e^{\alpha_2\eta}. \tag{2.23}$$

For the calculations and simulations in the following sections we will use

$$\alpha_1 \approx 0.27, \quad \alpha_2 \approx 0.55. \tag{2.24}$$

37

Therefore, the equation of state modified by interactions that we will be using is

$$P_{\text{fit}} = \alpha_1 \left(\frac{2\pi a_{2d}^2}{m} \right)^{\alpha_2/2} \frac{\pi}{2m^3} \rho^{2+\alpha_2/2} \,, \tag{2.25}$$

rewriting η in terms of density and scattering length. Notably, this is also a polytropic equation of state which is beneficial for both numerical and analytical calculations.
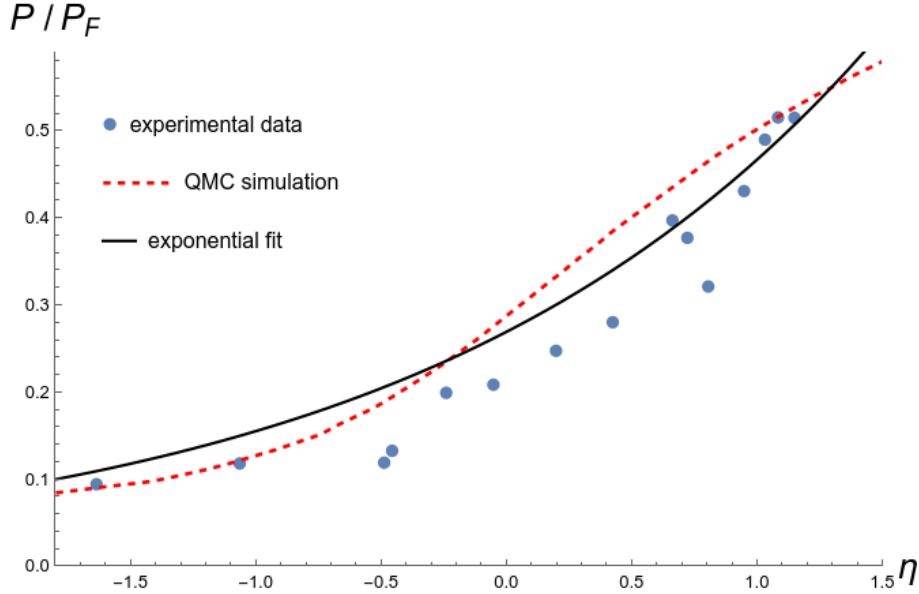

Figure 2.4: Exponential fit (solid black curve) of the multiplicative correction to the equation of state compared to the interpolated results of a quantum Monte Carlo simulation (dashed red curve) and experimental data (blue dots). For $\eta > 1.3$ the fit starts to diverge from the data as it does not capture the convergence towards the ideal Fermi gas pressure. Experimental and quantum Monte Carlo data taken from [76].

2.2.2 Real space prediction

With this approximate equation of state, we can return to the fluid dynamic equations of motions and try to solve them. However, we also need to know the initial configuration of system in order to predict its evolution. For the velocity, this is an easy problem to solve. The system is at rest initially and as such cannot have any macroscopic motion, i.e. fluid velocity. In order to arrive at a form for the initial density, we make use of the hydrostatic situation before the expansion of the atom cloud. At that point in time, there are still the external forces of the trap acting on the fluid. Inserting those into the Euler equation and rewriting the pressure as a chemical potential as in section 1.3, we get

$$\rho(\partial_t + \vec{u} \cdot \vec{\nabla})\vec{u} + \frac{\rho}{m}\vec{\nabla}\mu = -\frac{\rho}{m}\vec{\nabla}V_{\text{trap}} \,. \tag{2.26}$$

However, considering that the fluid is completely at rest before and at the very start ($t = t_0$) of the expansion, the fluid velocity must vanish. This leaves a very simple solution for the chemical potential at initial time,

$$\rho \vec{\nabla} \mu = -\rho \vec{\nabla} V_{\text{trap}}$$
$$\mu(t_0, \vec{x}) = \mu_0 - V_{\text{trap}}(\vec{x}) \,, \tag{2.27}$$

where μ_0 is just an integration constant for now. Since arriving at this equation required dividing by the mass density, it is only valid where the mass density is non-vanishing. Starting from a polytropic equation of state,

$$P = cn^{\kappa} \,, \tag{2.28}$$

we can express the chemical potential via $\mathrm{d}p = n\,\mathrm{d}\mu = c\kappa n^{\kappa-1}\,\mathrm{d}n$ as a function of the density,

$$\mu = \frac{c\kappa}{\kappa - 1} n^{\kappa-1} \,. \tag{2.29}$$

Inverting this gives us the particle number density and hence the mass density in terms of the chemical potential,

$$\rho = m \left(\frac{\kappa - 1}{c\kappa} \right)^{\frac{1}{\kappa-1}} \mu^{\frac{1}{\kappa-1}} \,. \tag{2.30}$$

With that we can use equation (2.27) to define the initial fluid density. The integration constant μ_0 is fixed by the normalisation of ρ to the total mass in the system. Since for $\kappa > 1$ the chemical potential cannot be negative, according to (2.29), the density must vanish at all points at which $V_{\text{trap}}(\vec{x}) > \mu_0$. This usually leads to a non-smooth behavior of both density and chemical potential at the boundaries defined by $V_{\text{trap}}(\vec{x}_b) = \mu_0$. While this is fine in a classical context and in areas of high density, in a quantum-mechanical context one can consider contributions like the quantum pressure in equation (1.54). This makes the dependence of the particle density on the chemical potential in general very complicated, but alleviates some of the problems at the edges of the density [79].

We will stick with the classical approach for now and combine it with the Lagrange coordinates discussed in section 1.3. The first thing to notice is that due to the polytropic equation of state and the scaling of the comoving density, the chemical potential inherits a very similar scaling behavior,

$$\mu(t, \vec{r}(t, \vec{R})) = \frac{\mu(t_0, \vec{R})}{J(t, \vec{R})^{\kappa-1}} = \frac{\mu_0 - V_{\text{trap}}(\vec{R})}{J(t, \vec{R})^{\kappa-1}} \,. \tag{2.31}$$

Specifying the trapping potential to be harmonic,

$$V_{\text{trap}}(\vec{R}) = \frac{m}{2} \omega_{jk}^2 R_j R_k \,, \tag{2.32}$$

we can see that the initial chemical potential is invariant under parity transformations $\vec{R} \to -\vec{R}$. The initial fluid velocity field is zero everywhere and thus trivially has both

odd and even parity. Considering that the gradient of the chemical potential is the driving force of any movement in the system, this symmetry translates to the parcel position as

$$\vec{r}(t, -\vec{R}) = -\vec{r}(t, \vec{R}) \,. \tag{2.33}$$

Contributions breaking this symmetry cannot be generated without being present in the initial conditions. In order to solve the Euler equation, we make the assumption that the position of a fluid parcel is linearly related to its initial position, equivalent to the assumption in [80],

$$r_k(t, \vec{R}) = \zeta_{jk}(t) R_j \,. \tag{2.34}$$

While this is just an ansatz, if it solves the differential equations for the given conditions, we can infer the uniqueness of that solution from the physicality of the situation and the local version of Picard-Lindelöf, if we restrict ourselves to analytical dependence on $\vec{R}$. As a consequence of this form of the parcel position we find

$$\begin{aligned} J_{jk}(t) &= \zeta_{jk}(t) \,, \\ J(t) &= \det(\zeta_{jk}(t)) = \zeta_{11}\zeta_{22} - \zeta_{12}\zeta_{21} \,. \end{aligned} \tag{2.35}$$

The fact that the Jacobian no longer depends on the initial parcel position also lets us express the gradient of the chemical potential in equation (1.44) in terms of a gradient of the trapping potential. Assuming the Jacobian does not vanish, which it should not for a physically viable solution, we can derive

$$\det(\zeta(t))^{\kappa-1}\zeta_{jk}(t)\frac{\mathrm{d}^2}{\mathrm{d}t^2}\zeta_{lk}(t) = \omega^2_{(jl)} \,, \tag{2.36}$$

with initial conditions inherited from the parcel position,

$$\begin{aligned} \vec{r}(t_0, \vec{R}) &= \vec{R} \Leftrightarrow \zeta_{jk}(t_0) = \delta_{jk} \,, \\ \vec{u}(t_0, \vec{R}) &= 0 \Leftrightarrow \dot{\zeta}_{jk}(t_0) = 0 \,. \end{aligned} \tag{2.37}$$

Since the trap frequency matrix $\omega^2_{(jl)}$ is symmetric, we diagonalise it only by applying rotations of or coordinate system,

$$\omega^2_{(jl)} = \mathrm{diag}(\omega^2_x, \omega^2_y)_{jl} \,. \tag{2.38}$$

Expanding the differential equation (2.36) into its four components,

$$\begin{aligned} (\zeta_{11}\zeta_{22} - \zeta_{12}\zeta_{21})^{\kappa-1}(\zeta_{11}\ddot{\zeta}_{11} + \zeta_{12}\ddot{\zeta}_{12}) &= \omega^2_x \,, \\ (\zeta_{11}\zeta_{22} - \zeta_{12}\zeta_{21})^{\kappa-1}(\zeta_{11}\ddot{\zeta}_{21} + \zeta_{12}\ddot{\zeta}_{22}) &= 0 \,, \\ (\zeta_{11}\zeta_{22} - \zeta_{12}\zeta_{21})^{\kappa-1}(\zeta_{21}\ddot{\zeta}_{11} + \zeta_{22}\ddot{\zeta}_{12}) &= 0 \,, \\ (\zeta_{11}\zeta_{22} - \zeta_{12}\zeta_{21})^{\kappa-1}(\zeta_{21}\ddot{\zeta}_{21} + \zeta_{22}\ddot{\zeta}_{22}) &= \omega^2_y \,, \end{aligned} \tag{2.39}$$

we can see that their solution for our given initial conditions is compatible with $\zeta_{jk}(t)$ also being diagonal, $\zeta_{12}(t) = \zeta_{21}(t) = 0$. With the notation $\zeta_{11} = \zeta_x$ and $\zeta_{22} = \zeta_y$ we can thus formulate the differential equations as

$$\begin{aligned} \ddot{\zeta}_x &= \omega^2_x \zeta_x^{-\kappa} \zeta_y^{1-\kappa} \,, \\ \ddot{\zeta}_y &= \omega^2_y \zeta_y^{-\kappa} \zeta_x^{1-\kappa} \,. \end{aligned} \tag{2.40}$$

These equations differ only by the exchange $(x \leftrightarrow y)$. One of them can be equivalently replaced by

$$\frac{1}{\omega_x^2} \zeta_x \ddot{\zeta}_x = \frac{1}{\omega_y^2} \zeta_y \ddot{\zeta}_y \,. \tag{2.41}$$

Specifically for the isotropic case $\omega_x = \omega_y = \omega$, with isotropic initial conditions, equation (2.41) implies $\zeta_x = \zeta_y = \zeta_{\text{iso}}$. For the remaining one independent function the differential equation is

$$\ddot{\zeta}_{\text{iso}} = \omega^2 \zeta_{\text{iso}}^{1-2\kappa} \,. \tag{2.42}$$

For an ideal Fermi gas with $\kappa = 2$, this is easily solved as

$$\zeta_{\text{iso}}(t) = \sqrt{1 + \omega^2 (t - t_0)^2} \,, \tag{2.43}$$

which asymptotically approaches a linear time depedence as would be expected for a freely streaming fluid. For our modified equation of state $(\kappa = 2 + \alpha_2/2)$, the solution can be written implicitly as

$$\zeta_{\text{iso}}(t)^2 \, {}_2F_1\left(\frac{1}{2}, -\frac{1}{2+\alpha_2}; 1 - \frac{1}{2+\alpha_2}; \zeta_{\text{iso}}(t)^{-2-\alpha_2}\right)^2 = \frac{2\omega^2}{2+\alpha_2}\left(t - t_0 + \frac{\sqrt{2+\alpha_2} c_F}{\sqrt{2}\omega}\right)^2 \,, \tag{2.44}$$

where ${}_2F_1$ is a hypergeometric function and c_F its value for $\zeta_{\text{iso}} = 1$. While it is hard to obtain to an explicit form for ζ_{iso} from this, we can draw some conclusions about its asymptotic behavior. The second time derivate of the function is strictly positive as long as the function itself is strictly positive according to equation (2.42). Therefore, the initial conditions imply that ζ_{iso} is strictly monotonously increasing in time. As such, the last argument of the hypergeometric function will vanish at late times if ζ_{iso} is not bounded from above. We make use of the identity ${}_2F_1(a, b; c; 0) = 1$ to find the asymptotic behavior

$$\lim_{t \to \infty} \frac{\zeta_{\text{iso}}(t)}{t} = \sqrt{\frac{2}{2+\alpha_2}} \omega \,. \tag{2.45}$$

We again see the asymptotically linear scaling that we associate with free streaming at late times.

Within the linear ansatz we find that the transformation back to Euler coordinates becomes particularly simple. The density can be expressed in terms of the scaling function,

$$\rho(t, \vec{x}) = \frac{\rho(t_0, \vec{R}(t, \vec{x}))}{J(t)} = \frac{\rho(t_0, \zeta^{-1}(t) \cdot \vec{x})}{\zeta_x(t) \zeta_y(t)} \,, \tag{2.46}$$

with the notation $\zeta^{-1} = \text{diag}(\zeta_x^{-1}, \zeta_y^{-1})$. The functional form of the fluid velocity is similarly straightforward,

$$u_k(t, \vec{x}) = \dot{\zeta}_{jk}(t) R_j(t, \vec{x}) = \dot{\zeta}_{jk} \zeta_{jl}^{-1} x_l = \text{diag}\left(\frac{\dot{\zeta}_x}{\zeta_x}, \frac{\dot{\zeta}_y}{\zeta_y}\right)_{jk} x_j \,. \tag{2.47}$$

41

Another advantage of the linear ansatz is that it makes some expectation values very easy to calculate, e.g.

$$\left\langle x^2 \right\rangle_{\rho(t,\vec{x})} = \frac{1}{m_{\text{tot}}} \int \mathrm{d}^2 R \; x^2(t,\vec{R}) \rho(t_0,\vec{R}) = \zeta_x^2(t) \left\langle x^2 \right\rangle_{\rho(t_0,\vec{x})} . \qquad (2.48)$$

Notably, the ratio between expectation values like this and their initial value only depends indirectly on the initial density profile. For the given example, $\left\langle x^2 \right\rangle(t)/\left\langle x^2 \right\rangle(t_0)$ only depends on ζ_{jk}. The differential equations determining ζ_{jk} directly contain the derivative of the initial chemical potential and thus of the initial density, but is not sensitive to μ_0 and thereby also insensitive to the number of particles in the fluid. With our knowledge about the initial chemical potential and its relation to the density, we can go one step further. At initial time the width in x-direction is

$$\left\langle x^2 \right\rangle_{\rho(t_0,\vec{x})} = \frac{1}{m_{\text{tot}}} \int \mathrm{d}^2 x \; x^2 m \left(\frac{\kappa-1}{c\kappa} \right)^{\frac{1}{\kappa-1}} (\mu_0 - V(\vec{x}))^{\frac{1}{\kappa-1}} \Theta(\mu_0 - V(\vec{x})) . \qquad (2.49)$$

We can introduce a coordinate transformation that accounts for the elliptical symmetry of the trapping potential,

$$
\begin{aligned}
x &= \frac{\tilde{r}}{\omega_x} \cos(\tilde{\varphi}) \\
y &= \frac{\tilde{r}}{\omega_y} \sin(\tilde{\varphi}) \\
\left| \det \frac{\partial(x,y)}{\partial(\tilde{r},\tilde{\varphi})} \right| &= \frac{\tilde{r}}{\omega_x \omega_y} .
\end{aligned}
\qquad (2.50)
$$

With this transformation, we find that the integral decomposes into the product of a radial and an angular integral,

$$\left\langle x^2 \right\rangle_{\rho(t_0,\vec{x})} = \frac{1}{m_{\text{tot}}} \frac{1}{\omega_x^2} \int_0^{2\pi} \mathrm{d}\tilde{\varphi} \cos^2 \tilde{\varphi} \int_0^{\sqrt{2\mu_0/m}} \mathrm{d}\tilde{r} \; \frac{\tilde{r}}{\omega_x \omega_y} \tilde{r}^2 m \left(\frac{\kappa-1}{c\kappa} \right)^{\frac{1}{\kappa-1}} (\mu_0 - \frac{m}{2}\tilde{r}^2)^{\frac{1}{\kappa-1}} . \qquad (2.51)$$

Looking at the aspect ratio at initial time, we find that the radial part is identical for $\left\langle x^2 \right\rangle$ and $\left\langle y^2 \right\rangle$ and the angular part integrates to the same value. Therefore, the initial aspect ratio is entirely determined by the ratio of the trap frequencies,

$$\sqrt{\frac{\left\langle x^2 \right\rangle_{\rho(t_0,\vec{x})}}{\left\langle y^2 \right\rangle_{\rho(t_0,\vec{x})}}} = \sqrt{\frac{\omega_y^2 \int_0^{2\pi} \mathrm{d}\tilde{\varphi} \cos^2 \tilde{\varphi}}{\omega_x^2 \int_0^{2\pi} \mathrm{d}\tilde{\varphi} \sin^2 \tilde{\varphi}}} = \frac{\omega_y}{\omega_x} . \qquad (2.52)$$

This calculation of the initial aspect ratio does not require the equation of state to be polytropic. The separation works as soon as the initial density can be expressed a function of only $(\mu_0 - V(\vec{x}))$. In the polytropic case, however, the time evolution of the aspect ratio is also easy to formulate,

$$\sqrt{\frac{\left\langle x^2 \right\rangle_{\rho(t,\vec{x})}}{\left\langle y^2 \right\rangle_{\rho(t,\vec{x})}}} = \frac{\zeta_x(t)\omega_y}{\zeta_y(t)\omega_x} . \qquad (2.53)$$

Since the scaling functions ζ_x and ζ_y are independent of the integration constant μ_0 which fixes the number of particles in the system, this result is valid for an arbitrary number of particles.

The representation in Lagrange coordinates gives us a powerful tool for the solution of the problem specifically for the Thomas-Fermi density profile with a polytropic equation of state. For other initial density profiles it fails to reduce the fluid dynamic equations from partial to ordinary differential equations. We can also use this to our advantage. A violation of the very general prediction of the fluid's aspect ratio in a harmonic trap can be seen as an indicator for the relevance of effects like quantum pressure.

2.2.3 Momentum space prediction

If the real space dynamics of the system are well-described by hydrodynamics, we can go one step further by making predictions for momentum space observables as well, in our case specifically the root mean square of momentum in a certain spatial direction $\langle p_i^2 \rangle$. While hydrodynamics by itself does not include this quantity, we can still make predictions based on the information we already have by employing three assumptions.

The first one is that there is an underlying one-particle phase space distribution $f(t, x, p)$ that describes the real and momentum space moments of the system. This is a given for kinetic theory which, uses this as the central object of interest (see section 1.1). But non-collisional systems can have something similar as well. For a quantum-mechanical system one can define the Wigner pseudodistribution, introduced by Wigner in [81], which does not fulfill all of the criteria for a probability distribution, but still generates all the moments of the system. In general, we require an object $f(t, x, p)$ that allows us to define expectation values as

$$\langle p_i^2 \rangle = \frac{\int \mathrm{d}^2 x \, \frac{\mathrm{d}^2 p}{(2\pi)^2} p_i^2 f(t, \mathbf{x}, \mathbf{p})}{\int \mathrm{d}^2 x \, \frac{\mathrm{d}^2 p}{(2\pi)^2} f(t, \mathbf{x}, \mathbf{p})} \,. \tag{2.54}$$

We choose the distribution function to be normalized such that

$$\int \frac{\mathrm{d}^2 p}{(2\pi)^2} f(t, \mathbf{x}, \mathbf{p}) = n(t, x) \tag{2.55}$$

where $n(t, x)$ is the particle number density of the system.

The second assumption is the identification of the momentum flux tensor for this distribution as in (1.14) or equivalently as an object like the relativistic energy momentum tensor,

$$T_{\mu\nu} = \int \frac{\mathrm{d}^2 p}{(2\pi)^2} \frac{p_\mu p_\nu}{p_0} f(x, p) \,, \tag{2.56}$$

in a relativistic setting. If this identification can be made for the given system and distribution function, the expectation value can be rewritten as

$$\langle p_i^2 \rangle = m^2 \frac{\int \mathrm{d}^2 x \, T_{ii}(t, x)}{\int \mathrm{d}^2 x \, \rho(t, \mathbf{x})} \,. \tag{2.57}$$

This reduces the momentum space expectation value to an integral over spatial quantities and leads to a definition of momentum anisotropy as presented in [47, 82].

The third and final assumption is, as in the derivative expansions introduced before, the specific choice of the stress tensor in terms of the hydrodynamic variables, which is necessarily already contained in the fluid dynamic simulations. For our purposes we use the ideal fluid stress tensor from equation (1.17), which leaves us with

$$
\begin{aligned}
\left\langle p_i^2/m^2 \right\rangle &= \frac{1}{Nm} \int \mathrm{d}^2 x \, \rho \left(u_i^2 + \frac{P}{\rho} \right) \\
&:= \left\langle u_i^2 \right\rangle_\rho + \left\langle P/\rho \right\rangle_\rho \; .
\end{aligned} \tag{2.58}
$$

Given the equation of state, fluid density and velocity of a system, this allows us to determine the momentum space width in either spatial direction. This method is not restricted to ideal fluids. If the first two assumptions hold, viscous corrections can be added to formula (2.58) without issue.

The reality of experimental measurement procedures, however, can add some complications to this. If the momentum variance measurement requires quenching off the interactions (as in [28]), this causes a sudden and hard to predict change in the equation of state of the system. In that case, the momentum variance in each individual direction is no longer a robustly predictable quantity. Instead, we consider the traceless part of the stress tensor, which is insensitive to the pressure and only depends on the fluid dynamic quantities ρ and $\vec{u}$ that are guaranteed to be continuous due to their evolution equations. The observable to be compared to experiments then becomes the difference between momentum variances,

$$
\begin{aligned}
\frac{1}{m^2} \left\langle p_x^2 - p_y^2 \right\rangle &= \frac{1}{Nm} \int \mathrm{d}^2 x \, \rho \left(u_x^2 - u_y^2 \right) \\
&= \left\langle u_x^2 \right\rangle_\rho - \left\langle u_y^2 \right\rangle_\rho \; .
\end{aligned} \tag{2.59}
$$

At higher orders of the derivative expansion, this acquires corrections due to shear viscosity. These would be discontinuous over the interaction quench, but are expected to be small corrections so that the prediction in (2.59) can still be fairly robust.

2.3 Numerical results

The theoretical predictions made in the previous section all still rely on a set of differential equations being solved in order to obtain predictions comparable to experiments. First, I will present a numerical solution to the inhomogeneous setting with the initial conditions predicted by hydrostatics. Noticing discrepancies in the initial condition compared to the experiment, this is complemented by a fluid dynamic simulation with an initial density profile fitted to experimental data in the second part. This prediction will be compared to experimental data for both real and momentum space. For this purpose, all numerical results will be calculated with $\omega_x = 2\pi \cdot 1.280\text{kHz}$, $\omega_y = 2\pi \cdot 3.384\text{kHz}$ and $a_{2d} = 1.17\mu\text{m}$. The number of particles in the system is

$N = 10 = 5 + 5$ unless explicitly stated otherwise. The numerical simulations were done in cooperation with Giuliano Giacalone and the experimental results were obtained and statistically evaluated by Philipp Lunt, Sandra Brandstetter, Carl Heintze and Selim Jochim (paper in preparation [74]).

2.3.1 Thomas-Fermi type density profile

In order to solve the dynamics of the Thomas-Fermi type initial condition, we need to solve the differential equations (2.40) with the initial conditions $\zeta_x(t_0) = \zeta_y(t_0) = 1$ and $\dot{\zeta}_x(t_0) = \dot{\zeta}_y(t_0) = 0$. Since this is a set of coupled ordinary differential equations without any singular behavior, this can be easily achieved numerically. Setting $t_0 = 0$ for simplicity, the solutions obtained from Mathematica's NDSolve method (which uses the method of lines [83, 84]) are shown in figure 2.5. As expected, we find that the expansion along the x-axis is slower in comparison to the initially more strongly confined y-direction. Both scaling functions become approximately linear in the long-time limit with expansion speeds,

$$\begin{aligned}
\lim_{t \to \infty} \dot{\zeta}_x &\approx 4.64 \, \mathrm{ms^{-1}} \,, \\
\lim_{t \to \infty} \dot{\zeta}_y &\approx 23.6 \, \mathrm{ms^{-1}} \,.
\end{aligned} \tag{2.60}$$

This solution leads to the time evolution of the aspect ratio as shown in the blue curve of figure 2.6. By design, it starts at the theoretically predicted ratio $\langle x^2 \rangle / \langle y^2 \rangle|_{t=0} = \omega_y/\omega_x$ and decreases from there. The cloud is round, $\langle x^2 \rangle / \langle y^2 \rangle = 1$, at $t \approx 0.172 \, \mathrm{ms}$ and for late times approaches the aspect ratio

$$\lim_{t \to \infty} \frac{\langle x^2 \rangle}{\langle y^2 \rangle} \approx 0.52 \,. \tag{2.61}$$

The evolution of the aspect ratio for different ratios of the trap frequency, but the same geometric average $\sqrt{\omega_x \omega_y}$ is shown in the other curves of figure 2.6. Overall, the time at which the ratio of the cloud's width becomes unity only weakly depends on the aspect ratio.

This ansatz does have some problems however. It predicts a non-smooth behavior of the initial density and does not feature tails, which we see in the experimental data [74]. The Thomas-Fermi profile is also overall narrower and has a larger peak density (cf. figure 2.7). Due to this, the fluid builds up more velocity and thereby elliptic flow in the long time limit.

2.3.2 Initial density from experimental data

In order to remedy the issues of the fluid static initial conditions, we instead make use of an initial density profile that is a fit to experimental data. For our simulations we use a distribution remotely similar to a Fermi-Dirac distribution,

$$\rho(t_0, \vec{x}) = \rho_0 \left[1 + \exp\left(\frac{|x|^{a_x} - b_x}{c_x} \right) \right]^{-d_x} \left[1 + \exp\left(\frac{|y|^{a_y} - b_y}{c_y} \right) \right]^{-d_y} \,, \tag{2.62}$$
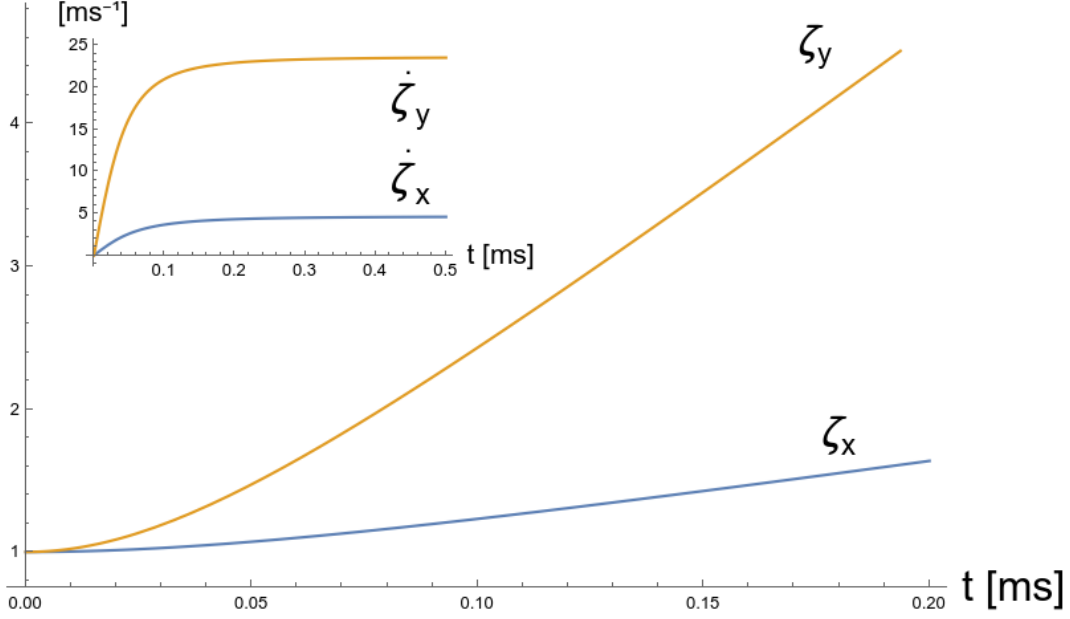
Figure 2.5: Numerical solution for the scaling functions ζ_x (orange) and ζ_y (blue) and their time derivatives (inset; same colors) for trap frequencies $\omega_x = 2\pi \cdot 1.280\text{kHz}$ and $\omega_y = 2\pi \cdot 3.384\text{kHz}$. This can also be interpreted as the position and velocity of a test particle starting at the point $(1, 1)$ in arbitrary units. The velocity converges towards a constant value after $\sim 0.15\text{ms}$ which indicates a transition to free streaming.

which allows for a flatter peak compared to a gaussian ansatz that would work well for the one particle states. This model has nine fit parameters. The normalization ρ_0 is fixed such that the integratal over the initial density becomes the total mass in the system ($m_{\text{tot}} = 10m_{\text{Li}}$). The other parameters are determined as the best fit to the two-dimensional histogram obtained from position measurements of the particles in the initial state (cf. figure 2.7), performed using a magnification technique instead of purely time of flight [74]. The values obtained for the fit parameters, obtained with scipy.optimize curve_fit, which uses a non-linear least squares method [85], are

$$a_x = 1.11643445\,, \; b_x = 3.14663841\,, \; c_x = 0.90498455\,, \; d_x = 2.14615622\,,$$
$$a_y = 0.34480747\,, \; b_y = 0.92854198\,, \; c_y = 0.11874637\,, \; d_y = 0.88257451\,. \tag{2.63}$$

The initial cloud is almost Gaussian, but with a slightly flatter plateau towards the trap center. Naturally, this fit compares much better to the experimental data than the fluid static initial conditions as shown in figure 2.7. The assumption of vanishing fluid velocity at initial time does not change. With this and the equation of state (2.25), we have all we need in order to numerically solve the continuity and Euler equation.

We chose not to implement a new numerical solver for the fluid dynamic equations ourselves, but instead modified a preexisting code. This code, named pyro [86], was
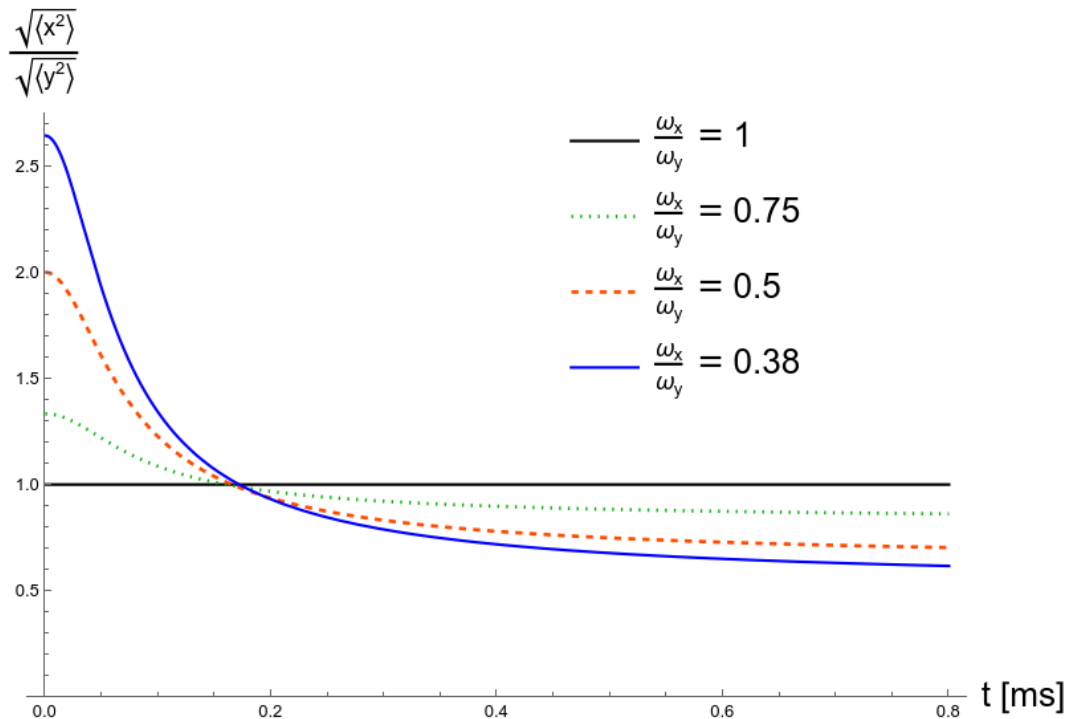
Figure 2.6: Time evolution of the aspect ratio for different trap frequency ratios at $\sqrt{\omega_x \omega_y} = 2\pi \cdot 2.081$kHz. The aspect ratio becomes unity for all anisotropic cases at similar times close to ~ 0.175ms. The initial shape inverts in all these, but not completely to the inverse of its initial aspect ratio.

used to run simulations for our initial conditions and equation of state. The compressible hydrodynamics solver contained within uses a piecewise linear reconstruction to solve the Euler equations with an upwind algorithm based on [87]. Running the code with our initial conditions, we get snapshots at different simulation times for both the density and fluid velocities in each spatial direction. From this data we calculate the three quantities we want to compare quantitatively which are $\sqrt{\langle x^2 \rangle}(t)$, $\sqrt{\langle y^2 \rangle}(t)$ and $\langle p_x^2 - p_y^2 \rangle (t)$.

The comparisons of the real space widths (figure 2.8) and the difference of squared momenta (figure 2.9) strongly suggest that the pressure predicted by our fitted equation of state (2.25) is an underestimate. This leaves our predictions for both real and momentum space consistently below the measured values. Considering that we used a macroscopic equation of state for the few-particle case, that is expected. We do not include finite size corrections. Considering that interparticle spacing, scattering length and overall system size are on the same order of magnitude in the initial state, we would have to consider the atoms not as distinct particles, but as overlapping wave packets or even a full multiparticle wave functions. These quantum contributions could increase the pressure (cf. quantum pressure in section 1.5.1). Another possible reason for the discrepancy might be that the experimental system is not exactly at zero temperature

and the resulting contributions are not negligible. In the macroscopic case, we can account for this by a temperature dependent correction to the equation of state. If we assume that there are no other scales in the system besides the scattering length, we can argue that the finite temperature correction can be modeled by multiplication with a function that only depends on the dimensionless quantity $\beta\mu$ or, equivalently, the ratio of entropy and particle number density s/n which is conserved along flowlines for ideal fluids [5]. Therefore, we choose to approximate the finite size and temperature corrections by multiplying the pressure (2.25) by a constant factor, equivalent to a spatially constant non-vanishing entropy per particle, which is an additional free parameter. As shown in figures 2.8 and 2.9 this leads to a fairly good agreement with the experimental data. We conclude that for $N = 5 + 5$ ^{6}Li atoms with $a_{2d} = 1.17\mu$m we have strong evidence for fluid dynamic behavior in the early stages of the expansion, albeit with a modified equation of state. The influence of finite size and temperature has to be investigated further in order to properly understand this modification. Experimental results and numerical simulations for other particle numbers show that this behavior breaks down below a certain number of particles (for fixed scattering length) and below a certain interaction strength (for fixed particle number) [74].
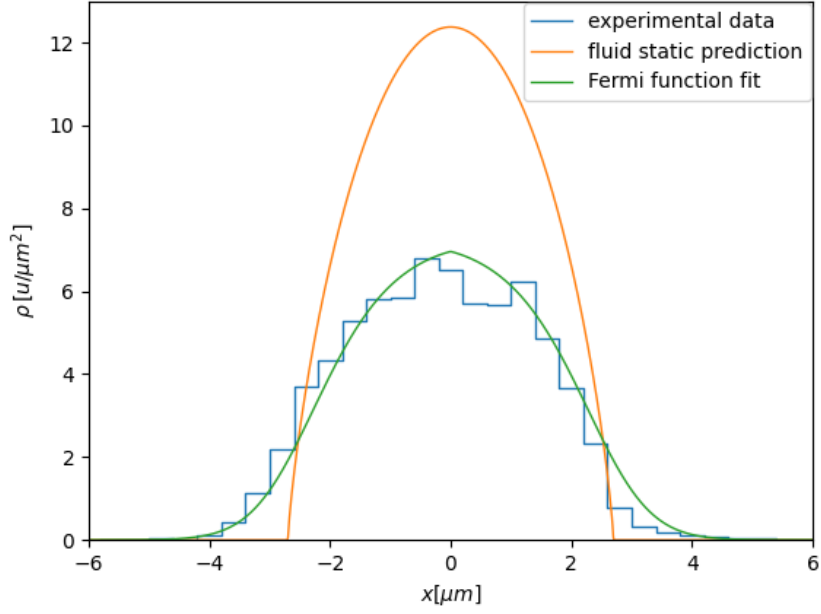
(a) Cross section of the initial density along the plane $y = 0$
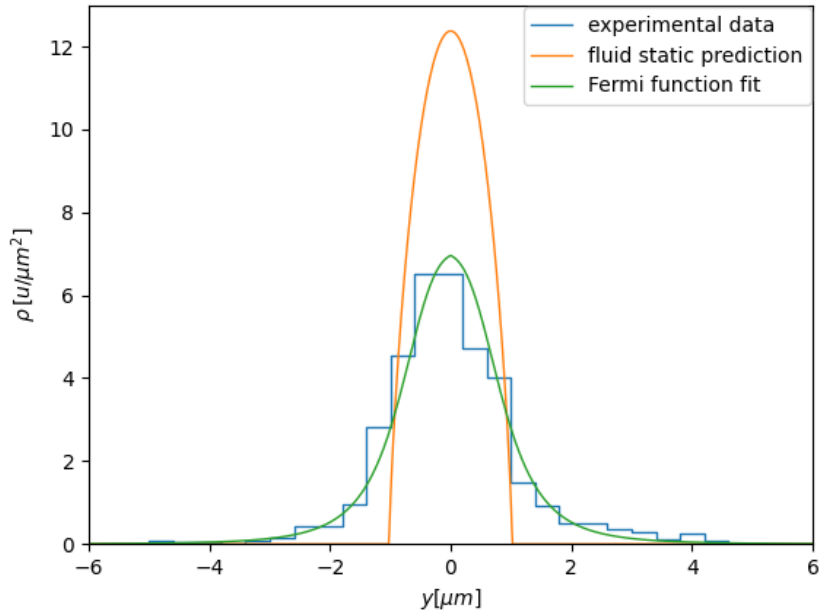
(b) Cross section of the initial density along the plane $x = 0$

Figure 2.7: Comparison of cross sections of the initial density profile along the $y = 0$ (a) and the $x = 0$ plane (b). The Thomas-Fermi type profile (orange) is much narrower than the experimentally observed one (blue). The fit of the form (2.62) (green) captures the tails and central height of the distribution much better. The experimental data is obtained as a two-dimensional histogram of the particle positions with bin size $(0.4\mu m \times 0.4\mu m)$. All density profiles were normalized to a total mass equal to the mass of 10 ^{6}Li atoms. The experimental data shown here was measured and analyzed by Sandra Brandstetter, Philipp Lunt and Carl Heintze, supervised by Selim Jochim.
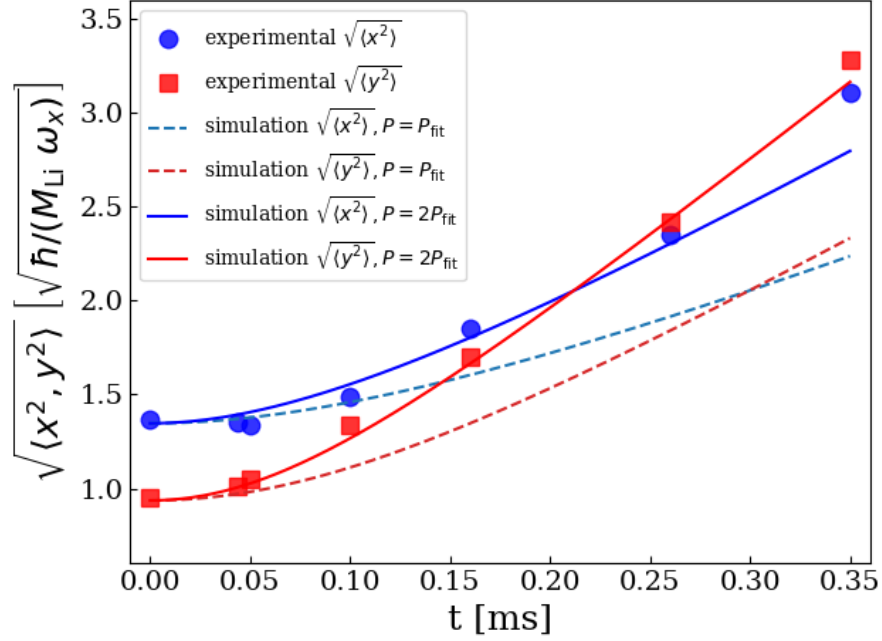
Figure 2.8: Comparison of the early time evolution of the real space widths from experiments (dots, boxes) and simulations (curves). Simulations were made with pressure both as in (2.25) (dashed curves) and at twice that value (solid curves). The simulations with increased pressure match the experimental data well and predict sign change of ellipticity at ~ 0.21ms while the curves with just the fitted pressure predict a slower expansion than observed. The experimental data shown here was measured and analyzed by Sandra Brandstetter, Philipp Lunt and Carl Heintze, supervised by Selim Jochim. Adapted from [74].
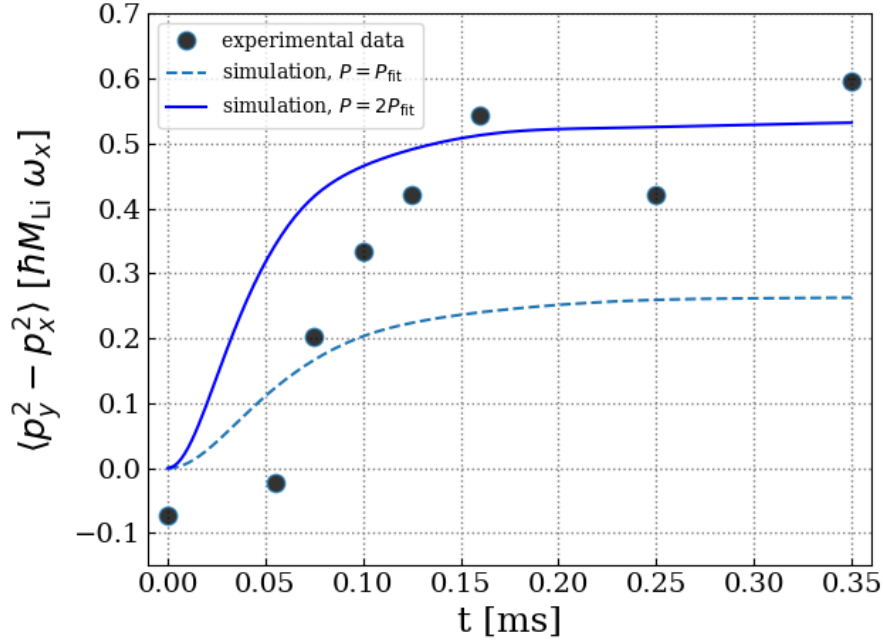
Figure 2.9: Comparison of the early time evolution of the momentum variance difference from experiments (dots) and simulations (curves). Simulations were made with pressure both as in (2.25) (dashed curve) and at twice that value (solid curve). Both curves flatten at around ~ 0.15ms in agreement with experimental results, marking the end of the acceleration of the fluid. The magnitude is much better predicted by the simulation with increased pressure. The first experimental values are negative which cannot be captured by the fluid dynamic simulations and should be investigated further. The experimental data shown here was measured and analyzed by Sandra Brandstetter, Philipp Lunt and Carl Heintze, supervised by Selim Jochim. Adapted from [74].

Chapter 3

Prediction of transport coefficients from microscopic theory

Now we approach the problem from the other side. Instead of asking what properties a microscopic system needs to have in order to qualify for a macroscopic description with fluid dynamics, we come from a macroscopic fluid and study how we can determine its transport coefficients, specifically in our case shear viscosity, from knowledge of its microscopic properties. The goal we will try to achieve is to specifically predict the shear viscosity of a scalar $\lambda\phi^4$ toy model that is comparatively easy to explore. This has been studied before in a perturbative expansion scheme [29, 30] which involves complex resummations of ladder diagrams. We will instead make use of non-perturbative functional renormalization group flow methods in order to obtain our results.

I start by introducing the elements of quantum field theory (QFT) at finite temperature that are needed for the description of the microscopic system. The next step towards the prediction of the viscosity is the idea of linear response. Utilizing the Green-Kubo relations and reformulating them in terms of functional derivatives of the 1PI effective action, it is possible to express the shear viscosity in a way that allows us to make use of functional renormalization group methods. We construct a minimalist ansatz for the effective action that can still produce non-trivial results. The last section formulates flow equations for the free parameters of our approximation and finally also for the shear viscosity. The work presented in this chapter was done together with Stefan Floerchinger and Tim Stötzel [88].

3.1 Basic objects of quantum field theory

In order to investigate the underlying microscopic theories of the macroscopic fluid systems discussed in the previous chapter, in general one needs to make use of QFT at non-zero temperature for a proper description. As such I will shortly (re)introduce in this section the mathematical objects and notations that I will work with, following along the lines of [89, 90].

In QFT, a theory is defined by knowledge of its microscopic action S which in general is a functional of a set of field operators. Observables are formulated as free

vacuum expectation values of correlation functions of these fields. They can be obtained from the generating functional (for simplicity only with one field),

$$Z[J] = \int \mathcal{D}\phi \exp\left(-iS[\phi] - i \int \mathrm{d}^4x \, J(x)\phi(x)\right),$$ (3.1)

by taking the functional derivative with respect to their corresponding source, e.g.

$$\langle \phi(x_1)\phi(x_2) \rangle = \frac{1}{Z[0]} \frac{\delta^2 Z[J]}{(-i)^2 \, \delta J(x_2)\delta J(x_1)}\bigg|_{J=0}.$$ (3.2)

The individual terms that contribute to this can be noted in the form of Feynman diagrams which encode them graphically. From the Lehmann-Symanzik-Zimmermann (LSZ) reduction formula [91] we can conclude that we need to consider amputated diagrams. Also, for the cases we are interested in only connected diagrams are relevant for physical results. The Schwinger functional can be introduced to address this,

$$W[J] = \ln(Z[J]),$$
$$\langle \phi(x_1)\phi(x_2) \rangle_c = \frac{\delta^2 W[J]}{(-i)^2 \, \delta J(x_2)\delta J(x_1)}\bigg|_{J=0}.$$ (3.3)

One can go even further to define a generating functional for only one-particle irreducible (1PI) diagrams by considering the Legendre-Fenchel transformation of the Schwinger functional,

$$\Gamma[\Phi] = \sup_J \int \mathrm{d}^4x \, J(x)\Phi(x) - W[J[\Phi]],$$
$$\Phi(x) = \frac{\delta W[J]}{\delta J} = \langle \phi \rangle_J.$$ (3.4)

$\Gamma[\Phi]$ is called the 1PI or quantum effective action since for vanishing source it provides an exact equation of motion for the one point expectation value (here for vanishing source $J = 0$)

$$\frac{\delta \Gamma[\Phi]}{\delta \Phi} = 0.$$ (3.5)

Since this can be considered like a classical action, but for Φ instead of ϕ, and $\Gamma[\Phi]$ also generates one-particle irreducible correlation functions of ϕ, we can consider most problems solved if we have exact knowledge of the form of the quantum effective action. In the following, we will assume that we are in the symmetric phase, i.e. that a possible solution to (3.5) is $\Phi = 0$ and that $\Gamma[\Phi]$ has a global minimum at this point as well.

3.1.1 Finite temperature field theory

One thermodynamic degree of freedom that we have so far neglected is the temperature. While the absence of any disordered motion in a classical picture is a reasonable assumption for the cold atom system discussed in the last chapter, it is not a good one

to make if we want to calculate a finite shear viscosity. For this purpose we need to look into how to calculate equilibrium expectation values at non-zero temperatures.

When dealing with finite temperature we can no longer treat our system as just being in any one definitive state $|\phi\rangle$, but instead need to use a density operator ρ, also called density matrix, to describe it. It can be imagined as a probability weighted projection to different states in an orthonormal basis $\{|\phi_i\rangle\}$ of the Hilbert space,

$$\rho = \sum_i p_i |\phi_i\rangle\langle\phi_i| \,. \tag{3.6}$$

It is hermitian, positive semidefinite and its trace is normalized to one. This simply reflects natural properties of the probability distribution $\{p_i\}$,

$$\begin{aligned} p_i &\in \mathbb{R}\,, \\ p_i &\geq 0\,, \\ \sum_i p_i &= 1\,. \end{aligned} \tag{3.7}$$

Expectation values of an operator $\mathcal{O}$ with respect to the density matrix are defined as the weighted average of expectation values with respect to the basis states,

$$\langle\mathcal{O}\rangle_\rho = \mathrm{tr}(\rho\mathcal{O}) = \sum_i p_i \langle\phi_i|\mathcal{O}|\phi_i\rangle \,. \tag{3.8}$$

For a thermal system we go back to a description originating from classical statistical physics, the canonical ensemble. It describes an equilibrium system that has a fixed temperature and particle number within a fixed volume. The probability of being occupied for a discrete set of states with energies $\{E_i\}$ is

$$p_i = \frac{e^{-\beta E_i}}{\sum_j e^{-\beta E_j}} \,, \tag{3.9}$$

where $\beta = T^{-1}$ is the inverse temperature. For a quantum system this translates into an equilibrium density matrix

$$\rho_{\mathrm{eq}} = \frac{e^{-\beta H}}{\mathrm{tr}(e^{-\beta H})} \,, \tag{3.10}$$

which reproduces exactly that distribution for an eigenstate basis of the Hamiltonian [3]. Neglecting the normalization $Z = \mathrm{tr}(e^{-\beta H})$, this density operator has a very similar structure to the time evolution operator $U(t) = e^{-iHt}$ known from zero-temperature QFT. Matsubara connected this to an evolution in an imaginary time coordinate $\tau = it$ [92]. With this Wick rotation we can express the density operator instead as a time evolution,

$$\rho_{\mathrm{eq}} = U(t = -i\beta) = U(\tau = \beta)\,. \tag{3.11}$$

We can confirm this interpretation by looking at a thermal expectation value of a two-point correlation function,

$$
\begin{aligned}
\langle \phi(it, x)\phi(0, y)\rangle_\rho &= \frac{1}{Z}\,\mathrm{tr}\big(e^{-\beta H}\phi(it, x)\phi(0, y)\big) \\
&= \frac{1}{Z}\,\mathrm{tr}\big(\phi(it, x)e^{-\beta H}\phi(-i\beta, y)\big) = \langle \phi(-i\beta, y)\phi(it, x)\rangle_\rho \\
&= \langle \phi(\tau = \beta, y)\phi(\tau, x)\rangle_\rho \,.
\end{aligned}
\tag{3.12}
$$

At $t = 0$ we directly find the Kubo-Martin-Schwinger (KMS) boundary condition (here with bosonic sign),

$$
\phi(\tau = 0, x) = \phi(\tau = \beta, x)\,,
\tag{3.13}
$$

implying that bosonic fields must be periodic with respect to the imaginary time (fermions would be antiperiodic). The KMS condition and Wick rotation transform our generating functional to

$$
Z_E[J] = \int \mathcal{D}\phi \; e^{-S_E[\phi] - J\cdot\phi}\,,
\tag{3.14}
$$

where we now have a structure very similar to the one we find in classical statistical field theory [89] with a euclidean action and Lagragian,

$$
S_E[\phi] = \int_0^\beta \mathrm{d}\tau \int \mathrm{d}^3 x \, \mathcal{L}_E[\phi]\,.
\tag{3.15}
$$

Like before in the zero-temperature case, derivatives of this thermal generating functional will lead to expectation values of correlation functions with respect to a thermal equilibrium state instead of a vacuum. In the same way as before we can also construct a euclidean Schwinger functional W_E and 1PI effective action Γ_E.

3.1.2 Matsubara formalism

All these changes in the construction of the path integral can be implemented into calculations in a straightforward manner. Due to the periodicity condition, the frequency space of the theory is discrete with the bosonic Matsubara frequencies,

$$
\omega_n = 2\pi n T\,.
\tag{3.16}
$$

The first step in the transition from a calculation at zero temperature to a thermal one is thus the replacement of any frequency integral by the corresponding Matsubara sum,

$$
\int \frac{\mathrm{d}p_0}{2\pi} f(p_0) \to T\sum_n f(i\omega_n)\,,
\tag{3.17}
$$

where the i in the righthand side argument automatically takes into account the change to a euclidean action. We can interpret the Matsubara sum as a sum over the poles of the function $g(z) = (1 + 2n_B(z))/2$, where $n_B(z)$ is the Bose distribution. Provided

that $f(z)$ is meromorphic, does not have any poles on the imaginary axis and converges to zero fast enough as $|z| \to \infty$, the residue theorem lets us replace this by the sum over residues of the combined function at the poles of f, here called $\{z_f\}$,

$$T \sum_n f(i\omega_n) = -\sum_{\{z_f\}} \text{Res}(f, z_f) \frac{1 + 2n_B(z_f)}{2} \, . \tag{3.18}$$

For most objects, this turns the infinite Matsubara sum into a finite one over e.g. the poles of a zero temperature propagator. In some cases however we need to chose a more complex contour to integrate along. As discussed in more detail in section 3.6, this can happen if the function in question has e.g. branch cuts.

Another thing that we need to be aware of is the fact that the Green-Kubo relation we will use to calculate the shear viscosity is formulated for real, not imaginary time. When calculating thermal expectation values using the Matsubara formalism, any incoming and outgoing frequencies also have to be treated as part of the discrete spectrum given by the KMS condition. Since in thermal equilibrium there are no net dynamics, this is usually not a problem. The slightly out of equilibrium approach of linear response theory however forces us to treat the system as if it had a meaningful real time evolution. Translating the Matsubara frequencies back to continuous frequencies corresponding to real time requires an analytic continuation of the calculated quantity. Given an expectation value calculated in the euclidean thermal framework $A_E(\omega_n)$ depending on an external Matsubara frequency, we can invert the Wick rotation to obtain a version of it in Minkowski spacetime $A_M(\omega)$ by inverting the Wick rotation [93],

$$A_M(\omega) = \lim_{\varepsilon \searrow 0} A_E(i\omega_n = \omega + i\varepsilon) \, . \tag{3.19}$$

The small positive parameter ε ensures that the poles of the Minkowski object on the real frequency axis are handled correctly (which leads to e.g. causal retarded propagators). Going back to real time correlations in this way can however lead to some problems if one does not properly ensure validity of the underlying mathematical statements. A more rigorous way that I will not explore here is the Schwinger-Keldysh formalism [94].

3.2   Linear response theory

We now have a description of a microscopic QFT at finite temperature that we will use as the basis of our investigation of transport coefficients. The next step is to approach from the macroscopic side and identify how we can relate the shear viscosity we want to predict to observables in the system and how to translate those back to the functionals we want to formulate our theory in. For this we make use of linear response theory which will be introduced following [34, 95].

As implied by the name, linear response theory deals with the leading order behavior a system previously in equilibrium exhibits when subjected to an external force. Given an observable A and an unperturbed Hamiltonian H_0 with respect to which

the system is in equilibrium, the expectation value A_{eq} will be constant in time. If at some point the system is perturbed by an external force $f(t)$, the expectation value of A is likely to change. If we assume an analytical dependence of this change on the perturbation, we can formulate the deviation of the non-equilibrium expectation value from its equilibrium counterpart as

$$\delta A(t) = A_{\mathrm{neq}}(t) - A_{\mathrm{eq}} = \int_{-\infty}^{t} G(t-t')f(t') + \mathcal{O}(f^2) \, \mathrm{d}t' \, . \qquad (3.20)$$

For a sufficiently small external force we can drop all terms above first order. In that case the response of the observable is governed by the weight $G(t-t')$ which contains the information about the systems response to the perturbation and conversely also how it relaxes back to its equilibrium state when the force goes away. For reasons of causality this response function must vanish for negative arguments. We can get access to this information loaded quantity by functional derivation

$$G(t-t') = \left. \frac{\delta A(t)}{\delta f(t')} \right|_{f=0} . \qquad (3.21)$$

Notably, the response function does not depend on the external force. It is a property already encoded in the equilibrium system. In a field theoretical context we reformulate the external force as a perturbation to the action containing an external gauge field A_μ that couples to the observable j^μ,

$$S = S_0 + S_{\mathrm{int}} = S_0[j^\mu] + \int \mathrm{d}^4x \, A_\mu(x)j^\mu(x) \, . \qquad (3.22)$$

The deviation in expectation value takes the form

$$\delta \langle j^\mu \rangle (x) = \int \mathrm{d}^4x' \, K^{\mu\nu}(x-x')A_\nu(x') + \mathcal{O}(A^2) \qquad (3.23)$$

with a response kernel $K^{\mu\nu}(x-x')$ that vanishes for any separation between x and x' that is spacelike or past-pointing. Seeing that our observable can be expressed as

$$j^\mu = \frac{\delta S}{\delta A_\mu} \, , \qquad (3.24)$$

we can construct a generating functional $W[A_\mu]$ of the external gauge field that allows the expectation value to be formulated as (using a euclidean signature)

$$\langle j^\mu \rangle = - \left. \frac{\delta W[A_\mu]}{\delta A_\mu} \right|_{A=0} . \qquad (3.25)$$

This functional also automatically contains the response kernel as the next higher functional derivative,

$$K^{\mu\nu}(x-x') = - \left. \frac{\delta^2 W[A]}{\delta A_\mu(x)\delta A_\nu(x')} \right|_{A=0} . \qquad (3.26)$$

The object $W[A_\mu]$ has a straightforward interpretation in QFT as the Schwinger functional.

3.2.1 Green-Kubo relations

Kubo managed to find formulas for the response of an observable A of a statistical or quantum ensemble to an adiabatically switched on external force [96]. If that force is proportional to some other observable B of the system, $F(t) = B \cdot f(t)$, the linear response function of A to a perturbation in B becomes

$$
\begin{aligned}
G_{AB}(t - t') &= -i \operatorname{tr}(\rho[B, A(t - t_0)]) \,, \\
A(t) &= e^{iHt} A e^{-iHt} \,,
\end{aligned}
\tag{3.27}
$$

for a density matrix ρ that commutes with the unperturbed Hamiltonian. In the case of a canonical density matrix $\rho \sim e^{-\beta H}$, the commutator can even be eliminated in favor of an integration in complex time direction,

$$
G_{AB}(t - t') = - \int_0^\beta \mathrm{d}\lambda \operatorname{tr}\left(\rho B(-i\lambda) \dot{A}(t - t_0) \right) .
\tag{3.28}
$$

Kubo's method can even be applied multiple times in order to obtain higher order, i.e. non-linear, response functions [96].

This means in order to arrive at an expression for the shear viscosity in terms of QFT functionals, we need to first identify what type of response it quantifies. In this thesis we will limit ourselves to the response to a static displacement, i.e. the static susceptibility χ_{AB} of the system. For the Green-Kubo relations this translates into the zero frequency mode of the regularized Laplace transform of the real time response function,

$$
\begin{aligned}
G_{AB}(\omega) &= \lim_{\varepsilon \searrow 0} \int_0^\infty \mathrm{d}t \, G_{AB}(t) e^{-i\omega t - \varepsilon t} \,, \\
\chi_{AB} &= \lim_{\omega \to 0} G_{AB}(\omega) \,.
\end{aligned}
\tag{3.29}
$$

Instead of a Laplace transformation this can also be interpreted as the Fourier transformation of the retarded response function $G_{AB}^R(t) = \theta(t) G_{AB}(t)$. In the quantum field theoretical formulation we want to archieve, we need to make some changes that let us express the involved quantities as field operators,

$$
\begin{aligned}
G_{AB}^R(\omega, \vec{p}) &= \lim_{\varepsilon \searrow 0} \int_0^\infty \mathrm{d}t \int \mathrm{d}^3 p \, (-i) \operatorname{tr}(\rho[B(0,0), A(t, \vec{x})]) \, e^{-i(\omega t - \vec{p} \cdot \vec{x}) - \varepsilon t} \,, \\
\chi_{AB} &= \lim_{\omega \to 0} \lim_{\vec{p} \to 0} G_{AB}^R(\omega, \vec{p}) \,.
\end{aligned}
\tag{3.30}
$$

What remains to be determined is the specific nature of the operators A and B. Shear viscosity disperses gradients in the fluid velocity perpendicular to the local flow of the fluid. In that way it can be seen as a transversal transport of momentum as a response to the presence of transversal anisotropy of momentum. As shown in [31, 32] this can be related to the retarded response function of the energy momentum tensor or in QFT terms, its retarded two-point correlation function,

$$
G_{T^{xy}T^{xy}}^R(\omega, \vec{p} \to 0) = P - i\omega\eta + \dots .
\tag{3.31}
$$

We can construct this function from the standard QFT functionals by introducing an external spacetime metric $g_{\mu\nu}$ which is minimally coupled to the fields,

$$S[\phi] = \int \mathrm{d}^4 x \, \mathcal{L}[\phi, \eta_{\mu\nu}] \to S[\phi, g_{\mu\nu}] = \int \mathrm{d}^4 x \, \sqrt{-g} \mathcal{L}[\phi, g_{\mu\nu}] \,. \tag{3.32}$$

The energy momentum tensor of the matter content of the theory can be obtained as metric derivatives of the action,

$$T^{\mu\nu}(x) = \frac{2}{\sqrt{-g}} \frac{\delta S[\phi, g_{\alpha\beta}]}{\delta g_{\mu\nu}(x)} \,, \tag{3.33}$$

and its connected expectation value correspondingly as a derivative of the Schwinger functional parametrized with the external metric,

$$\langle T^{\mu\nu} \rangle (x) = \frac{2}{\sqrt{-g}} \left. \frac{\delta W[J, g_{\alpha\beta}]}{\delta g_{\mu\nu}(x)} \right|_{J=0} \,. \tag{3.34}$$

Identifying the deviations of the metric from the Minkowski metric as the force causing the energy momentum tensor to respond, we can formulate the response function as in (3.23),

$$\delta \langle T^{\mu\nu} \rangle (x) = - \int \mathrm{d}^4 x' \, \sqrt{-g} \, G^{\mu\nu\alpha\beta}(x - x') \, \delta(g_{\alpha\beta}(x') - \eta_{\alpha\beta}) \,. \tag{3.35}$$

Relating this back to a functional derivative of the Schwinger functional, we find

$$W^{(0,2)\mu\nu\alpha\beta}[J = 0; g_{\mu\nu} = \eta_{\mu\nu}](x, x') = -G^{\mu\nu\alpha\beta}(x - x') + \eta^{\alpha\beta} \langle T^{\mu\nu} \rangle (x') \delta(x - x') \,, \tag{3.36}$$

with the shorthand notation

$$W^{(i,j)\alpha_1\beta_1\cdots\alpha_j\beta_j}(x_1, \ldots, x_i, y_1, \ldots, y_j) = \prod_{n_i=1}^{i} \frac{\delta}{\delta J(x_{n_i})} \prod_{n_j=1}^{j} \frac{\delta}{\delta g_{\alpha_{n_j}\beta_{n_j}}(y_{n_j})} W \,, \tag{3.37}$$

up to powers of $-i$ or -1 depending on whether we work in a Minkowskian or euclidean theory. The second term in equation (3.36) is a contact term that we can ignore for our calculation since it vanishes for $\alpha \neq \beta$. Under the assumption that the field vacuum expectation value $\Phi = \langle \phi \rangle$ is not directly dependent on the metric, it can be shown from definition (3.4) that we can reformulate this in terms of the 1PI effective action as [88]

$$W^{(0,2)\mu\nu\alpha\beta}|_{J=0} = -\Gamma^{(0,2)\mu\nu\alpha\beta}|_{\Phi=0} \,. \tag{3.38}$$

We can thus relate the shear viscosity η as a macroscopic transport coefficient on one side to functional derivatives of the quantum effective action Γ on the other side. With the right approach to the Wick rotation, we can obtain the retarded correlation function automatically from the thermal QFT formalism. The functional representation of the shear viscosity then becomes [88]

$$\eta = \lim_{\omega \to 0} \lim_{\vec{p} \to 0} \partial_\omega \, \mathrm{Im} \lim_{\varepsilon \searrow 0} \Gamma_E^{(0,2)xyxy}(\omega + i\varepsilon, \vec{p})|_{g_{\mu\nu}=\eta_{\mu\nu}, \Phi=0} \,. \tag{3.39}$$

3.3 Non-relativistic limit of scalar field theory

We now have a way to express the shear viscosity using the 1PI effective action of a relativistic QFT on a general background metric. The fluid dynamic description that we have been working with so far is however a non-relativistic one. This can be resolved by either going to relativistic fluid dynamics using for example the Isreal-Stewards equations [97] or by considering the non-relativistic limit on the field theory side. In this section I will do the latter following the paper [98] by Stefan Floerchinger and myself.

3.3.1 Minkowskian background

In order to understand how the non-relativistic limit of a scalar field theory works for a general spacetime metric, we first approach the problem specifically for a Minkowskian background. A transformation from the relativistic field ϕ to a non-relativistic one ψ that works for QFT needs to both transform the classical field theory in the desired way and not be anomalous with respect to the path integral measure. For a complex scalar field, a straightforward approach is to separate out the oscillation due to rest mass energy,

$$\phi = \frac{1}{\sqrt{2m}} e^{-imc^2} \psi \, , \tag{3.40}$$

and do an expansion of the Klein-Gordon equation in terms of orders in the speed of light and take the limit $c \to \infty$. The non-relativistic field obeys the free Schroedinger equation,

$$i\dot{\psi} = -\frac{\vec{\nabla}^2}{2m} \psi \, . \tag{3.41}$$

This transformation however neglects the antiparticle excitations that would be contained in a relativistic theory of a complex scalar. This can also be seen as equivalent to going from the second order (in time) Klein-Gordon equation to the first order Schroedinger equation. Further, the equivalent transformation for real scalar fields, defined as the real part of equation (3.40) (cf. [99]), produces equations of motions with fast-oscillating terms ($\sim e^{\pm 2imc^2}$) which are usually neglected, but can in principle backreact onto the slower modes [100]. All in all this transformation is not invertible for complex scalars and not fit for our purposes in general.

There is however a more involved way of handling this problem. Namjoo, Guth and Kaiser found a transformation for a real scalar field that does not lose any information [100]. Starting from the Lagrangian of a free real scalar field,

$$\mathcal{L} = \frac{1}{2} \eta^{\mu\nu} (\partial_\mu \phi)(\partial_\nu \phi) - \frac{1}{2} m^2 \phi^2 \, , \tag{3.42}$$

the non-relativistic field is defined as a combination of the relativistic field and its time

derivative,

$$\psi = \sqrt{\frac{m}{2}} e^{imt} \left(\mathcal{P}^{\frac{1}{2}} \phi + \frac{i}{m} \mathcal{P}^{-\frac{1}{2}} \dot{\phi} \right),$$
$$\psi^* = \sqrt{\frac{m}{2}} e^{-imt} \left(\mathcal{P}^{\frac{1}{2}} \phi - \frac{i}{m} \mathcal{P}^{-\frac{1}{2}} \dot{\phi} \right),$$

(3.43)

where $\mathcal{P}$ is the differential operator

$$\mathcal{P} = \sqrt{1 - \frac{\vec{\nabla}^2}{m^2}} = 1 - \frac{\vec{\nabla}^2}{2m^2} - \frac{(\vec{\nabla}^2)^2}{8m^4} + \dots .$$

(3.44)

We will refer to this transformation as the NGK transformation in the following. Fractional powers of the differential operator are defined via the corresponding modification of the Taylor series. With the Fourier space identification $-\vec{\nabla}^2 \sim \vec{p}^2$ this series can also be understood as an expansion for kinetic energies small compared to the rest mass $\vec{p}^2/m^2 \ll 1$. Also, $\mathcal{P}$ is notably non-local in space since it contains arbitrarily large derivatives. The Lagrangian and equation of motion for the transformed field are

$$\mathcal{L} = \frac{i}{2}(\psi^* \dot{\psi} - \dot{\psi}^* \psi) - \psi^* m(\mathcal{P} - 1)\psi ,$$
$$i\dot{\psi} = m(\mathcal{P} - 1)\psi \approx -\frac{\vec{\nabla}^2}{2m}\psi .$$

(3.45)

To lowest non-trivial order in $\vec{p}^2/m^2$ this recovers the Schroedinger equation that we are looking for. Instead of a second order in time differential equation for a real scalar field, we now have a first order equation for a complex field. Thus, we do not lose any information in the transformation. It is invertible. Relativistic corrections can be added systematically by taking into account higher order terms in the expansion. The NGK transformation can be also applied to an interacting $\lambda \phi^4$ theory [100]. At lowest order this again reproduces a $c \to \infty$ result for a complex scalar while higher orders add derivative interactions.

3.3.2   General background metric

In order to apply this transformation to the generic metric case we are interested in, we try to formulate the problem in a covariant way as opposed to specifically singling out time as before. This more general approach will also help us understand whether this type of transformation affects the path integral measure in general. We start from the action of a free massive real scalar field this time on a general background metric g with minimal coupling,

$$S = \int \mathrm{d}^4 x \sqrt{-g} \left\{ -\frac{1}{2} g^{\mu\nu} (\nabla_\mu \phi)(\nabla_\nu \phi) - \frac{1}{2} m^2 \phi^2 \right\} .$$

(3.46)

The equation of motion that governs the dynamics of ϕ is

$$-g^{\mu\nu}\nabla_\mu\partial_\nu\phi + m^2\phi = 0 \,, \tag{3.47}$$

where ∇_μ denotes a metric covariant derivative. Next, we need to choose to which observers the system appears to be non-relativistic. This is done by the choice of a time-like vector field u^μ normalized to minus unity. In essence this defines rest frames of the observers as the ones in which all components except the zero-component vanish. This specifies a time direction for the non-relativistic dynamics. We define the projector to the spatial directions as

$$\Delta_{\mu\nu} = g_{\mu\nu} + u_\mu u_\nu \,. \tag{3.48}$$

Similarly to the NGK transformation, we define the non-relativistic field as a linear combination of the relativistic field and its time derivative with possibly different spatial derivative operators applied to them,

$$\psi = \alpha \left(\phi + i\gamma\, u^\mu\partial_\mu\phi \right). \tag{3.49}$$

If a particle has 4-momentum p^μ, the non-relativistic limit from the perspective of an observer defined by u^μ can be understood as

$$\frac{\Delta_{\mu\nu}p^\mu p^\nu}{(u_\sigma p^\sigma)^2} \ll 1 \,. \tag{3.50}$$

By making use of equation (3.47) we can write down the time derivative of the non-relativistic field as

$$\begin{aligned}
u^\mu\partial_\mu\psi =& [u^\mu\partial_\mu\alpha + i\alpha\gamma(-m^2 + \nabla_\mu\Delta^{\mu\nu}\partial_\nu)]\phi \\
&+ [\alpha + iu^\nu\partial_\nu\alpha\gamma - i\alpha\gamma\nabla_\mu u^\mu](u^\mu\partial_\mu\phi) \,.
\end{aligned} \tag{3.51}$$

In order for the equation of motion of ψ to be first order in time derivatives, the righthand side of this equation needs to be proportional to ψ itself (up to spatial derivates). This restricts γ to solutions of the differential equation

$$u^\nu\partial_\nu\gamma + i(m^2 - \nabla_\mu\Delta^{\mu\nu}\partial_\nu)\gamma^2 - (\nabla_\mu u^\mu)\gamma - i = 0 \,. \tag{3.52}$$

Here the spatial derivatives are to be understood as a variable akin to the momentum $\vec{p} \sim -i\vec{\nabla}$ in the non-relativistic case. The solutions to this equation are time dependent series of spatial derivatives. We can formulate another restraint by demanding that the equal time commutation relations of the relativistic and non-relativistic field differ only by a phase factor,

$$[\phi(t,x), \phi(t,y)] = i[\psi(t,x), \psi^*(t,y)] = i\delta(x-y) \,. \tag{3.53}$$

On the side of the transformation this is equivalent to

$$|\alpha|^2 = (2\,\mathrm{Re}(\gamma))^{-1} \,, \tag{3.54}$$

where the operations on α and γ are to be understood on an eigenbasis of $\nabla_\mu \Delta^{\mu\nu} \partial_\nu$. The remaining freedom that we have is the choice of initial condition for the differential equation (3.52) and the complex argument of α. The equation of motion and Lagrangian for the non-relativistic field are

$$i \left[u^\mu \partial_\mu \psi + \frac{1}{2}(\nabla_\mu u^\mu)\psi \right] = - \left[u^\mu \partial_\mu \arg(\alpha) - (m^2 - \nabla_\mu \Delta^{\mu\nu}\partial_\nu)\operatorname{Re}(\gamma) \right] \psi \,,$$

$$\mathcal{L} = \frac{i}{2} \left[(u^\mu \partial_\mu \psi)\psi^* - \psi(u^\mu \partial_\mu \psi^*) \right] + \psi^* \left[u^\mu \partial_\mu \arg(\alpha) - (m^2 - \nabla_\mu \Delta^{\mu\nu}\partial_\nu)\operatorname{Re}(\gamma) \right] \psi \,. \tag{3.55}$$

A more detailed calculation of this can be found in [98]. We recover the NGK transformation for $g_{\mu\nu} = \eta_{\mu\nu}$ with the choices $u^\mu = (1,0,0,0)^T$, $u^\mu \partial_\mu \arg(\alpha) = m$ and $u^\mu \partial_\mu \gamma|_{t_0} = 0$. In that case the solutions for (3.52) and α are

$$\gamma = (m\mathcal{P})^{-1} \,,$$
$$\alpha = \sqrt{\frac{m}{2}} \mathcal{P}^{1/2} e^{imt} \,, \tag{3.56}$$

which agree perfectly with (3.43). In the context of a clearly defined time direction we can also go to a Hamiltonian formulation of the problem. We find that the near-conservation of the commutation relations is equivalent to the transformation from the relativistic field and its conjugate momentum to the real and imaginary parts of the non-relativistic field being a canonical transformation (cf. [98]).

3.3.3 Transformation of the path integral measure

So far, the transformation works well on a classical level. It transforms the action in the way that we want in order to formulate a non-relativistic limit. We are, however, working in a QFT so we also need to make sure that there are no anomalies introduced to the theory by this transformation. Such an anomaly could manifest in a non-unity Jacobian of the change of coordinates from the relativistic to the non-relativistic degrees of freedom. On the relativistic side we consider the relativistic field and its conjugate momentum field $\pi = u^\mu \partial_\mu \phi$ as independent while on the non-relativistic side the relevant fields are ψ and its complex conjugate ψ^*. In order to study the transformation of the path integral measure, we make use of Fujikawa's method [101]. We consider a complete orthonormal basis of eigenfunctions $\hat{\lambda}_n$ of the generalized Laplace-Beltrami operator $-\nabla_\mu \Delta^{\mu\nu} \partial_\nu$ with eigenvalues λ_n. We do not explicitly prove the existence of such a basis, but instead restrict the space of fields we consider to the span of the maximal choice of $\{\hat{\lambda}_n\}$ that are sufficiently well-behaved for our calculations. This allows us to decompose the involved field into (possibly infinite) linear combinations,

$$\phi = \sum_n a_n(t)\hat{\lambda}_n \,, \qquad u^\mu \partial_\mu \phi = \sum_n b_n(t)\hat{\lambda}_n \,,$$
$$\psi = \sum_n a'_n(t)\hat{\lambda}_n \,, \qquad \psi^* = \sum_n b'_n(t)\hat{\lambda}_n \,. \tag{3.57}$$

63

The operators α and γ can now be explicitly treated as functions of λ_n for each summand. The transformation from relativistic to non-relativistic field can in this formulation be understood as the transformation from (a_n, b_n) to (a'_n, b'_n). It is given by the projection onto the corresponding eigenfunction and can be inferred directly from (3.49),

$$
\begin{aligned}
a'_n(t) &= \hat{\lambda}_n^\dagger \cdot \psi = \alpha(\lambda_n)[a_n(t) + i\gamma(\lambda_n)b_n(t)]\,, \\
b'_n(t) &= \hat{\lambda}_n^\dagger \cdot \psi^* = \alpha^*(\lambda_n)[a_n(t) - i\gamma^*(\lambda_n)b_n(t)]\,.
\end{aligned}
\tag{3.58}
$$

The Jacobian of the transformation can be understood as the determinant of a block matrix,

$$
\begin{aligned}
J &= \left| \det \begin{pmatrix} \frac{\partial a'_m}{\partial a_n} & \frac{\partial a'_m}{\partial b_n} \\ \frac{\partial b'_m}{\partial a_n} & \frac{\partial b'_m}{\partial b_n} \end{pmatrix} \right| \\
&= \left| \det \begin{pmatrix} \delta_{mn}\alpha(\lambda_n) & i\delta_{mn}\alpha(\lambda_n)\gamma(\lambda_n) \\ \delta_{mn}\alpha^*(\lambda_n) & -i\delta_{mn}\alpha^*(\lambda_n)\gamma^*(\lambda_n) \end{pmatrix} \right| \\
&= \left| \det\left(-i\delta_{mn}|\alpha(\lambda_n)|^2(\gamma^*(\lambda_n) + \gamma(\lambda_n))\right) \right| \\
&= |\det(-i\delta_{mn})| = 1\,,
\end{aligned}
\tag{3.59}
$$

where we applied condition (3.54) in the next-to-last step. Exactly when the transformation is canonical (from the Hamiltonian point of view) and conserves the equal time commutation relations (from the point of view of canonical quantisation), it also leaves the path integral measure invariant. Hence this transformation is a viable way to move towards a non-relativistic limit on the QFT side of things. For interacting theories we use the same transition to non-relativistic degrees of freedom and expand the new terms in the equations of motion up to the desired order in p^2/m^2 as shown in [100] and also section 3.3.5.

3.3.4 Further properties of the transformation

Besides the properties that make it fit for an interpretation as a non-relativistic limit, our real scalar transformation brings with it some other features. First of all, the transformation of the real scalar fields can naturally be expanded to cover complex scalar fields. For that, we consider the standard decomposition of a complex scalar Φ into two real scalar fields,

$$
\Phi = \frac{1}{\sqrt{2}}(\phi_1 + i\phi_2)\,.
\tag{3.60}
$$

Each of these real scalars can be transformed in the previously discussed way into their non-relativistic counterparts ψ_1 and ψ_2. The non-relativistic equivalent of the complex relativistic field are two complex fields defined as transformations of the effectively independent fields Φ and Φ^*,

$$
\begin{aligned}
\Psi_1 &= \alpha(\Phi + i\gamma u^\mu \nabla_\mu \Phi) = \frac{1}{\sqrt{2}}(\psi_1 + i\psi_2)\,, \\
\Psi_2 &= \alpha(\Phi^* + i\gamma u^\mu \nabla_\mu \Phi^*) = \frac{1}{\sqrt{2}}(\psi_1 - i\psi_2)\,.
\end{aligned}
\tag{3.61}
$$

With the same conditions on α and γ as before, this transforms the action of a relativistic free complex scalar field,

$$S_{\text{rel}} = \int \mathrm{d}^4x \,\sqrt{-g} \left\{ -\frac{1}{2} g^{\mu\nu} (\nabla_\mu \Phi^*)(\nabla_\nu \Phi) - \frac{1}{2} m^2 |\Phi|^2 \right\} , \qquad (3.62)$$

into that of two completely decoupled non-relativistic fields,

$$
\begin{aligned}
S_{\text{NR}} = \int \mathrm{d}^4x \sqrt{-g} \sum_{n=1}^{2} & \left\{ \frac{i}{2} ((u^\mu \partial_\mu \Psi_n)\Psi_n^* - \Psi_n (u^\mu \partial_\mu \Psi_n^*)) \right. \\
& \left. + \Psi_n^* \left(u^\mu \partial_\mu \arg(\alpha) - (m^2 - \nabla_\mu \Delta^{\mu\nu} \partial_\nu) \operatorname{Re}(\gamma) \right) \Psi_n \right\} .
\end{aligned}
\qquad (3.63)
$$

Here we also find the true analogon to the $c \to \infty$ limit for the complex scalar. That is exactly the result you obtain by truncating the expansion in Laplace-Beltrami operators at the lowest non-trivial order and demanding that $\Phi_2 = 0$ everywhere. This explicitly demonstrates that method's neglect of the degrees of freedom associated with antiparticles which are demoted from a decoupled, but still dynamical field to a constant. Especially in interacting scenarios which mix Ψ_1 and Ψ_2 this would lose terms that could contribute significantly to the dynamics of the system.

The second important property of the transformation is that it lets additional symmetries emerge. In addition to the invariance under coordinate transformations guaranteed by the covariant formulation, we find that there is an additional global $U(1)$ symmetry in the non-relativistic action,

$$\psi \to e^{i\varphi} \psi , \quad \psi^* \to e^{-i\varphi} \psi^* , \qquad (3.64)$$

that is not present in the relativistic one. A look at the associated Noether charge,

$$Q = \int \mathrm{d}^3x \,\sqrt{-g} |\psi|^2 , \qquad \dot{Q} = 0 , \qquad (3.65)$$

tells us that this new symmetry can be interpreted as the conservation of total particle number from the perspective of a quantum-mechanical wave function. This includes any loss effects due to e.g. cosmological expansion. Correspondingly, this symmetry can in general be broken by additional interaction terms that introduce particle number changing processes. In the expansion scheme presented by NGK, however, the symmetry is explicitly kept and can thus never account for these processes. This is no surprise since a change in particle number always involves at least one particle with kinetic energy on the same scale as its rest mass and can as such never be considered non-relativistic. We find a similar emergent symmetry for the complex scalar field where the $U(1)$ symmetry of the non-interacting relativistic action is promoted to a $U(2)$ symmetry for the non-relativistic fields which accounts for individual particle and antiparticle number conservations as well as symmetry under rotating Ψ_1 and Ψ_2 into each other. Interaction terms also break this symmetry, but if the new term conserves the $U(1)$ symmetry present in the relativistic action, there is a remaining $U(1)$ on the non-relativistic side as well,

$$\Psi_1 \to e^{i\varphi} \Psi_1, \qquad \Psi_2 \to e^{-i\varphi} \Psi_2 . \qquad (3.66)$$

The corresponding Noether charge,

$$Q = \int \mathrm{d}^3x \, \sqrt{-g}(|\Psi_1|^2 - |\Psi_2|^2) \,, \qquad \dot{Q} = 0 \,, \tag{3.67}$$

is the net particle number which is also conserved in the relativistic description. This feature is present without any expansion in non-relativistic momentum.

The last property discussed here is that, in specific cases, the transformation to a non-relativistic field can be understood as a Bogoliubov transformation, i.e. a transformation of the annihilation and creation operators, which will be shortly introduced following [102]. For this we use the standard decomposition for the relativistic field,

$$\phi = \int \frac{\mathrm{d}^3k}{(2\pi)^3}(a_{\vec{k}} f_{\vec{k}}(t)e^{i\vec{k}\vec{x}} + a_{\vec{k}}^\dagger f_{\vec{k}}^*(t)e^{-i\vec{k}\vec{x}}) \,,$$
$$\dot{\phi} = \int \frac{\mathrm{d}^3k}{(2\pi)^3}(a_{\vec{k}} \dot{f}_{\vec{k}}(t)e^{i\vec{k}\vec{x}} + a_{\vec{k}}^\dagger \dot{f}_{\vec{k}}^*(t)e^{-i\vec{k}\vec{x}}) \,, \tag{3.68}$$

where $f_{\vec{k}}(t)$ is an appropriately chosen mode function that is (in combination with the Fourier factor) a solution to the classical field equations and ensures that the integral transforms properly under coordinate transformations. In order to get the standard commutation relations for creation and annihilation operators, they must be normalized such that

$$\mathrm{Im}(f_{\vec{k}}^*(t)\dot{f}_{\vec{k}}(t)) = -\frac{1}{2} \,. \tag{3.69}$$

For a general background metric, the mode function might not just depend on the non-relativistic observer time, but also the spatial position. In these scenarios the concept of a spatial Fourier transformation also breaks down. We will neglect this possibility in the following considerations. The non-relativistic field can be expressed through annihilation and creation operators in a similar way,

$$\psi = \int \frac{\mathrm{d}^3k}{(2\pi)^3}b_{\vec{k}}e^{i\vec{k}\vec{x}} \,,$$
$$\psi^* = \int \frac{\mathrm{d}^3k}{(2\pi)^3}b_{\vec{k}}^\dagger e^{-i\vec{k}\vec{x}} \,. \tag{3.70}$$

If we can represent this change of operators as a linear transformation

$$b_{\vec{k}} = u_{\vec{k}} a_{\vec{k}} + v_{-\vec{k}}^* a_{-\vec{k}}^\dagger \,,$$
$$b_{\vec{k}}^\dagger = u_{\vec{k}}^* a_{\vec{k}}^\dagger + v_{-\vec{k}} a_{-\vec{k}} \,, \tag{3.71}$$

and the coefficients fulfill $|u_{\vec{k}}|^2 - |v_{-\vec{k}}|^2 = 1$, this is a so-called Bogoliubov transformation and the commutation relations for the old and new creation and annihilation operators remain the same. Indeed we find that the transformation is linear under the

assumption $f_{\vec{k}} = f_{-\vec{k}}$ with

$$u_{\vec{k}} = \alpha_k \left(1 + i\gamma_k \frac{\dot{f}_{\vec{k}}}{f_{\vec{k}}}\right) f_{\vec{k}} \,,$$

$$v^*_{-\vec{k}} = \alpha_k \left(1 + i\gamma_k \frac{\dot{f}^*_{\vec{k}}}{f^*_{\vec{k}}}\right) f^*_{\vec{k}} \,,$$

(3.72)

where α_k and γ_k are the transformation operators with each instance of the generalized Laplace-Beltrami operator replaced by k^2. The normalization condition is also fulfilled,

$$|u_{\vec{k}}|^2 - |v_{-\vec{k}}|^2 = -4|\alpha_k|^2 \operatorname{Re}(\gamma_k) \operatorname{Im}(f^*_{\vec{k}} \dot{f}_{\vec{k}}) = 1 \,. \tag{3.73}$$

We see that the validity of the description as a Bogoliubov transformation again hinges on condition (3.54). In the case of a Minkowski metric with standard mode function $f_{\vec{k}} = (2\sqrt{\vec{k}^2 + m^2})^{-1/2} \exp\left(i\sqrt{\vec{k}^2 + m^2} t\right)$ we even find that $v_k = 0$ which implies that the relativistic and non-relativistic theory have the same vacuum state. Such a statement is difficult to prove for more general spacetime choices since both the choice of the mode functions and the initial condition for γ are not unique.

3.3.5 Real scalar on a cosmological background

As a specific example in this section I will discuss the non-realtivistic transformation for the case of a Friedmann-Lemaître-Robertson-Walker (FLRW) metric,

$$g_{\mu\nu} = \operatorname{diag}(-1, a^2(t), a^2(t), a^2(t)) \,. \tag{3.74}$$

The scale factor $a(t)$ is in this case treated as an external parameter fixed by the content of our chosen universe. The FLRW metric allows us to choose the observer frame $u^\mu = (1, 0, 0, 0)^T$. The concept of a Fourier transformation from real to momentum space is however not by default valid for this spacetime anymore. The choice of frame lets us formulate the derivative operators as

$$u^\mu \partial_\mu \psi = \partial_t \psi \,,$$

$$\nabla_\mu \Delta^{\mu\nu} \partial_\nu \psi = a^{-2} \vec{\nabla}^2 \psi \,.$$

(3.75)

With the further identification $\nabla_\mu u^\mu = 3H$, introducing the Hubble function $H = \dot{a}/a$, we have everything we need to solve (3.52) except the initial condition. We resolve that by selecting the solution that matches the NGK transformation in the limit $a(t) \to 1$ everywhere. For this purpose we define a slightly modified version of the differential operator used before,

$$\mathcal{P}_a = \sqrt{1 - \frac{\vec{\nabla}^2}{a^2 m^2}} \,, \tag{3.76}$$

and expand γ in terms of this operator and orders in the quantity H/m which will be small in the aforementioned limit (and in a standard cosmology at late times),

$$\gamma = \sum_{n=0}^{\infty} f_n(\mathcal{P}_a) \left(\frac{H}{m}\right)^n, \tag{3.77}$$

where the coefficients f_n are analytical (or meromorphic) functions and the expression $f_n(\mathcal{P}_a)$ is to be understood as a differential operator defined by the corresponding power series. The lowest order of this is fixed by our chosen initial condition to be $f_0(x) = 1/(mx)$. From that point we can solve equation (3.52) order by order in H/m. At next-to-leading order the coefficient function becomes complex-valued (assuming a real argument),

$$f_1(x) = -\frac{i}{2m}(x^{-4} + 2x^{-2}). \tag{3.78}$$

Hence the solution for the transformation up to that order becomes

$$\alpha = \sqrt{\frac{m}{2}} \mathcal{P}_a^{1/2} e^{imt}, \quad \gamma = \frac{1}{m}\left[\mathcal{P}_a^{-1} - \frac{iH}{2m}(\mathcal{P}_a^{-4} + 2\mathcal{P}_a^{-2})\right],$$

$$\psi = \sqrt{\frac{m}{2}} \mathcal{P}_a^{1/2} e^{imt} \phi + i\frac{1}{\sqrt{2m}} \mathcal{P}_a^{1/2} e^{imt}\left[\mathcal{P}_a^{-1} - \frac{iH}{2m}\left(\mathcal{P}_a^{-4} + 2\mathcal{P}_a^{-2}\right)\right]\dot{\phi}. \tag{3.79}$$

This transforms a free real scalar on a FLRW background to a non-relativistic field with a very similar equation of motion to the Minkowskian case,

$$i\left[\dot{\psi} + \frac{3}{2}H\psi\right] = m(\mathcal{P}_a - 1)\psi. \tag{3.80}$$

The main difference is the modification of the spatial derivatives by a factor of a^{-1} each and the presence of a damping term on the lefthand side. This Hubble damping represents the dilution of the wave function due to the expansion of the universe.

The next step is adding an interaction term to the relativistic theory. With a standard $\lambda\phi^4$ interaction term the action becomes

$$S = \int \mathrm{d}^4x\, a^3 \left\{\frac{1}{2}(\partial_t\phi)^2 - \frac{1}{2}a^{-2}(\vec{\nabla}\phi)\cdot(\vec{\nabla}\phi) - \frac{1}{2}m^2\phi^2 - \frac{\lambda}{4!}\phi^4\right\}. \tag{3.81}$$

With the same transformation as for the non-interacting case we now find an interaction term also in the non-relativistic equation of motion,

$$i\left[\dot{\psi} + \frac{3}{2}H\psi\right] = m(\mathcal{P}_a - 1)\psi + \frac{\lambda}{3!}\alpha\gamma(\alpha^*\gamma^*\psi + \alpha\gamma\psi^*)^3. \tag{3.82}$$

If we want to expand this in orders of $\vec{\nabla}^2/(a^2m^2)$, we need to split the non-relativistic field into modes oscillating with different multiples of $\arg(\alpha) = mt$,

$$\psi = \sum_{\nu=-\infty}^{\infty} e^{i\nu mt}\psi_\nu \tag{3.83}$$

similar to the decomposition discussed in [100]. Further we need to assume that, beyond $(\vec{\nabla}^2\psi)/(a^2m^2\psi)$ and H/m, the variation of the field in time $\dot{\psi}/(m\psi)$ and the interaction strength λ can also be considered small. Identifying the zero mode $\psi_{\nu=0}$ with the bulk of the wave function and treating all other modes as corrections to this, we can find an expression for the equation of motion up to second order in small quantities,

$$
\begin{aligned}
i\left[\dot{\psi}_s + \frac{3}{2}H\psi_s\right] &\approx -\frac{1}{2a^2m}\vec{\nabla}^2\psi_s + \frac{\lambda}{8m^2}|\psi_s|^2\psi_s - \frac{1}{8a^4m^3}\nabla^4\psi_s \\
&+ \frac{\lambda}{32a^2m^4}\left[\psi_s^2\vec{\nabla}^2\psi_s^* + 2|\psi_s|^2\vec{\nabla}^2\psi_s + \vec{\nabla}^2(|\psi_s|^2\psi_s)\right] \\
&+ i\frac{7\lambda H}{32a^2m^5}\left[-\psi_s^2\vec{\nabla}^2\psi_s^* + 2|\psi_s|^2\vec{\nabla}^2\psi_s - \vec{\nabla}^2(|\psi_s|^2\psi_s)\right] \\
&- \frac{17\lambda^2}{768m^5}|\psi_s|^4\psi_s\,.
\end{aligned}
\tag{3.84}
$$

This is the Euler-Lagrange equation of the effective Lagrangian

$$
\begin{aligned}
\mathcal{L}_{\text{eff}} =& \frac{i}{2}(\dot{\psi}_s\psi_s^* - \psi_s\dot{\psi}_s^*) - \frac{1}{2a^2m}(\vec{\nabla}\psi_s)(\vec{\nabla}\psi_s^*) - \frac{\lambda}{16m^2}|\psi_s|^4 \\
&+ \frac{1}{8a^4m^3}(\vec{\nabla}^2\psi_s)(\vec{\nabla}^2\psi_s^*) - \frac{\lambda}{32a^2m^4}|\psi_s|^2(\psi_s^*\vec{\nabla}^2\psi_s + \psi_s\vec{\nabla}^2\psi_s^*) \\
&+ \frac{7\lambda H}{16a^2m^5}|\psi_s|^2\,\text{Im}(\psi_s^*\vec{\nabla}^2\psi_s) + \frac{17\lambda^2}{9\cdot 2^8 m^5}|\psi_s|^6\,.
\end{aligned}
\tag{3.85}
$$

A fully detailed calculation of this can be found in [98]. All the terms that are already known from the Minkowski metric case are present in the FLRW action as well with the only difference being the additional factors of a^{-1} per spatial derivative. At this order in the expansion there is one new term other than the Hubble damping that is proportional to the Hubble expansion rate. This term is a derivate interaction term, i.e. it is present in neither the non-interacting theory nor at a lower order of the momentum expansion. At higher orders in H/m the real part of the transformation will also be modified which introduces further effects of the cosmological expansion even in the non-interacting case. One thing of note here is that the expansion scheme that we used preserves the $U(1)$ symmetry that is present in the free non-relativistic theory. This means that particle number changing processes are not captured by this approach, leaving the particle number conserved up to dilution due to expansion. This also removes the possibility of vacuum instabilities. The $|\psi|^6$ term with a positive sign in the Lagrangian causes the energy spectrum to be unbounded from below. However, since the particle number cannot change, this can never result in the vacuum decaying into particles. This can also be understood as a decoupling of the N-particle problem from all higher particle number problems [103].

All in all, we found a formalism that allows us to obtain a non-relativistic formulation of quantum field theories even on general curved background metrics. The limit of small momenta from the perspective of a well-defined class of observers can be taken to arbitrary order. This method does however require exact knowledge of the metric

in question in order to solve equation (3.52). On top of that corrections to interacting theories are in general limited to the perturbative regime $\lambda \ll 1$. It is also at this point not completely clear whether the transformation could be anomalous in the quantum theory by means other than a corresponding Jacobian of the path integral measure. The transformation discussed in this section shows that a non-relativistic limit can lead to a theory close to quantum mechanics and merits further investigation, possibly in application to Majorana fermions, by that alone as well as the mathematical implications of a non-relativistic QFT [103]. However, its requirements do not align with the typical fluid picture of strong interactions. Therefore, we need to consider relativistic fluid dynamics if we want to link its transport properties to a quantum field theory. Fortunately, the Green-Kubo formulas require only equilibrium expectation values, which allows us to neglect terms from dynamic contributions such as bulk viscous pressure and shear stress that appear in the Israel-Stewart equations [97].

3.4   Wetterich equation

The last problem that remains is the calculation of the 1PI effective action. This is, however, problematic since it contains an infinite resummation of quantum corrections that usually cannot be analytically resolved. For this reason we turn to functional renormalization group (fRG) flow methods in order to obtain integro-differential equations that allow us to solve this issue non-perturbatively. An extensive discussion of these methods is given in [104], following which I will outline the concepts needed for our calculation. The method presented here is only applicable to euclidean field theories. We are working with a finite temperature Matsubara formulation, so this is not a problem and as a consequence we will drop the subscript $\cdot_E$ for euclidean functionals from here on.

The basic idea of this approach to finding the 1PI effective action is to add quantum corrections one after another to the classical action starting from the ultraviolet regime and moving towards infrared in a controlled way. This is done by adding a supression term with a momentum scale k to the action,

$$
\begin{aligned}
S[\phi] &\to S_k[\phi] = S[\phi] + \Delta S_k[\phi]\,, \\
\Delta S_k[\phi] &= \frac{1}{2} \int \mathrm{d}^4x\, \mathrm{d}^4y\, \phi(x) R_k(x-y)\phi(y)\,,
\end{aligned}
\tag{3.86}
$$

where R_k is the so-called regulator. If the Fourier transform of the regulator $R_k(p)$ is chosen such that it fulfills the conditions,

$$
\begin{aligned}
&\lim_{p^2 \to 0} R_k(p^2) > 0\,, \\
&\lim_{k \to 0} R_k(p^2) = 0\,, \\
&\lim_{k \to \infty} R_k(p^2) = \infty\,,
\end{aligned}
\tag{3.87}
$$

then this additional term suppresses quantum effects at momentum scales smaller than k (meaning $p^2 < k^2$) by effectively adding a heavy artificial mass to particles

in that momentum regime, suppressing all contributions beyond tree level. From this modified action we can construct in the same way as before a Schwinger functional W_k and preliminary quantum effective action $\tilde{\Gamma}_k$. Instead of using $\tilde{\Gamma}_k$, we will work with $\Gamma_k[\Phi] = \tilde{\Gamma}_k[\Phi] - \Delta S_k[\Phi]$. That way we find the limiting behavior,

$$
\begin{aligned}
\Gamma_{k\to\infty}[\Phi] &= S[\Phi]\,, \\
\Gamma_{k\to 0}[\Phi] &= \Gamma[\Phi]\,.
\end{aligned}
\tag{3.88}
$$

If the theory has an ultraviolet cutoff Λ, the limit of infinite k in the first formula is replaced by the limit $k \to \Lambda$. The object Γ_k, the 1PI effective action at scale k, thus interpolates between the microscopic classical action and the macroscopic 1PI effective action including all relevant quantum corrections. Wetterich [33] found that the change of Γ_k with the scale k is governed by a functional differential equation,

$$
\partial_t \Gamma_k = \frac{1}{2}\mathrm{STr}\left(\frac{\partial_t R_k}{\Gamma_k^{(2,0)} + R_k}\right) = \frac{1}{2}\mathrm{STr}\left(G_k \partial_t R_k\right)\,,
\tag{3.89}
$$

where we use the short notation $t = \ln(k/\Lambda)$, $G_k = (\Gamma_k^{(2,0)} + R_k)^{-1}$ and STr denotes a super trace that connects all open indices and spacetime or, equivalently, momentum dependencies. The object G_k is the scale dependent propagator and will be represented by a line in Feynman diagrams. Using a cross over a propagator line to indicate the insertion of a regulator derivative $\partial_t R_k$, we can represent the Wetterich equation (3.89) in a diagrammatic form,

$$
\partial_t \Gamma_k = \frac{1}{2}\ \bigcirc\!\!\!\!\times \ .
\tag{3.90}
$$

From this, we can construct a scale dependent shear viscosity,

$$
\eta_k = \lim_{\omega\to 0}\lim_{\vec{p}\to 0}\partial_\omega\,\mathrm{Im}\lim_{\epsilon\searrow 0}\Gamma_k^{(0,2)xyxy}(\omega + i\epsilon,\vec{p})\,.
\tag{3.91}
$$

The variation of this object with the scale k (or flow) can be derived from the Wetterich equation, starting at its value as can be derived from the classical action $\eta_{k\to\infty} = 0$.

Even though we now have a differential equation and a known boundary condition in $\Gamma_{k\to\infty} = S$, we cannot simply solve this equation to obtain the full 1PI effective action since the righthand side of the Wetterich equation depends on the second field derivative of Γ_k. The flow of $\Gamma_k^{(2,0)}$ can be derived from the Wetterich equation, but will depend on higher order field derivatives itself. Therefore, the equation in this form is not closed and one has to chose a sensible truncation.

3.5 Constructing the ansatz for the effective action Γ_k

Our intention is to calculate the shear viscosity of a real scalar $\lambda\phi^4$ theory in a simple but not trivial way. We start from the classical action

$$
S[\phi] = \int \mathrm{d}^4 x \left\{ -\frac{1}{2}\eta^{\mu\nu}(\partial_\mu\phi)(\partial_\nu\phi) - \frac{m^2}{2}\phi^2 - \frac{\lambda}{4!}\phi^4 \right\}\,.
\tag{3.92}
$$

This is a well-known system that has been investigated extensively in the past. An important fact about this system for our considerations is that it in principle renormalizes towards triviality in more than four spacetime dimensions and likely also in exactly four [105]. This would manifests in the flow in that, if we simply replaced the mass and coupling strength by scale dependent ones m_k and λ_k, we would find that the coupling flows to zero. Therefore, we will work with a ultraviolet cutoff Λ that we will try to remove at the end. We also leave the mass and quartic interaction constant with respect to the flow scale. With this our ansatz is restricted to

$$\begin{aligned}
\Gamma_k[\Phi] &= S[\Phi] + \Gamma_k^{\mathrm{dis}}[\Phi]\,, \\
\Gamma_{k\to\Lambda}^{\mathrm{dis}} &= 0\,.
\end{aligned} \tag{3.93}$$

We further choose to use the Callan-Symanzik regulator [106]

$$R_k(x-y) = k^2 \frac{\delta(x-y)}{\sqrt{-g}}\,, \tag{3.94}$$

which reproduces a Callan-Symanzik type renormalization group flow [107, 108]. This makes its momentum space representation in Minkowski and euclidean spacetime simply $R_k = k^2$ and also gives the typical scale derivative insertion the form $\partial_t R_k = 2k^2$. Both R_k and $\partial_t R_k$ are independent of the involved momenta, aside from enforcing momentum conservation, and can thus be pulled out of any integral which simplifies the calculations. In order to identify which dissipative terms to add in order to archieve a non-trivial flow of the shear viscosity, we look at the flow equation of the second metric derivative of the effective action already evaluated at a trivial euclidean metric [88],

$$\begin{aligned}
\partial_t \Gamma_k^{(0,2)\mu\nu\alpha\beta}[\Phi,\delta^{\mu\nu}](x,y) &= \frac{\partial_t R_k}{2}\Bigg[\frac{1}{4}\delta^d(x-y)\delta^{\mu\nu}\delta^{\alpha\beta}G_k(x,x) \\
&\quad -\frac{1}{2}\delta^d(x-y)\delta^{\mu(\alpha}\delta^{\beta)\nu}G_k(x,x) \\
&\quad -\int_{v,w}(\frac{1}{2}\delta^{\alpha\beta}G_k(y,v)\Gamma_k^{(2,1)\mu\nu}(v,w;x)G_k(w,y) + (\alpha\beta,y)\leftrightarrow(\mu\nu,x)) \\
&\quad -\int_{u,v,w}G_k(u,v)\Gamma_k^{(2,2)\mu\nu\alpha\beta}(v,w;x,y)G_k(w,u) \\
&\quad +\int_{u,v,w,r,s}(G_k(u,r)\Gamma_k^{(2,1)\alpha\beta}(r,v;y)G_k(v,w)\Gamma_k^{(2,1)\mu\nu}(w,s;x)G_k(s,u) \\
&\quad +(\alpha\beta,y)\leftrightarrow(\mu\nu,x))\Bigg]\,,
\end{aligned} \tag{3.95}$$

where $(\alpha\beta,y) \leftrightarrow (\mu\nu,x)$ represents the same terms as before within the the same brackets, but with the indices and coordinates exchanged correspondingly, and $\int_x = \int \mathrm{d}^4 x$ for shortness of notation. Specifically in the case of $\mu\nu\alpha\beta = xyxy$ that is relevant

to the shear viscosity, this reduces to

$$\partial_t \Gamma_k^{(0,2)xyxy}[\Phi, \delta^{\mu\nu}](x,y) = \frac{\partial_t R_k}{2} \Bigg[-\int_{u,v,w} G_k(u,v)\Gamma_k^{(2,2)xyxy}(v,w;x,y)G_k(w,u)$$

$$+\int_{u,v,w,r,s} (G_k(u,r)\Gamma_k^{(2,1)xy}(r,v;y)G_k(v,w)\Gamma_k^{(2,1)xy}(w,s;x)G_k(s,u) + (x \leftrightarrow y)) \Bigg].$$
$$(3.96)$$

We can see that this only contains two types of contribution which can be diagramatically represented as

$$\partial_t \;\; xy \;\; \underset{p \quad p}{\wwave{\bullet}} \;\; xy \;\; = \frac{1}{2} \cdot \Bigg[\;\; xy \;\; \underset{p \qquad p}{\wwave} \overset{q}{\underset{p-q}{\otimes}} \;\; xy \;\; - 2 \;\; xy \;\; \underset{p \qquad p}{\wwave} \overset{q}{\bigcirc} \;\; xy \;\; \Bigg],$$
$$(3.97)$$

where the wavy lines represent the external metric. In order to generate a non-vanishing shear viscosity, the righthand side of this needs to have an imaginary part that is dependent on the external frequency $\omega = p^0$ (cf. equation (3.91)). The tadpole diagram (right) can only achieve this if $\Gamma_k^{(2,2)xyxy}$ is frequency dependent since no external momentum flows through its loop, while for the polarization diagram (middle) this can be achieved by a modification of the propagator alone.

3.5.1 Källén-Lehmann spectral representation

In the 1950s, Källén [109] and Lehmann [110] found a spectral representation of the two-point function. Feynman, retarded, advanced and Matsubara propagator can be represented as integrations along different contours of a spectral density $\rho(k, \vec{p})$ which contains the complete information of the two-point function and is introduced briefly here, following the discussions in [90, 111]. For the retarded propagators that we are interested in in our finite temperature real time description, this relation is

$$G_k^R(\omega, \vec{p}) = \lim_{\varepsilon \searrow 0} \int_{-\infty}^{\infty} \frac{\mathrm{d}\omega'}{2\pi} \frac{\rho(\omega', \vec{p})}{\omega' - (\omega + i\varepsilon)} \,. \tag{3.98}$$

The spectral function has to be normalized,

$$\int_{-\infty}^{\infty} \frac{\mathrm{d}\omega'}{\pi} \omega' \rho(\omega', \vec{p}) = 1 \,, \tag{3.99}$$

non-negative for positive frequencies and odd in its frequency argument. We can make use of the Sokhotski-Plemelj theorem,

$$\frac{1}{x \pm i\varepsilon} \xrightarrow{\varepsilon \to 0} P\left(\frac{1}{x}\right) \mp i\pi\delta(x) \,, \tag{3.100}$$

73

where $P(f(x))$ means that an integral over f should be treated as its Cauchy principle value, in order to invert this relation. The spectral density can be obtained from the imaginary part of the retarded propagator,

$$\rho(\omega, \vec{p}) = -2 \operatorname{Im} G_k^R(\omega, \vec{p}) . \tag{3.101}$$

Using the spectral function, we can freely transform between different forms of the propagator as long as we know one of them. For free particles and including the regulator term the spectral density takes the form

$$\rho(\omega, \vec{p}) = 2\pi\delta(\omega^2 - \omega_{\vec{p},k}^2)\operatorname{sign}(\omega) ,$$
$$\omega_{\vec{p},k}^2 = \vec{p}^2 + m^2 + k^2 . \tag{3.102}$$

We can straightforwardly introduce a dissipative term into the ansatz for the effective action by broadening the mass peak of the density. We introduce the scale dependent damping γ_k via

$$\rho(\omega, \vec{p}) = \frac{2\gamma_k \omega}{(\omega^2 - \omega_{\vec{p},k}^2)^2 + \gamma_k^2 \omega^2} . \tag{3.103}$$

This form of the spectral density reduces to the free one in the limit $\gamma_k \to 0$ and fulfills all of the required conditions. The modification to the inverse propagator that we need to make is

$$\Gamma_k^{(2,0)\mathrm{dis}} \sim -i\omega\gamma_k . \tag{3.104}$$

This lets us express the real part of the retarded and advanced propagators as

$$\operatorname{Re} G_k^R(\omega, \vec{p}) = \operatorname{Re} G_k^A(\omega, \vec{p}) = \frac{\omega^2 - \omega_{\vec{p},k}^2}{(\omega^2 - \omega_{\vec{p},k}^2)^2 + \gamma_k^2 \omega^2} . \tag{3.105}$$

From this we can directly read off the projector to the damping to be

$$\gamma_k = -\operatorname{Im}\partial_\omega|_{\omega=0} \lim_{\varepsilon \searrow 0} \Gamma_k^{(2,0)}(\omega + i\varepsilon, \vec{p} = 0) . \tag{3.106}$$

In real space representation for a Minkowski metric background the damping term would correspond to

$$\Gamma^{\mathrm{dis},\gamma}[\Phi, \eta_{\mu\nu}] = \int \mathrm{d}^4 x \frac{1}{2}\gamma_k \Phi s_R(\partial_t)\partial_t \Phi \tag{3.107}$$

with the differential operator $s_R(\partial_t)\partial_t$ (introduced in [112]) defined via its Fourier representation

$$s_R(\partial_t)\partial_t \Phi(t) \to -i\omega s_I(\omega)\Phi(\omega) ,$$
$$s_I(\omega) := \operatorname{sign}(\operatorname{Im}\omega) . \tag{3.108}$$

This can be generalised to an arbitrary metric background where Fourier transformations are not clearly defined as done in [112].

3.5.2 Modification of the interaction

The initial condition for the damping is $\gamma_{k\to\Lambda} = 0$ since no term in the microscopic action is dissipative. From the projector to the damping factor, we can directly construct its flow equation. Under the assumption that the effective action conserves the $\mathbb{Z}_2$ symmetry of the microscopic action and hence $\Gamma_k^{(3,0)}[\Phi = 0] = 0$, the diagrammatic representation is

$$\partial_t \gamma_k = \frac{1}{2}\,\mathrm{Im}\,\partial_\omega\big|_{\omega=0} \lim_{\vec{p}\to 0} \underset{p \qquad p}{\overset{q}{\bigotimes}} .$$

(3.109)

It shows that in order to generate damping as part of the flow, there must also be correction to the scalar four-point function. Specifically, we need an imaginary term that is dependent on a non-trivial, meaning in this case not just s-channel, combination of the in- and outgoing momenta. Using the same differential operator as for the γ_k term, we introduce an imaginary derivative interaction with strength λ_k as

$$\Gamma^{\mathrm{dis},\lambda}[\Phi, \eta_{\mu\nu}] = -\int \mathrm{d}^4x\,\frac{\lambda_k}{4}\Phi^2 s_{\mathrm{R}}(\partial_t)\partial_t\left(\Phi^2\right).$$

(3.110)

Due to the higher number of involved frequencies, the projector to this new flowing quantity is slightly more complicated

$$\lambda_k = -\mathrm{Im}\,\frac{1}{12}\left(\sum_i \frac{\partial}{\partial\omega_i}\Big|_{\omega_i=0}\right)\Gamma_k^{(4,0)}[\Phi = 0].$$

(3.111)

The diagram that determines the flow of the derivative interaction strength,

$$\partial_t\lambda_k = \frac{1}{24}\,\mathrm{Im}\left(\sum_{i=1}^{4}\partial_{\omega_i}\Big|_{\omega_i=0}\right)\underset{p_1 \qquad p_+ - q \qquad p_3}{\overset{p_2 \qquad q \qquad p_4}{\bigotimes}},$$

(3.112)

can have frequency dependent imaginary parts with only the flow parameters that we have so far. Additional terms could be added by considering non-zero contributions from $\Gamma^{(5,0)}$ and $\Gamma^{(6,0)}$. We chose not to include these in this relatively minimalist treatment. Thus, we have now arrived at a non-trivial ansatz for the effective action that can generate shear viscosity.

3.5.3 Wave function renormalization

As mentioned at the beginning of this chapter, the shear viscosity of a real scalar $\lambda\phi^4$ theory has already been investigated perturbatively by Jeon and Yaffe [29, 30]. They use a resummation of ladder diagrams that accounts for scaling with inverse interaction strength in the thermal perturbation theory. Such ladder diagrams cannot be generated in our ansatz so far, since they are neither contained in the propagator nor

in the four-point function corrections. While this means giving up the minimality in flow parameters, including these diagrams allows us to compare our theory to tested results. In order to do so, we need to include a correction to $\Gamma^{(2,1)}$. The most straight-forward way to do this is to add a wave function renormalization Z_k to the kinetic term,

$$\Gamma_k^{\mathrm{dis},Z}[\Phi] = -\int \mathrm{d}^4x\,\sqrt{-g}\,\frac{Z_k-1}{2}g^{\mu\nu}(\partial_\mu\Phi)(\partial_\nu\Phi)\,. \tag{3.113}$$

The new parameter can be obtained, like γ_k, from derivatives of the two-point function,

$$Z_k = \partial_\omega^2 \lim_{\varepsilon\searrow 0}\Gamma_k^{(2,0)}[\Phi=0](\omega+i\varepsilon,\vec{p}=0)\,, \tag{3.114}$$

and the diagram that determines its flow is the same with different derivatives applied to it. The wave function renormalization scales the momentum term in the inverse propagator by a factor of Z_k and changes the spectral density accordingly. The damped spectral function becomes

$$\rho(\omega,\vec{p}) = \frac{2\gamma_k\omega}{(Z_k(\omega^2-\vec{p}^2)-m^2-k^2)^2+\gamma_k^2\omega^2}\,, \tag{3.115}$$

which is no longer normalized to 1 but instead to $1/Z_k$. With this we have a closed system of three flow coefficients, γ_k, λ_k and Z_k, which account for resummations of propagator, interaction and dependence on the external metric. For consistency, we also have to add an in principle metric and temperature dependent vacuum energy U_k that is necessary to capture non-zero values of the thermodynamic and transport quantities we are interested in. While this parameter is conceptually very important, being closely related to the thermodynamic potentials [104], it does not directly contribute to the flows of the other parameters. The complete correction to the classical action in our ansatz is
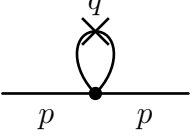
$$\Gamma_k^{\mathrm{dis}}[\Phi, g_{\mu\nu}] = \int \mathrm{d}^4x\,\sqrt{-g}\left[\frac{Z_k-1}{2}g^{\mu\nu}(\partial_\mu\Phi)(\partial_\nu\Phi) - U_k[g_{\mu\nu}]\right.$$
$$\left. + \frac{1}{2}\gamma_k\Phi s_R(\partial_t)\partial_t\Phi - \frac{\lambda_k}{4}\Phi^2 s_{\mathrm{R}}(\partial_t)\partial_t\left(\Phi^2\right)\right]\,. \tag{3.116}$$

3.6   Flow equations

With our ansatz for the scale dependent 1PI effective action we can now explicit write out the flow equations for γ_k, λ_k and Z_k and express the flow of the shear viscosity in terms of these parameters.

3.6.1 Flow of the damping γ_k

We start by investigating the tadpole diagram that determines the flow of the damping and wave function renormalization,

$$\qquad =: I(\omega + i0^+, \vec{p})\,. \qquad (3.117)$$

We are interested only in the part of this amplitude that depends on the external momentum which we will call I_1,

$$I(\omega, \vec{p}) = I_0 + I_1(\omega, \vec{p})\,. \qquad (3.118)$$

The imaginary part of I_1 is relevant for the flow of γ_k while its real part determines the flow of Z_k. We express the Matsubara form of the momentum dependent part of the amplitude as an integral,

$$
\begin{aligned}
I_1(i\omega_n, \vec{p} = 0) &= 2k^2 \int_{\vec{q}} T \sum_{\omega_m} G_k^2(i\omega_m, \vec{q}) \Gamma_k^{(4,0)\mathrm{dis}}(i\omega_n, -i\omega_n, i\omega_m, -i\omega_m) \\
&= -4ik^2\lambda_k \int_{\vec{q}} T \sum_{\omega_m} G_k^2(i\omega_m, \vec{q})[S(i\omega_n + i\omega_m) + S(i\omega_m - i\omega_n)]\,,
\end{aligned}
\qquad (3.119)
$$

with the short notation $S(\omega) = s_I(\omega)\,\omega$. If we want to express the Matsubara sum as as contour integration over $z = i\omega_m$, we find that the function inside has three branch cuts, located at $\mathrm{Im}\, z = \pm i\omega_n$ from the sign functions and at $\mathrm{Im}\, z = 0, z \neq 0$ from the branch cut of the propagators. The external frequencies $i\omega_n$ are Matsubara frequencies and thus the corresponding branch cuts cross the poles on the imaginary axis. We choose to integrate parallel to the real axis in positive direction an infinitesimal displacement above and negative direction similarly below each of the branch cuts as shown in figure 3.1 (cf. [113]). Notably, this choice of contour excludes the Matsubara poles at the branch cuts which will be treated separately. For the integrals around the branch cut at $\mathrm{Im}\, z = i\omega_n$ we find, neglecting the $\vec{q}$ argument of the propagators,

$$
\begin{aligned}
&\int_{C_{i\omega_n}} \frac{\mathrm{d}z}{2\pi i} \frac{1 + 2n_B(z)}{2} G_k^2(z)[S(i\omega_n + z) + S(z - i\omega_n)] \\
&= \int_{\mathbb{R}} \frac{\mathrm{d}z}{2\pi i}(1 + 2n_B(z + i\omega_n))z G_k^2(z + i\omega_n)\,,
\end{aligned}
\qquad (3.120)
$$

and similarly for the path around $\mathrm{Im}\, z = -i\omega_n$,

$$
\begin{aligned}
&\int_{C_{-i\omega_n}} \frac{\mathrm{d}z}{2\pi i} \frac{1 + 2n_B(z)}{2} G_k^2(z)[S(i\omega_n + z) + S(z - i\omega_n)] \\
&= \int_{\mathbb{R}} \frac{\mathrm{d}z}{2\pi i}(1 + 2n_B(z - i\omega_n))z G_k^2(z - i\omega_n)\,.
\end{aligned}
\qquad (3.121)
$$

We can now make the Wick rotation back to a real external frequency $i\omega_n \to \omega + i\varepsilon$. This lets us express the propagator terms in their retarded and advanced form respectively. Making use of the identity $G^R(-\omega) = G^A(\omega)$ and symmetry properties of the Bose distribution, we can formulate the sum of these two contributions as

$$
\int_{C_{\pm i\omega_n}} \frac{\mathrm{d}z}{2\pi i} \frac{1 + 2n_B(z)}{2} G_k^2(z)[S(\omega + i\varepsilon + z) + S(z - \omega - i\varepsilon)]
$$
$$
= 2\omega \int_{\mathbb{R}} \frac{\mathrm{d}z}{2\pi} (1 + 2n_B(z))\rho(z) \operatorname{Re} G_k^R(z) \tag{3.122}
$$
$$
+ 2 \int_{\mathbb{R}} \frac{\mathrm{d}z}{2\pi i} z(1 + 2n_B(z)) \left[(\operatorname{Re} G_k^R(z))^2 - \frac{1}{4}\rho^2(z) \right].
$$

This contribution has a linear dependence on the external frequency as desired. The dependence on the flow parameters is entirely contained in the retarded propagator and spectral density. Unfortunately, these integrals in general cannot be resolved analytically since they contain products of rational functions with the Bose distribution. The contour around the real axis can be simplified in a similar manner and yields

$$
\int_{C_0} \frac{\mathrm{d}z}{2\pi i} \frac{1 + 2n_B(z)}{2} G_k^2(z)[S(\omega + i\varepsilon + z) + S(\omega + i\varepsilon - z)]
$$
$$
= 2\omega \int_{\mathbb{R}} \frac{\mathrm{d}z}{2\pi} (1 + 2n_B(z))\rho(z) \operatorname{Re} G_k^R(z). \tag{3.123}
$$

Lastly, we need to account for the excluded terms of the Matsubara sum manually, since they are not covered by the integrations,

$$
\sum_{\omega_m \in \{0, \pm\omega_n\}} TG_k^2(i\omega_m, \vec{q})[S(i\omega_n + i\omega_m) + S(i\omega_m - i\omega_n)]|_{i\omega_n = \omega + i\varepsilon}
$$
$$
= 2\omega T(\operatorname{Re} G_k^R(0, \vec{q}))^2. \tag{3.124}
$$

We find that the contributions of the poles at $z = \pm i\omega_n$ exactly cancel. Notably, the dependence of (3.117) on the external frequency is only linear. Therefore, the flow of wave number renormalization cannot be generated,

$$
\partial_t Z_k = 0. \tag{3.125}
$$

This shows a clear weakness in our choice of the imaginary interaction term. A non-vanishing flow of Z_k can be generated by choosing an interaction correction that depends on higher orders in the ingoing frequencies and momenta. However, this does not change the calculations by much as long as the branch cuts and poles of the interaction term with respect to the frequencies are known so that the Matsubara sums can be resolved. Therefore, I will continue to work with our fairly simple definition (3.110). For the flow of the damping following (3.109) we find

$$
\partial_t \gamma_k = -4k^2 \lambda_k \int_{\vec{q}} \left[T(\operatorname{Re} G_k^R(0, \vec{q}))^2 \right.
$$
$$
\left. + 2 \int_{\mathbb{R}} \frac{\mathrm{d}z}{2\pi} (1 + 2n_B(z))\rho(z) \operatorname{Re} G_k^R(z, \vec{q}) \right]. \tag{3.126}
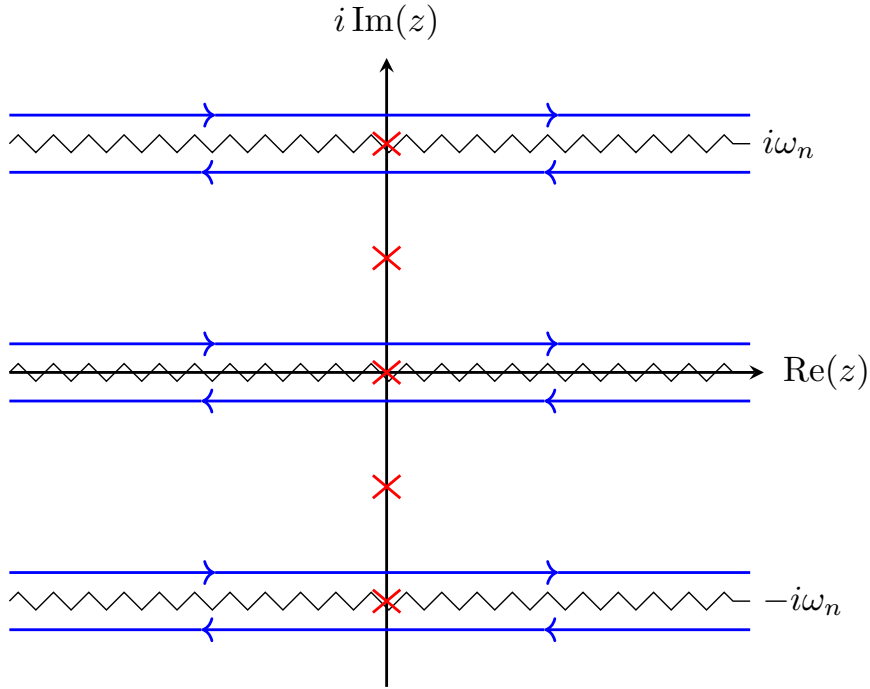$$

Figure 3.1: Pole structure and integration contours (blue lines) used to solve the Matsubara sum in (3.119). The integration paths go parallel to the real axis infinitesimally above and below each of the branch cuts (zigzag lines) with the indicated direction of integration. The Matsubara poles (red crosses) at the branch cuts are not included in the shown contour. The central branch cut at $\mathrm{Im}(z) = 0$ comes from the propagator, the other two from the dissipative interaction term.

3.6.2 Flow of the interaction correction λ_k

The flow of the last remaining parameter λ_k is determined by a (1PI) one-loop two-to-two scattering,

$$=: J(\omega_1 + i0^+, \vec{p}_1, \ldots, \omega_4 + i0^+, \vec{p}_4,). \qquad (3.127)$$

Here we have relevant contributions from both the dissipative and the bare interaction. Using again external imaginary frequencies $i\bar{\omega}_i$ and defining the center of mass

quantities $\omega_+ = \omega_1 + \omega_2 = \omega_3 + \omega_4$ and $\vec{p}_+ = \vec{p}_1 + \vec{p}_2$, we can express J as

$$
J(i\bar{\omega}_1, \ldots, i\bar{\omega}_4) = 2k^2 \int_{\vec{q}} T \sum_{\omega_m} G_k^2(i\omega_m, \vec{q}) G_k(i\bar{\omega}_+ - i\omega_m, \vec{p}_+ - \vec{q})
$$

$$
\Gamma^{(4,0)}(i\bar{\omega}_1, i\bar{\omega}_2, -i\omega_m, i\omega_m - i\bar{\omega}_+) \Gamma^{(4,0)}(-i\bar{\omega}_3, -i\bar{\omega}_4, i\omega_m, -i\omega_m + i\bar{\omega}_+)
$$

$$
= -2k^2 \lambda_k^2 \int_{\vec{q}} T \sum_{\omega_m} G_k^2(i\omega_m, \vec{q}) G_k(i\bar{\omega}_+ - i\omega_m, \vec{p}_+ - \vec{q}) \left(\frac{\lambda}{i\lambda_k} + S(i\bar{\omega}_+) \right.
$$

$$
+ S(i\bar{\omega}_1 - i\omega_m) + S(i\bar{\omega}_2 - i\omega_m) \bigg) \left(\frac{\lambda}{i\lambda_k} + S(i\bar{\omega}_+) + S(i\bar{\omega}_3 - i\omega_m) \right.
$$

$$
\left. + S(i\bar{\omega}_4 - i\omega_m) \right) .
$$

(3.128)

From symmetry arguments we can see that this expression is invariant under the exchanges $(\omega_1 \leftrightarrow \omega_2)$, $(\omega_3 \leftrightarrow \omega_4)$ and $(\omega_1, \omega_2 \leftrightarrow \omega_3, \omega_4)$. Thus, without loss of generality we assume $\omega_1 < \omega_3 < \omega_4 < \omega_2$. Since $S^2(z) = z^2$ is not discontinuous, this can also capture cases where some of the frequencies are equal. The projection to the interaction correction we have chosen sets all external frequecies to zero in the end. Therefore, we will handle all the calculations under the further assumption $\omega_1 \geq 0$ for simplicity. Interpreting the Matsubara sum as a contour integration, the integrand now has six branch cuts, one each at $\operatorname{Im} z \in \{0, \bar{\omega}_+, \bar{\omega}_1, \bar{\omega}_2, \bar{\omega}_3, \bar{\omega}_4\}$. The first two of those come from the propagators, while the other ones are caused by the discontinuity of the sign function in the interaction. We choose integration paths in a similar way to the previous section infinitesimally above and below each branch cut as shown in figure 3.2. This choice excludes the Matsubara terms at the branch cut frequencies which after analytical continuation contribute to the flow as

$$
\Sigma_0(\omega_+) = T(\operatorname{Re} G_k^R(0, \vec{q}))^2 G_k^R(\omega_+, \vec{p}_+ - \vec{q}) \left(\frac{\lambda}{i\lambda_k} + 2\omega_+ \right)^2
$$

$$
+ T(G_k^R(\omega_1, \vec{q}))^2 G_k^R(\omega_2, \vec{p}_+ - \vec{q}) \left(\frac{\lambda}{i\lambda_k} + 2\omega_2 \right)^2
$$

$$
+ T(G_k^R(\omega_2, \vec{q}))^2 G_k^R(\omega_1, \vec{p}_+ - \vec{q}) \left(\frac{\lambda}{i\lambda_k} + 2\omega_2 \right)^2
$$

$$
+ T(G_k^R(\omega_3, \vec{q}))^2 G_k^R(\omega_4, \vec{p}_+ - \vec{q}) \left(\frac{\lambda}{i\lambda_k} + 2\omega_2 \right) \left(\frac{\lambda}{i\lambda_k} + 2\omega_4 \right)
$$

$$
+ T(G_k^R(\omega_4, \vec{q}))^2 G_k^R(\omega_3, \vec{p}_+ - \vec{q}) \left(\frac{\lambda}{i\lambda_k} + 2\omega_2 \right) \left(\frac{\lambda}{i\lambda_k} + 2\omega_4 \right)
$$

$$
+ T(G_k^R(\omega_+, \vec{q}))^2 \operatorname{Re} G_k^R(0, \vec{p}_+ - \vec{q}) \left(\frac{\lambda}{i\lambda_k} + 2\omega_+ \right)^2 .
$$

(3.129)

While not explicitly part of the projector, λ_k in our ansatz does not depend on spatial momenta. Therefore, we will express all further contributions evaluated at $\vec{p}_+ = 0$.

This dependency can be reintroduced by changing the momentum dependency of the non-squared propagator to $\vec{p}_+ - \vec{q}$. For shortness of notation, dependencies on the loop momentum $\vec{q}$ will not be not written out. With this in mind we consider the paths around each of the branch cuts and label the terms $C_i, i \in \{0, +, 1, 2, 3, 4\}$ correspondingly. For the contour around the real axis we find

$$C_0 = \int_{\mathbb{R} \pm i\varepsilon} \frac{\mathrm{d}z}{2\pi i} \frac{1 + 2n_B(z)}{2} G_k^2(z) G_k(i\bar{\omega}_+ - z) \left(\frac{\lambda}{i\lambda_k} + S(i\bar{\omega}_+) + S(i\bar{\omega}_1 - z) \right.$$

$$\left. + S(i\bar{\omega}_2 - z) \right) \left(\frac{\lambda}{i\lambda_k} + S(i\bar{\omega}_+) + S(i\bar{\omega}_3 - z) + S(i\bar{\omega}_4 - z) \right)$$

$$\to -4 \int_{\mathbb{R}} \frac{\mathrm{d}z}{2\pi} (1 + 2n_B(z)) \operatorname{Re} G_k^R(z) \rho(z) G_k^R(\omega_+ - z) (\omega_+ - z) \left(\frac{\lambda}{2i\lambda_k} + \omega_+ - z \right)^2 .$$

$$(3.130)$$

The other propagator induced branch cut gives

$$C_+ = -2 \int_{\mathbb{R}} \frac{\mathrm{d}z}{2\pi} (1 + 2n_B(z))(G_k^R(z))^2 \rho(z - \omega_+) \left(z + \frac{\lambda}{2i\lambda_k} \right)^2 . \qquad (3.131)$$

These two terms include the contribution to λ_k that is generated from the presence of the bare interaction λ and, implicitly via the spectral function, the damping γ_k. The terms that come from the branch cuts of the interaction can be summarised as

$$\sum_{i=1}^{4} C_i = 2 \int_{\mathbb{R}} \frac{\mathrm{d}z}{2\pi i} (1 + 2n_B(z))(G_k^R(z))^2 G_k^R(\omega_+ - z) \omega_+ (2z - \omega_+) . \qquad (3.132)$$

While the individual terms depend on the individual frequencies, their sum only depends on the total frequency ω_+ that goes into and out of the loop. Finally, with equation (3.112) we can formulate the flow of the interaction correction as

$$\partial_t \lambda_k = -k^2 \lambda_k^2 \int_{\vec{q}} \left\{ T(\operatorname{Re} G_k^R(0))^2 \left(\frac{3\lambda^2}{2\lambda_k^2} \gamma_k (\operatorname{Re} G_k^R(0))^2 - \frac{8\lambda}{3\lambda_k} \operatorname{Re} G_k^R(0) \right) \right.$$

$$- \frac{1}{3} \int_{\mathbb{R}} \frac{\mathrm{d}z}{2\pi} (1 + 2n_B(z)) \left[2\rho(z) \operatorname{Re} G_k^R(z) \left\{ \frac{\lambda}{2\lambda_k} (2 \operatorname{Re} G_k^R(z) - \rho^2(z)) \right. \right.$$

$$+ 2z \left(z^2 - \frac{\lambda^2}{4\lambda_k^2} \right) \rho(z) \operatorname{Re} G_k^R(z) - \frac{4\lambda}{\lambda_k} z^2 (\operatorname{Re} G_k^R(z))^2$$

$$+ \left(\left(\frac{\lambda}{\gamma_k \lambda_k} - 1 \right) z - \frac{1}{2z} \left(z^2 - \frac{\lambda^2}{4\lambda_k^2} \right) \right) \rho(z) \right\} \qquad (3.133)$$

$$+ \left((\operatorname{Re} G_k^R(z))^2 - \frac{1}{4} \rho^2(z) - \rho(z) \operatorname{Re} G_k^R(z) \left(z^2 - \frac{\lambda}{4\lambda_k^2} \right) \right)$$

$$\cdot \left(\frac{1}{z} \rho(z) - 4z\rho(z) \operatorname{Re} G_k^R(z) \right) + 2z \operatorname{Re} G_k^R(z)$$

$$\left. \left. \cdot \left((\operatorname{Re} G_k^R(z))^2 + \frac{1}{4} \rho^2(z) \right) \right] \right\} .$$

With this and the initial conditions at $k = \Lambda$ for γ_k and λ_k we can now numerically solve equations (3.126) and (3.133) as a coupled system of integro-differential equations. Notably, at first look, none of the involved loop momentum integrals diverge upon removal of the cutoff as all terms scale at least as $|\vec{q}|^{-4}$. What remains is to translate this into a flow of the shear viscosity.
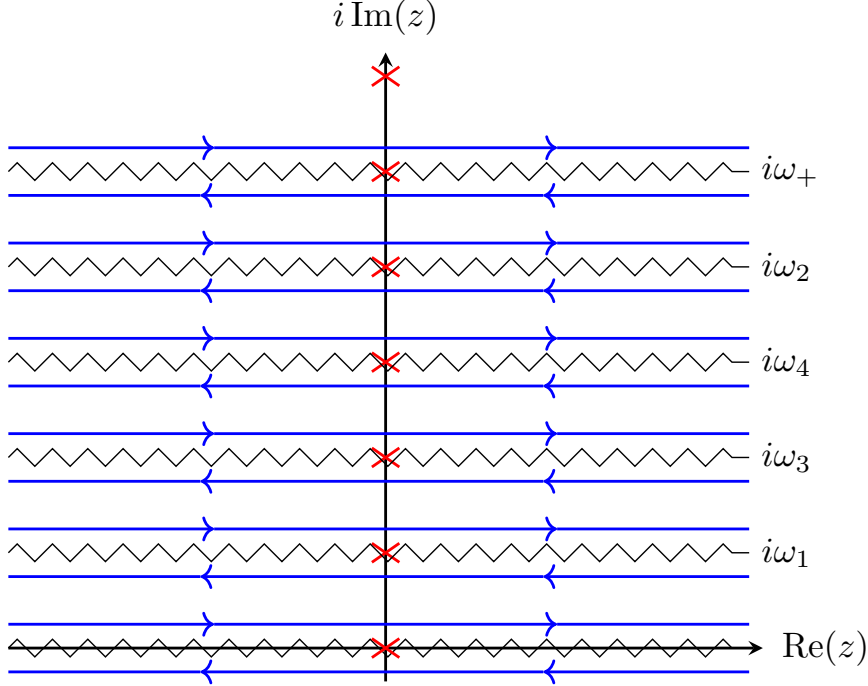

Figure 3.2: Pole structure and integration contours (blue lines) used to solve the Matsubara sum in (3.128). The integration paths go parallel to the real axis infinitesimally above and below each of the branch cuts (zigzag lines) with the indicated direction of integration. The Matsubara poles (red crosses) at the branch cuts are not included in the shown contour. The two outer branch cuts at $\text{Im}(z) = 0$ and $\text{Im}(z) = \omega_+$ come from the propagators, the other four from the dissipative interaction term.
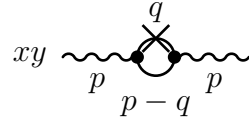
3.6.3   Flow of the shear viscosity η_k

The last quantities that we have not yet explicitly written out and are needed for the flow of η_k are the vertices that involve the metric background. In the projection to the scale time derivative of the shear viscosity, there is a derivative with respect to the external frequency. As mentioned before, the tadpole diagram that contains $\Gamma_k^{(2,2)xyxy}$ would need a dependence on the external frequency within the vertex in order to contribute. While the vertex is modified in a frequency dependent way by our addition of a damping term, it involves only the momenta of the scalar field, i.e. only the loop momentum. For the $\Gamma_k^{(2,1)xy}$ vertex only the original kinetic term contributes

82

after setting the metric to a euclidean one,

$$\Gamma_k^{(2,1)xy}(q_1, q_2; p)[\Phi = 0] = \frac{1}{2}\left(q_1^x q_1^y + q_2^x q_2^y - p^x p^y\right),\qquad(3.134)$$

where the term that ensures momentum conservation is excluded. In the case of vanishing metric momentum, as in the projection to η_k, this simplifies even further to $q^x q^y$. Most importantly, the vertex does not depend on the external frequency which means that the pole and branch cut structure of the amplitude is entirely determined by the involved propagators. We define

$$xy\ \underset{p\quad\ \ p}{\overset{q}{\wedge}}\ xy\ =: K(\omega + i\varepsilon, \vec{p})\qquad(3.135)$$

$$p - q$$

and can express this again with an external imaginary frequency,

$$K(i\omega_n, \vec{p}) = 2k^2 \int_{\vec{q}} T \sum_{\omega_m} G_k^2(i\omega_m) G_k(i\omega_n - i\omega_m, \vec{p} - \vec{q})\left(\Gamma^{(2,1)}(\vec{q}, \vec{p} - \vec{q}; -\vec{p})\right)^2.\quad(3.136)$$

The branch cuts of the Matsubara summand lie at $\operatorname{Im} z = 0$ and $\operatorname{Im} z = i\omega_n$. The contour we choose to reexpress this is of the same type as in the two cases before. Likewise, we have three contributions, Σ_0 from the zero and external frequency Matsubara terms, C_0 from the path around the real axis and $C_{i\omega_n}$ from the path around $\mathbb{R} + i\omega_n$. We define them such that

$$K(\omega + i\varepsilon, \vec{p} = 0) = 2k^2 \int_{\vec{q}} (q^x q^y)^2 (\Sigma_0(\omega + i\varepsilon) + C_0(\omega + i\varepsilon) + C_{i\omega_n}(\omega + i\varepsilon)).\quad(3.137)$$

For the zero frequency term we find

$$\Sigma_0(\omega + i\varepsilon) = T(\operatorname{Re} G_k^R(0, \vec{q}))^2 G_k^R(\omega, \vec{q}) + T\operatorname{Re} G_k^R(0, \vec{q})(G_k^R(\omega, \vec{q}))^2,\qquad(3.138)$$

while the contour integrals give

$$C_0(\omega + i\varepsilon) = \int_{\mathbb{R}} \frac{\mathrm{d}z}{2\pi}(1 + 2n_B(z))\rho(z, \vec{q})\operatorname{Re} G_k^R(z, \vec{q}) G_k^R(\omega - z, \vec{q}),$$

$$C_{i\omega_n}(\omega + i\varepsilon) = \int_{\mathbb{R}} \frac{\mathrm{d}z}{2\pi}\frac{1 + 2n_B(z)}{2}(G_k^R(z, \vec{q}))^2 \rho(\omega - z, \vec{q}).$$

$$(3.139)$$

Inserting this into equation (3.91) gives us the final form of the flow equation for the shear viscosity (not writing out the dependencies on the loop momentum),

$$\partial_t \eta_k = -2k^2 \int_{\vec{q}} (q^x q^y)^2 \left[\frac{3}{2}T\gamma_k(\operatorname{Re} G_k^R(0))^4 + \int_{\mathbb{R}} \frac{\mathrm{d}z}{2\pi}\frac{1 + 2n_B(z)}{2}\rho(z)\operatorname{Re} G_k^R(z)\right.$$

$$\left.\cdot\left(\frac{1}{z}\rho(z) - 4z\rho(z)\operatorname{Re} G_k^R(z)\right)\right].$$

$$(3.140)$$

With the solution for γ_k as a function of the scale, this becomes an ordinary differential equation in k after all the integrals are evaluated. In the limit $k \to 0$ of the solution, we recover a non-perturbative expression for the shear viscosity.

However, this ansatz as it is is flawed. It does not generate terms that are relevant in the perturbative regime which manifests as a lack of scaling of Z_k. This can be fixed by assuming the presence of higher order frequency (and possibly also spatial momentum) dependencies in the correction to the interaction. There is also another problem. With the equations for γ_k and λ_k in their current form, the initial conditions $\gamma_{k \to \Lambda} = 0$ and $\lambda_{k \to \Lambda} = 0$ imply that they stay at zero since all terms in equations (3.126) and (3.133) are proportional to either γ_k or λ_k themselves. A small deviation from the zero initial conditions is sufficient to generate non-vanishing flow, hence the fixed point at $(\gamma_k, \lambda_k) = (0, 0)$ is not a stable one. A deviation from the initial condition, however, means starting from a different microscopic theory. This problem might instead be solvable by choosing different projections for the flow parameters. While in principle this should not influence the effective action we end up at following the Wetterich equation, we break this feature by choosing an ansatz for the effective action. In that sense, the choice of projector is comparable to perturbative calculations assigning the meaning of a thermal decay width to the imaginary part of the self-energy evaluated on-shell [29]. In summary, while the calculation given here does not generate a non-trivial shear viscosity, it can be expanded to do so with only small modifications.

Conclusions

In the first half of this thesis, we investigated the lower particle number limit of the applicability of fluid dynamics. While this was originally motivated by results from heavy-ion physics, we concluded that the expansion dynamics of ultracold atoms were better suited to study this question experimentally. Therefore, we presented multiple predictions of their dynamics for different situations. We found that, at unitarity in a three dimensional system, the time dependency of the moment of inertia can be separated from the initial condition and isotropic expansion and oscillation can be described in a simple fashion. Slight deviations from the isotropic case might be within reach by means of a perturbative treatment. In order to achieve the small particle numbers required for our investigation, experiments work in a quasi two-dimensional harmonic trap. We use the elliptic flow v_2, adapted from heavy-ion physics, as an indicator of fluidlike behavior in these systems. Our qualitative prediction of v_2 from basic arguments about relative contributions from effects of non-interacting quantum mechanics and a classical image of interactions is confirmed by experiments [74]. From there, we proceeded by using a fitted polytropic equation of state to make quantitative predictions. For fluid static initial conditions in the trap, we reduced the expansion dynamics to a set of two coupled ordinary differential equations by using Lagrange coordinates and solved them numerically. For the special case of an isotropic trap, the equations can be solved implictly for a general polytropic exponent κ and explicitly in the case $\kappa = 2$. The aspect ratio of the fluid static trapped system was found to be a general prediction for any equation of state without derivative contributions like quantum pressure. The discrepancy between the predicted and experimental initial density profile is therefore seen as an indicator that quantum effects play an important role in the few particle system. We simulated the fluid dynamic evolution starting from an initial condition fitted to the experimental data. The early time evolution in simulation and experiment with $N = 5 + 5$ atoms matches if the equation of state is rescaled by a constant factor. We therefore concluded that, **at early times in the expansion, a set of ten strongly interacting ^{6}Li atoms behaves like a fluid.** This behavior is shown to break down for fewer particles in the upcoming paper [74]. Further work needs to be put into understanding the rescaling of the pressure, which is possibly due to finite size and finite temperature effects. The next step in the study of few fermion systems could be testing its rotational properties to determine whether it is superfluid. Similarly, oscillatory motion might give insight into its viscosity.

The second question this thesis addressed was the prediction of transport coefficients from an underlying quantum field theory. Using the corresponding Green-Kubo

relation, the shear viscosity can be expressed as a second derivative of the one particle irreducible effective action with respect to the metric, treated in this case as an external field. We investigated the non-relativistic limit of real scalar quantum field theory and generalized an existing canonical transformation to work on an arbitrary metric background. This lets us systematically obtain relativistic corrections to both interacting and non-interacting non-relativistic equations of motion. While their in general complex dependency on the metric makes them less fit as a simplification for our calculation of shear viscosity, they might be suited for the description of axionic dark matter [98]. This type of transformation and potential equivalents for Majorana fermions could help in the study of structure formation and thus merit further investigation. For the calculation of shear viscosity we turned to a relativistic real scalar theory with a quartic interaction term. We employed functional renormalization group methods, applied to a minimalist ansatz containing a broadening of the spectral function (γ_k), a frequency dependent correction to the interaction (λ_k) and a wave function renormalization (Z_k) as scale dependent parameters. We found that this simple truncation still leads to a trivial result with the given initial conditions, not generating any flow for Z_k and staying at a fixed point in parameter space for vanishing γ_k and λ_k at initial time. This problem can be solved by assuming a more complex frequency and momentum dependence of the contribution to the four-point function. After these issues have been resolved, **a numerical solution of the integro-differential flow equations leads directly to a non-perturbative prediction of the shear viscosity.**

List of Publications

- Lars H. Heyen and Stefan Floerchinger. "Real scalar field, the nonrelativistic limit, and the cosmological expansion". *Phys. Rev. D* 102 (3 Aug. 2020), p. 036024. DOI: `10.1103/PhysRevD.102.036024`. URL: `https://link.aps.org/doi/10.1103/PhysRevD.102.036024` in the text referred to as [98], results used in section 3.3

- Stefan Floerchinger, Giuliano Giacalone, Lars H. Heyen, and Leena Tharwat. "Qualifying collective behavior in expanding ultracold gases as a function of particle number". *Phys. Rev. C* 105 (4 Apr. 2022), p. 044908. DOI: `10.1103/PhysRevC.105.044908`. URL: `https://link.aps.org/doi/10.1103/PhysRevC.105.044908` in the text referred to as [71], results used in section 2.1

Results from the at the time of this writing unpublished manuscript

> Sandra Brandstetter, Philipp Lunt, Carl Heintze, Giuliano Giacalone, Lars H. Heyen, Marvin Holten, Keerthan Subramanian, Philipp M. Preiss, Stefan Floerchinger, and Selim Jochim. "A mesoscopic fluid of 10 Fermions". *in preparation* (2023) in the text referred to as [74]

were used in sections 2.2 and 2.3. The experimental data that is discussed in these sections was measured and analyzed by Sandra Brandstetter, Philipp Lunt and Carl Heintze, supervised by Selim Jochim.

Bibliography

[1] H. Poincaré. *Les méthodes nouvelles de la mécanique céleste*. Bd. 1. Gauthier-Villars, 1892.

[2] Karl F. Sundman. "Mémoire sur le problème des trois corps". *Acta Mathematica* 36 (1913), pp. 105–179.

[3] Franz Schwabl. *Statistical Mechanics*. Springer Berlin, Heidelberg, June 2006. DOI: `10.1007/3-540-36217-7`.

[4] R. B. Laughlin and David Pines. "The Theory of Everything". *Proceedings of the National Academy of Sciences* 97.1 (2000), pp. 28–31. DOI: `10.1073/pnas.97.1.28`. eprint: `https://www.pnas.org/doi/pdf/10.1073/pnas.97.1.28`. URL: `https://www.pnas.org/doi/abs/10.1073/pnas.97.1.28`.

[5] L.D. Landau and E.M. Lifshitz. *Fluid Mechanics*. Pergamon, Aug. 1987. DOI: `10.1016/C2013-0-03799-1`.

[6] L. P. (Lev Petrovich) Pitaevskiĭ and S Stringari. *Bose-Einstein condensation / Lev Pitaevskii, Sandro Stringari*. eng. International series of monographs on physics (Oxford, England); no. 116. Oxford ; New York: Clarendon Press, 2003. ISBN: 0198507194.

[7] K. H. Ackermann et al. "Elliptic Flow in $Au + Au$ Collisions at $\sqrt{s}_{\mathrm{NN}} = 130\mathrm{GeV}$". *Phys. Rev. Lett.* 86 (3 Jan. 2001), pp. 402–407. DOI: `10.1103/PhysRevLett.86.402`. URL: `https://link.aps.org/doi/10.1103/PhysRevLett.86.402`.

[8] S. Voloshin and Y. Zhang. "Flow study in relativistic nuclear collisions by Fourier expansion of azimuthal particle distributions". *Zeitschrift für Physik C Particles and Fields* 70.4 (Dec. 1996), pp. 665–671. ISSN: 1431-5858. DOI: `10.1007/s002880050141`. URL: `https://doi.org/10.1007/s002880050141`.

[9] A. M. Poskanzer and S. A. Voloshin. "Methods for analyzing anisotropic flow in relativistic nuclear collisions". *Phys. Rev. C* 58 (3 Sept. 1998), pp. 1671–1678. DOI: `10.1103/PhysRevC.58.1671`. URL: `https://link.aps.org/doi/10.1103/PhysRevC.58.1671`.

[10] Jean-Yves Ollitrault. "Anisotropy as a signature of transverse collective flow". *Phys. Rev. D* 46 (1 July 1992), pp. 229–245. DOI: `10.1103/PhysRevD.46.229`. URL: `https://link.aps.org/doi/10.1103/PhysRevD.46.229`.

[11] James L. Nagle and William A. Zajc. "Small System Collectivity in Relativistic Hadronic and Nuclear Collisions". *Ann. Rev. Nucl. Part. Sci.* 68 (2018), pp. 211–235. DOI: `10.1146/annurev-nucl-101916-123209`. arXiv: `1801.03477 [nucl-ex]`.

[12] Björn Schenke. "The smallest fluid on Earth". *Rept. Prog. Phys.* 84.8 (2021), p. 082301. DOI: `10.1088/1361-6633/ac14c9`. arXiv: `2102.11189 [nucl-th]`.

[13] Aleksi Kurkela et al. "Matching the Nonequilibrium Initial Stage of Heavy Ion Collisions to Hydrodynamics with QCD Kinetic Theory". *Phys. Rev. Lett.* 122 (12 Mar. 2019), p. 122302. DOI: `10.1103/PhysRevLett.122.122302`. URL: `https://link.aps.org/doi/10.1103/PhysRevLett.122.122302`.

[14] S. Acharya et al. "Investigations of Anisotropic Flow Using Multiparticle Azimuthal Correlations in pp, $p-$Pb, Xe-Xe, and Pb-Pb Collisions at the LHC". *Phys. Rev. Lett.* 123 (14 Oct. 2019), p. 142301. DOI: `10.1103/PhysRevLett.123.142301`. URL: `https://link.aps.org/doi/10.1103/PhysRevLett.123.142301`.

[15] Cheng Chin et al. "Feshbach resonances in ultracold gases". *Rev. Mod. Phys.* 82 (2 Apr. 2010), pp. 1225–1286. DOI: `10.1103/RevModPhys.82.1225`. URL: `https://link.aps.org/doi/10.1103/RevModPhys.82.1225`.

[16] K. M. O'Hara et al. "Observation of a Strongly Interacting Degenerate Fermi Gas of Atoms". *Science* 298.5601 (2002), pp. 2179–2182. DOI: `10.1126/science.1079107`.

[17] J. A. Joseph, E. Elliott, and J. E. Thomas. "Shear Viscosity of a Unitary Fermi Gas Near the Superfluid Phase Transition". *Phys. Rev. Lett.* 115 (2 July 2015), p. 020401. DOI: `10.1103/PhysRevLett.115.020401`. URL: `https://link.aps.org/doi/10.1103/PhysRevLett.115.020401`.

[18] I. Shvarchuck et al. "Hydrodynamic behavior in expanding thermal clouds of ^{87}Rb". *Phys. Rev. A* 68 (6 Dec. 2003), p. 063603. DOI: `10.1103/PhysRevA.68.063603`. URL: `https://link.aps.org/doi/10.1103/PhysRevA.68.063603`.

[19] F. Gerbier et al. "Experimental study of the thermodynamics of an interacting trapped Bose-Einstein condensed gas". *Phys. Rev. A* 70 (1 July 2004), p. 013607. DOI: `10.1103/PhysRevA.70.013607`. URL: `https://link.aps.org/doi/10.1103/PhysRevA.70.013607`.

[20] C. A. Regal and D. S. Jin. "Measurement of Positive and Negative Scattering Lengths in a Fermi Gas of Atoms". *Phys. Rev. Lett.* 90 (23 June 2003), p. 230404. DOI: `10.1103/PhysRevLett.90.230404`. URL: `https://link.aps.org/doi/10.1103/PhysRevLett.90.230404`.

[21] T. Bourdel et al. "Measurement of the Interaction Energy near a Feshbach Resonance in a ^{6}Li Fermi Gas". *Phys. Rev. Lett.* 91 (2 July 2003), p. 020402. DOI: `10.1103/PhysRevLett.91.020402`. URL: `https://link.aps.org/doi/10.1103/PhysRevLett.91.020402`.

[22] Richard J. Fletcher et al. "Elliptic flow in a strongly interacting normal Bose gas". *Phys. Rev. A* 98 (1 July 2018), p. 011601. DOI: 10.1103/PhysRevA.98.011601. URL: https://link.aps.org/doi/10.1103/PhysRevA.98.011601.

[23] A. Trenkwalder et al. "Hydrodynamic Expansion of a Strongly Interacting Fermi-Fermi Mixture". *Phys. Rev. Lett.* 106 (11 Mar. 2011), p. 115304. DOI: 10.1103/PhysRevLett.106.115304. URL: https://link.aps.org/doi/10.1103/PhysRevLett.106.115304.

[24] E. Elliott, J. A. Joseph, and J. E. Thomas. "Observation of Conformal Symmetry Breaking and Scale Invariance in Expanding Fermi Gases". *Phys. Rev. Lett.* 112 (4 Jan. 2014), p. 040405. DOI: 10.1103/PhysRevLett.112.040405. URL: https://link.aps.org/doi/10.1103/PhysRevLett.112.040405.

[25] E. Elliott, J. A. Joseph, and J. E. Thomas. "Anomalous Minimum in the Shear Viscosity of a Fermi Gas". *Phys. Rev. Lett.* 113 (2 July 2014), p. 020406. DOI: 10.1103/PhysRevLett.113.020406. URL: https://link.aps.org/doi/10.1103/PhysRevLett.113.020406.

[26] F. Serwane et al. "Deterministic Preparation of a Tunable Few-Fermion System". *Science* 332.6027 (2011), pp. 336–338. DOI: 10.1126/science.1201351. URL: https://www.science.org/doi/abs/10.1126/science.1201351.

[27] Luca Bayha et al. "Observing the emergence of a quantum phase transition shell by shell". *Nature* 587.7835 (Nov. 2020), pp. 583–587. ISSN: 1476-4687. DOI: 10.1038/s41586-020-2936-y. URL: https://doi.org/10.1038/s41586-020-2936-y.

[28] Marvin Holten et al. "Observation of Cooper pairs in a mesoscopic two-dimensional Fermi gas". *Nature* 606.7913 (June 2022), pp. 287–291. ISSN: 1476-4687. DOI: 10.1038/s41586-022-04678-1. URL: https://doi.org/10.1038/s41586-022-04678-1.

[29] Sangyong Jeon. "Hydrodynamic transport coefficients in relativistic scalar field theory". *Phys. Rev. D* 52 (6 Sept. 1995), pp. 3591–3642. DOI: 10.1103/PhysRevD.52.3591. URL: https://link.aps.org/doi/10.1103/PhysRevD.52.3591.

[30] Sangyong Jeon and Laurence G. Yaffe. "From quantum field theory to hydrodynamics: Transport coefficients and effective kinetic theory". *Phys. Rev. D* 53 (10 May 1996), pp. 5799–5809. DOI: 10.1103/PhysRevD.53.5799. URL: https://link.aps.org/doi/10.1103/PhysRevD.53.5799.

[31] Pavel Kovtun. "Lectures on hydrodynamic fluctuations in relativistic theories". *Journal of Physics A: Mathematical and Theoretical* 45.47 (Nov. 2012), p. 473001. DOI: 10.1088/1751-8113/45/47/473001. URL: https://dx.doi.org/10.1088/1751-8113/45/47/473001.

[32] Thomas Schäfer and Derek Teaney. "Nearly Perfect Fluidity: From Cold Atomic Gases to Hot Quark Gluon Plasmas". *Rept. Prog. Phys.* 72 (2009), p. 126001. DOI: 10.1088/0034-4885/72/12/126001. arXiv: 0904.3107 [hep-ph].

[33] Christof Wetterich. "Exact evolution equation for the effective potential". *Physics Letters B* 301.1 (1993), pp. 90–94. ISSN: 0370-2693. DOI: https://doi.org/10.1016/0370-2693(93)90726-X. URL: https://www.sciencedirect.com/science/article/pii/037026939390726X.

[34] R.L. Liboff. *Kinetic Theory: Classical, Quantum, and Relativistic Descriptions*. Graduate Texts in Contemporary Physics. Springer New York, 2013. ISBN: 9781475779103.

[35] Sa šo Grozdanov et al. "Convergence of the Gradient Expansion in Hydrodynamics". *Phys. Rev. Lett.* 122 (25 June 2019), p. 251601. DOI: 10.1103/PhysRevLett.122.251601. URL: https://link.aps.org/doi/10.1103/PhysRevLett.122.251601.

[36] Alaric Erschfeld. "Functional methods for cosmic structure formation". PhD thesis. Ruprecht-Karls-Universität Heidelberg, Jan. 2021.

[37] P. K. Kovtun, D. T. Son, and A. O. Starinets. "Viscosity in Strongly Interacting Quantum Field Theories from Black Hole Physics". *Phys. Rev. Lett.* 94 (11 Mar. 2005), p. 111601. DOI: 10.1103/PhysRevLett.94.111601. URL: https://link.aps.org/doi/10.1103/PhysRevLett.94.111601.

[38] Jean-Yves Ollitrault. "Relativistic hydrodynamics for heavy-ion collisions". *Eur. J. Phys.* 29 (2008), pp. 275–302. DOI: 10.1088/0143-0807/29/2/010. arXiv: 0708.2433 [nucl-th].

[39] Thomas Schaefer. "Fluid Dynamics and Viscosity in Strongly Correlated Fluids". *Ann. Rev. Nucl. Part. Sci.* 64 (2014), pp. 125–148. DOI: 10.1146/annurev-nucl-102313-025439. arXiv: 1403.0653 [hep-ph].

[40] B. Betz, D. Henkel, and D.H. Rischke. "From kinetic theory to dissipative fluid dynamics". *Progress in Particle and Nuclear Physics* 62.2 (2009). Heavy-Ion Collisions from the Coulomb Barrier to the Quark-Gluon Plasma, pp. 556–561. ISSN: 0146-6410. DOI: https://doi.org/10.1016/j.ppnp.2008.12.018. URL: https://www.sciencedirect.com/science/article/pii/S0146641008001361.

[41] P. Kapitza. "Viscosity of Liquid Helium below the λ-Point". *Nature* 141.3558 (Jan. 1938), pp. 74–74. ISSN: 1476-4687. DOI: 10.1038/141074a0. URL: https://doi.org/10.1038/141074a0.

[42] J. F. Allen and A. D. Misener. "Flow of Liquid Helium II". *Nature* 141.3558 (Jan. 1938), pp. 75–75. ISSN: 1476-4687. DOI: 10.1038/141075a0. URL: https://doi.org/10.1038/141075a0.

[43] Charles S. Peskin. "The immersed boundary method". *Acta Numerica* 11 (2002), pp. 479–517. DOI: 10.1017/S0962492902000077.

[44] Andrew Bennett. *Lagrangian Fluid Dynamics*. Cambridge Monographs on Mechanics. Cambridge University Press, 2006. DOI: 10.1017/CBO9780511734939.

[45] James Serrin. "Mathematical Principles of Classical Fluid Mechanics". *Fluid Dynamics I / Strömungsmechanik I*. Ed. by C. Truesdell. Berlin, Heidelberg: Springer Berlin Heidelberg, 1959, pp. 125–263. ISBN: 978-3-642-45914-6. DOI: `10.1007/978-3-642-45914-6_2`. URL: `https://doi.org/10.1007/978-3-642-45914-6_2`.

[46] Derek A. Teaney. "Viscous Hydrodynamics and the Quark Gluon Plasma". *Quark-Gluon Plasma 4*, pp. 207–266. DOI: `10.1142/9789814293297_0004`.

[47] Derek Teaney and Li Yan. "Triangularity and Dipole Asymmetry in Heavy Ion Collisions". *Phys. Rev. C* 83 (2011), p. 064904. DOI: `10.1103/PhysRevC.83.064904`. arXiv: `1010.1876 [nucl-th]`.

[48] J. Scott Moreland, Jonah E. Bernhard, and Steffen A. Bass. "Alternative ansatz to wounded nucleon and binary collision scaling in high-energy nuclear collisions". *Phys. Rev. C* 92 (1 July 2015), p. 011901. DOI: `10.1103/PhysRevC.92.011901`. URL: `https://link.aps.org/doi/10.1103/PhysRevC.92.011901`.

[49] Nicolas Borghini, Phuong Mai Dinh, and Jean-Yves Ollitrault. "Is the analysis of flow at the CERN Super Proton Synchrotron reliable?" *Phys. Rev. C* 62 (3 Aug. 2000), p. 034902. DOI: `10.1103/PhysRevC.62.034902`. URL: `https://link.aps.org/doi/10.1103/PhysRevC.62.034902`.

[50] Nicolas Borghini, Phuong Mai Dinh, and Jean-Yves Ollitrault. "Flow analysis from multiparticle azimuthal correlations". *Phys. Rev. C* 64 (5 Sept. 2001), p. 054901. DOI: `10.1103/PhysRevC.64.054901`. URL: `https://link.aps.org/doi/10.1103/PhysRevC.64.054901`.

[51] Fernando G. Gardim et al. "Thermodynamics of hot strong-interaction matter from ultrarelativistic nuclear collisions". *Nature Phys.* 16.6 (2020), pp. 615–619. DOI: `10.1038/s41567-020-0846-4`. arXiv: `1908.09728 [nucl-th]`.

[52] Albert Einstein. "Quantentheorie des einatomigen idealen Gases". *Sitzungberichte der Preußischen Akademie der Wissenschaften* (1925). URL: `https://www.uni-muenster.de/imperia/md/content/physik_ap/demokritov/mbecfornonphysicists/einstein_1924_1925.pdf`.

[53] M. H. Anderson et al. "Observation of Bose-Einstein Condensation in a Dilute Atomic Vapor". *Science* 269.5221 (1995), pp. 198–201. DOI: `10.1126/science.269.5221.198`. eprint: `https://www.science.org/doi/pdf/10.1126/science.269.5221.198`. URL: `https://www.science.org/doi/abs/10.1126/science.269.5221.198`.

[54] K. B. Davis et al. "Bose-Einstein Condensation in a Gas of Sodium Atoms". *Phys. Rev. Lett.* 75 (22 Nov. 1995), pp. 3969–3973. DOI: `10.1103/PhysRevLett.75.3969`. URL: `https://link.aps.org/doi/10.1103/PhysRevLett.75.3969`.

[55] L. Landau. "Theory of the Superfluidity of Helium II". *Phys. Rev.* 60 (4 Aug. 1941), pp. 356–358. DOI: `10.1103/PhysRev.60.356`. URL: `https://link.aps.org/doi/10.1103/PhysRev.60.356`.

[56] S. Jochim et al. "Bose-Einstein Condensation of Molecules". *Science* 302.5653 (2003), pp. 2101–2103. DOI: 10.1126/science.1093280. eprint: https://www.science.org/doi/pdf/10.1126/science.1093280. URL: https://www.science.org/doi/abs/10.1126/science.1093280.

[57] C. A. Regal, M. Greiner, and D. S. Jin. "Observation of Resonance Condensation of Fermionic Atom Pairs". *Phys. Rev. Lett.* 92 (4 Jan. 2004), p. 040403. DOI: 10.1103/PhysRevLett.92.040403. URL: https://link.aps.org/doi/10.1103/PhysRevLett.92.040403.

[58] J. Bardeen, L. N. Cooper, and J. R. Schrieffer. "Theory of Superconductivity". *Phys. Rev.* 108 (5 Dec. 1957), pp. 1175–1204. DOI: 10.1103/PhysRev.108.1175. URL: https://link.aps.org/doi/10.1103/PhysRev.108.1175.

[59] J. Dalibard. "Collisional dynamics of ultra-cold atomic gases". *Proceedings of the International School of Physics "Enrico Fermi", Vol. 140: Bose Einstein Condensation in Atomic Gases*, pp. 321–349. DOI: 10.3254/978-1-61499-225-7-321.

[60] Hossein Sadeghpour et al. "Collisions near threshold in atomic and molecular physics". *J. Phys. B: At. Mol. Opt. Phys* 33 (Mar. 2000), pp. 93–140. DOI: 10.1088/0953-4075/33/5/201.

[61] Moerdijk, Verhaar, and Axelsson. "Resonances in ultracold collisions of 6Li, 7Li, and 23Na." *Physical review. A, Atomic, molecular, and optical physics* 51 6 (1995), pp. 4852–4861.

[62] Jeff Maki and Fei Zhou. "Quantum many-body conformal dynamics: Symmetries, geometry, conformal tower states, and entropy production". *Phys. Rev. A* 100 (2 Aug. 2019), p. 023601. DOI: 10.1103/PhysRevA.100.023601. URL: https://link.aps.org/doi/10.1103/PhysRevA.100.023601.

[63] Maxim Olshanii, Hélène Perrin, and Vincent Lorent. "Example of a Quantum Anomaly in the Physics of Ultracold Gases". *Phys. Rev. Lett.* 105 (9 Aug. 2010), p. 095302. DOI: 10.1103/PhysRevLett.105.095302. URL: https://link.aps.org/doi/10.1103/PhysRevLett.105.095302.

[64] Johannes Hofmann. "Quantum Anomaly, Universal Relations, and Breathing Mode of a Two-Dimensional Fermi Gas". *Phys. Rev. Lett.* 108 (18 May 2012), p. 185303. DOI: 10.1103/PhysRevLett.108.185303. URL: https://link.aps.org/doi/10.1103/PhysRevLett.108.185303.

[65] Jeff Maki, Li-Ming Zhao, and Fei Zhou. "Nonperturbative dynamical effects in nearly-scale-invariant systems: The action of breaking scale invariance". *Phys. Rev. A* 98 (1 July 2018), p. 013602. DOI: 10.1103/PhysRevA.98.013602. URL: https://link.aps.org/doi/10.1103/PhysRevA.98.013602.

[66] Yusuke Nishida and Dam T. Son. "Nonrelativistic conformal field theories". *Phys. Rev. D* 76 (8 Oct. 2007), p. 086004. DOI: 10.1103/PhysRevD.76.086004. URL: https://link.aps.org/doi/10.1103/PhysRevD.76.086004.

[67] G. Zürn et al. "Precise Characterization of ^{6}Li Feshbach Resonances Using Trap-Sideband-Resolved RF Spectroscopy of Weakly Bound Molecules". *Phys. Rev. Lett.* 110 (13 Mar. 2013), p. 135301. DOI: 10.1103/PhysRevLett.110.135301. URL: https://link.aps.org/doi/10.1103/PhysRevLett.110.135301.

[68] Andrea Bergschneider et al. "Spin-resolved single-atom imaging of ^{6}Li in free space". *Phys. Rev. A* 97 (6 June 2018), p. 063613. DOI: 10.1103/PhysRevA.97.063613. URL: https://link.aps.org/doi/10.1103/PhysRevA.97.063613.

[69] I. Boettcher et al. "Equation of State of Ultracold Fermions in the 2D BEC-BCS Crossover Region". *Phys. Rev. Lett.* 116 (4 Jan. 2016), p. 045303. DOI: 10.1103/PhysRevLett.116.045303. URL: https://link.aps.org/doi/10.1103/PhysRevLett.116.045303.

[70] Jesper Levinsen and Meera M. Parish. "Strongly interacting two-dimensional Fermi gases". *Annual Review of Cold Atoms and Molecules.* Chap. 1, pp. 1–75. DOI: 10.1142/9789814667746_0001.

[71] Stefan Floerchinger et al. "Qualifying collective behavior in expanding ultracold gases as a function of particle number". *Phys. Rev. C* 105 (4 Apr. 2022), p. 044908. DOI: 10.1103/PhysRevC.105.044908. URL: https://link.aps.org/doi/10.1103/PhysRevC.105.044908.

[72] S. Weinberg. *Lectures on Quantum Mechanics.* Cambridge University Press, 2015. ISBN: 9781107111660.

[73] Aleksi Kurkela, Urs Achim Wiedemann, and Bin Wu. "Flow in AA and pA as an interplay of fluid-like and non-fluid like excitations". *Eur. Phys. J. C* 79.11 (2019), p. 965. DOI: 10.1140/epjc/s10052-019-7428-6. arXiv: 1905.05139 [hep-ph].

[74] Sandra Brandstetter et al. "A mesoscopic fluid of 10 Fermions". *in preparation* (2023).

[75] G. Bertaina and S. Giorgini. "BCS-BEC Crossover in a Two-Dimensional Fermi Gas". *Phys. Rev. Lett.* 106 (11 Mar. 2011), p. 110403. DOI: 10.1103/PhysRevLett.106.110403. URL: https://link.aps.org/doi/10.1103/PhysRevLett.106.110403.

[76] Vasiliy Makhalov, Kirill Martiyanov, and Andrey Turlapov. "Ground-State Pressure of Quasi-2D Fermi and Bose Gases". *Phys. Rev. Lett.* 112 (4 Jan. 2014), p. 045301. DOI: 10.1103/PhysRevLett.112.045301. URL: https://link.aps.org/doi/10.1103/PhysRevLett.112.045301.

[77] I. Boettcher et al. "Equation of State of Ultracold Fermions in the 2D BEC-BCS Crossover Region". *Phys. Rev. Lett.* 116 (4 Jan. 2016), p. 045303. DOI: 10.1103/PhysRevLett.116.045303. URL: https://link.aps.org/doi/10.1103/PhysRevLett.116.045303.

[78] Hao Shi, Simone Chiesa, and Shiwei Zhang. "Ground-state properties of strongly interacting Fermi gases in two dimensions". *Phys. Rev. A* 92 (3 Sept. 2015), p. 033603. DOI: 10.1103/PhysRevA.92.033603. URL: https://link.aps.org/doi/10.1103/PhysRevA.92.033603.

[79] C. F. v. Weizsäcker. "Zur Theorie der Kernmassen". *Zeitschrift für Physik* 96.7 (July 1935), pp. 431–458. ISSN: 0044-3328. DOI: 10.1007/BF01337700. URL: https://doi.org/10.1007/BF01337700.

[80] T. Schäfer and C. Chafin. "Scaling Flows and Dissipation in the Dilute Fermi Gas at Unitarity". *The BCS-BEC Crossover and the Unitary Fermi Gas*. Ed. by Wilhelm Zwerger. Berlin, Heidelberg: Springer Berlin Heidelberg, 2012, pp. 375–406. ISBN: 978-3-642-21978-8. DOI: 10.1007/978-3-642-21978-8_10. URL: https://doi.org/10.1007/978-3-642-21978-8_10.

[81] E. Wigner. "On the Quantum Correction For Thermodynamic Equilibrium". *Phys. Rev.* 40 (5 June 1932), pp. 749–759. DOI: 10.1103/PhysRev.40.749. URL: https://link.aps.org/doi/10.1103/PhysRev.40.749.

[82] P.F. Kolb, J. Sollfrank, and U. Heinz. "Anisotropic flow from AGS to LHC energies". *Physics Letters B* 459.4 (1999), pp. 667–673. ISSN: 0370-2693. DOI: https://doi.org/10.1016/S0370-2693(99)00720-0. URL: https://www.sciencedirect.com/science/article/pii/S0370269399007200.

[83] *Introduction to Advanced Numerical Differential Equation Solving in the Wolfram Language.* https://reference.wolfram.com/language/tutorial/NDSolveIntroductoryTutorial.html. Accessed: 2023-03-15.

[84] W.E. Schiesser. *The Numerical Method of Lines: Integration of Partial Differential Equations.* Academic Press, 1991. ISBN: 9780126241303.

[85] *Scipy documentation, scipy.optimize.curve$_f$it.* https://docs.scipy.org/doc/scipy/reference/generated/scipy.optimize.curve_fit.html. Accessed: 2023-03-15.

[86] Alice Harpole et al. "pyro: a framework for hydrodynamics explorations and prototyping". *Journal of Open Source Software* 4.34 (2019), p. 1265. DOI: 10.21105/joss.01265. URL: https://doi.org/10.21105/joss.01265.

[87] Phillip Colella. "Multidimensional upwind methods for hyperbolic conservation laws". *Journal of Computational Physics* 87.1 (1990), pp. 171–200. ISSN: 0021-9991. DOI: https://doi.org/10.1016/0021-9991(90)90233-Q. URL: https://www.sciencedirect.com/science/article/pii/002199919090233Q.

[88] Tim Stötzel. "Master thesis: Calculation of the Shear Viscosity of a Real Scalar Field Theory using FRG Methods". *unpublished* (Feb. 2022).

[89] J. Zinn-Justin. *Quantum Field Theory and Critical Phenomena: Fifth Edition.* International series of monographs on physics. Oxford University Press, 2021. ISBN: 9780198834625.

[90] Michel Le Bellac. *Thermal Field Theory.* Cambridge Monographs on Mathematical Physics. Cambridge University Press, 1996. DOI: 10.1017/CBO9780511721700.

[91] H. Lehmann, K. Symanzik, and W. Zimmermann. "Zur Formulierung quantisierter Feldtheorien". *Il Nuovo Cimento (1955-1965)* 1.1 (Jan. 1955), pp. 205–225. ISSN: 1827-6121. DOI: 10.1007/BF02731765. URL: https://doi.org/10.1007/BF02731765.

[92] Takeo Matsubara. "A New Approach to Quantum-Statistical Mechanics". *Progress of Theoretical Physics* 14.4 (Oct. 1955), pp. 351–378. ISSN: 0033-068X. DOI: 10.1143/PTP.14.351. eprint: https://academic.oup.com/ptp/article-pdf/14/4/351/5286981/14-4-351.pdf. URL: https://doi.org/10.1143/PTP.14.351.

[93] T.S. Evans. "N-point finite temperature expectation values at real times". *Nuclear Physics B* 374.2 (1992), pp. 340–370. ISSN: 0550-3213. DOI: https://doi.org/10.1016/0550-3213(92)90357-H. URL: https://www.sciencedirect.com/science/article/pii/055032139290357H.

[94] L. V. Keldysh. "Diagram technique for nonequilibrium processes". *Zh. Eksp. Teor. Fiz.* 47 (1964), pp. 1515–1527.

[95] M. Toda et al. *Statistical Physics II: Nonequilibrium Statistical Mechanics.* Springer Series in Solid-State Sciences. Springer Berlin Heidelberg, 1991. ISBN: 9783540538332.

[96] Ryogo Kubo. "Statistical-Mechanical Theory of Irreversible Processes. I. General Theory and Simple Applications to Magnetic and Conduction Problems". *Journal of the Physical Society of Japan* 12.6 (1957), pp. 570–586. DOI: 10.1143/JPSJ.12.570.

[97] W. Israel and J.M. Stewart. "Transient relativistic thermodynamics and kinetic theory". *Annals of Physics* 118.2 (1979), pp. 341–372. ISSN: 0003-4916. DOI: https://doi.org/10.1016/0003-4916(79)90130-1. URL: https://www.sciencedirect.com/science/article/pii/0003491679901301.

[98] Lars H. Heyen and Stefan Floerchinger. "Real scalar field, the nonrelativistic limit, and the cosmological expansion". *Phys. Rev. D* 102 (3 Aug. 2020), p. 036024. DOI: 10.1103/PhysRevD.102.036024. URL: https://link.aps.org/doi/10.1103/PhysRevD.102.036024.

[99] Eric Braaten, Abhishek Mohapatra, and Hong Zhang. "Classical nonrelativistic effective field theories for a real scalar field". *Phys. Rev. D* 98 (9 Nov. 2018), p. 096012. DOI: 10.1103/PhysRevD.98.096012. URL: https://link.aps.org/doi/10.1103/PhysRevD.98.096012.

[100] Mohammad Hossein Namjoo, Alan H. Guth, and David I. Kaiser. "Relativistic corrections to nonrelivistic effective field theories". *Phys. Rev. D* 98 (1 July 2018), p. 016011. DOI: 10.1103/PhysRevD.98.016011. URL: https://link.aps.org/doi/10.1103/PhysRevD.98.016011.

[101] Kazuo Fujikawa. "Path-Integral Measure for Gauge-Invariant Fermion Theories". *Phys. Rev. Lett.* 42 (18 Apr. 1979), pp. 1195–1198. DOI: `10.1103/PhysRevLett.42.1195`. URL: `https://link.aps.org/doi/10.1103/PhysRevLett.42.1195`.

[102] E.A. Calzetta and B.L.B. Hu. *Nonequilibrium Quantum Field Theory*. Cambridge Monographs on Mathematical Physics. Cambridge University Press, 2008. ISBN: 9780521641685.

[103] Stefan Floerchinger. "Few-body hierarchy in non-relativistic functional renormalization group equations and a decoupling theorem". *Nuclear Physics A* 927 (2014), pp. 119–133. ISSN: 0375-9474. DOI: `https://doi.org/10.1016/j.nuclphysa.2014.04.013`. URL: `https://www.sciencedirect.com/science/article/pii/S0375947414000955`.

[104] Jürgen Berges, Nikolaos Tetradis, and Christof Wetterich. "Non-perturbative renormalization flow in quantum field theory and statistical physics". *Physics Reports* 363.4 (2002). Renormalization group theory in the new millennium. IV, pp. 223–386. ISSN: 0370-1573. DOI: `https://doi.org/10.1016/S0370-1573(01)00098-9`. URL: `https://www.sciencedirect.com/science/article/pii/S0370157301000989`.

[105] R. Fernandez, J. Froehlich, and A.D. Sokal. *Random walks, critical phenomena, and triviality in quantum field theory*. Germany: Springer, 1992. ISBN: 3-540-54358-9. URL: `http://inis.iaea.org/search/search.aspx?orig_q=RN:23080215`.

[106] Jan M. Pawlowski. "Aspects of the functional renormalisation group". *Annals of Physics* 322.12 (2007), pp. 2831–2915. ISSN: 0003-4916. DOI: `https://doi.org/10.1016/j.aop.2007.01.007`. URL: `https://www.sciencedirect.com/science/article/pii/S0003491607000097`.

[107] K. Symanzik. "Small distance behaviour in field theory and power counting". *Communications in Mathematical Physics* 18.3 (Sept. 1970), pp. 227–246. ISSN: 1432-0916. DOI: `10.1007/BF01649434`. URL: `https://doi.org/10.1007/BF01649434`.

[108] Curtis G. Callan. "Broken Scale Invariance in Scalar Field Theory". *Phys. Rev. D* 2 (8 Oct. 1970), pp. 1541–1547. DOI: `10.1103/PhysRevD.2.1541`. URL: `https://link.aps.org/doi/10.1103/PhysRevD.2.1541`.

[109] Gunnar Kallen. "On the definition of the Renormalization Constants in Quantum Electrodynamics". *Helv. Phys. Acta* 25.4 (1952), p. 417. DOI: `10.1007/978-3-319-00627-7_90`.

[110] H. Lehmann. "Über Eigenschaften von Ausbreitungsfunktionen und Renormierungskonstanten quantisierter Felder". *Il Nuovo Cimento (1943-1954)* 11.4 (Apr. 1954), pp. 342–357. ISSN: 1827-6121. DOI: `10.1007/BF02783624`. URL: `https://doi.org/10.1007/BF02783624`.

[111] Alexander Altland and Ben D. Simons. *Condensed Matter Field Theory*. 2nd ed. Cambridge University Press, 2010. DOI: 10.1017/CBO9780511789984.

[112] Stefan Floerchinger. "Variational principle for theories with dissipation from analytic continuation". *Journal of High Energy Physics* 2016.9 (Sept. 2016), p. 99. ISSN: 1029-8479. DOI: 10.1007/JHEP09(2016)099. URL: https://doi.org/10.1007/JHEP09(2016)099.

[113] Ralf-Arno Tripolt. "Spectral Functions and Transport Coefficients from the Functional Renormalization Group". PhD thesis. Technische Universität Darmstadt, Apr. 2015.

Acknowledgements

I would like to thank everyone who accompanied me along my journey through the last few years. My time as a PhD student was interesting and fun, not just because of the engaging topics of research, but also the people around me who I could always discuss and laugh with.

First, I would like to thank my advisor Prof. Dr. Stefan Floerchinger who always took the time to discuss all my projects in detail, gave direction and advice whenever needed and always encouraged me to try and learn new things.

Second, I thank Prof. Dr. Richard Schmidt for agreeing to be my second referee and Prof. Dr. Selim Jochim and Prof. Dr. Ulrich Schwarz for being part of my examination committee.

I am grateful to my colleagues in the Quantum fields, fluids and information group, both in Heidelberg and in Jena, who were just generally great people to be around. Special thanks go to Tobias Haas who helped me a lot at the beginning of my PhD and was always willing to talk about all things physics, Tim Stötzel who I could always exchange ideas with and rely on to point out mistakes in my calculations, and Giuliano Giacalone who taught me many things, not only about the heavy-ion side of our project, but also how to improve the presentation of my work.

I would also like to thank our collaborators on the experimental side, especially Sandra Brandstetter, Philipp Lunt, Carl Heintze and Selim Jochim, for our many great discussions. Afterwards, I always felt like I had gained a deeper understanding of the physics of our project.

Last but not least, all of this would not have been possible without the constant support of my friends and family. Thank you for reassuring me and making me smile whenever I needed it.